



**HAL**  
open science

# Low-cost Millimeter antenna system based on the technology Air-filled SIW for satellite telecommunication application

Jingwen Zhang

► **To cite this version:**

Jingwen Zhang. Low-cost Millimeter antenna system based on the technology Air-filled SIW for satellite telecommunication application. Optics / Photonic. Université Grenoble Alpes [2020-..], 2024. English. NNT : 2024GRALT002 . tel-04558953

**HAL Id: tel-04558953**

**<https://theses.hal.science/tel-04558953>**

Submitted on 25 Apr 2024

**HAL** is a multi-disciplinary open access archive for the deposit and dissemination of scientific research documents, whether they are published or not. The documents may come from teaching and research institutions in France or abroad, or from public or private research centers.

L'archive ouverte pluridisciplinaire **HAL**, est destinée au dépôt et à la diffusion de documents scientifiques de niveau recherche, publiés ou non, émanant des établissements d'enseignement et de recherche français ou étrangers, des laboratoires publics ou privés.

THÈSE

Pour obtenir le grade de

**DOCTEUR DE L'UNIVERSITÉ GRENOBLE ALPES**

École doctorale : EEATS - Electronique, Electrotechnique, Automatique, Traitement du Signal (EEATS)

Spécialité : Optique et Radiofréquences

Unité de recherche : Institut de Microélectronique, Electromagnétisme et Photonique - Laboratoire d'hyperfréquences et de caractérisation

**Système antennaire millimétrique actif bas coût basé sur la technologie guide d'onde intégré au substrat creux pour application de télécommunication satellite**

**Low-cost Millimeter antenna system based on the technology Air-filled SIW for satellite telecommunication application**

Présentée par :

**Jingwen ZHANG**

Direction de thèse :

**Tan Phu VUONG**

PROFESSEUR DES UNIVERSITES, Université Grenoble Alpes

Directeur de thèse

**Yvan DUROC**

PROFESSEUR DES UNIVERSITES, Université Grenoble Alpes

Co-directeur de thèse

**Ke Wu**

Ecole Polytechnique de Montréal

Co-directeur de thèse

Rapporteurs :

**Habiba OUSLIMANI**

PROFESSEURE DES UNIVERSITES, Université Paris Nanterre

**Philippe LE-THUC**

PROFESSEUR DES UNIVERSITES, Université Côte d'Azur

Thèse soutenue publiquement le **12 janvier 2024**, devant le jury composé de :

**Tan Phu VUONG**

PROFESSEUR DES UNIVERSITES, Grenoble INP

Directeur de thèse

**Yvan DUROC**

PROFESSEUR DES UNIVERSITES, University Claude Bernard Lyon 1

Co-directeur de thèse

**Ke WU**

FULL PROFESSOR, Polytechnique Montréal

Co-directeur de thèse

**Anne VILCOT**

PROFESSEURE DES UNIVERSITES, Grenoble INP

Présidente

**Anthony GHIOTTO**

MAITRE DE CONFERENCES, Bordeaux INP

Examinateur

**Alexandru TAKACS**

MAITRE DE CONFERENCES, Université de Toulouse

Examinateur

**Habiba OUSLIMANI**

PROFESSEURE DES UNIVERSITES, Université Paris Nanterre

Rapporteuse

**Philippe LE-THUC**

PROFESSEUR DES UNIVERSITES, Université Côte d'Azur

Rapporteur

Invités :

**Alejandro Niembro**

INGENIEUR DOCTEUR, Schneider Electric



## ACKNOWLEDGEMENTS

First, I would like to express my deep gratitude to my supervisor and co-supervisors: PR. Tan-Phu VUONG from the laboratory IMEP-LaHC, Grenoble Alpes University; PR. Ke WU from the Poly-Grames research center, École Polytechnique de Montréal; PR. Yvan DUROC from the laboratory Ampère, University Claude Bernard Lyon 1 for their guidance and support. I would like to thank them for giving me this opportunity, for their help and accompany over these years.

I'm also very grateful to PR. Anne VILCOT from Grenoble Alpes University and MCF. Anthony GHIOTTO from the IMS research center, University of Bordeaux. As members of CSI (individual monitoring committee; 'Comité de Suivi Individuel' in French), they helped me solve the difficulties I encountered during this thesis.

My sincere thanks to all members in the IMEP-LaHC laboratory. I would like to thank leader of DHREAMS, PR. Pascal Xavier, for patiently answering all my questions and not only technical questions, but also with procedural and other questions I encountered during my PhD. I would like to thank the technical staffs: Nicolas CORRAO, Martine GRI, Gregory GROSA, who helped me a lot with fabrications and measurements. I would like also to thank the members of the administrative staffs, Dalhila ALOUANI, Brigitte RASOLOFONIAINA, Anais DESCHAUX BEAUME, Valerie MISCIOSCIA, Gwladys ANAGNI, Isabelle MICHELIN, Serge BAS for their support during my life in the lab.

I would like to send my sincere thanks to my colleagues and friends, especially Nhu Huan NGUYEN, Thi-Hong-Le DAM, Maxime WAWRZYNIAK, Clément PORNIN for their technical and living supports.

Finally, I would like to express a deep sense of gratitude to my family: my dear grandparents, my parents, Heng ZHANG, Min WANG. Although they are far away in China, their daily care has always supported me. I would also like to thank my life partner Bastien PERES. Thanks to him for accompanying and taking care of me during

these last six years. Also, a big thank you to his parents, Luc, Marie-Laure PERES and his siblings. Their care and attention made me feel like family in this country.

## RÉSUMÉ

La technologie des guides d'ondes et celle des circuits imprimés (PCB en anglais) constituent deux jalons dans l'histoire de l'ingénierie des micro-ondes. Les guides d'ondes sont à l'origine de différents types de dispositifs passifs tels que les antennes ou les filtres alors que la technologie des PCB a permis d'intégrer les composants actifs tels que les amplificateurs ou les mélangeurs sur de petits volumes. Les composants passifs basés sur les guides d'ondes présentent des avantages tels que de faibles pertes d'insertion, une capacité de tenue en puissance élevée et un blindage intrinsèque. La technologie des guides d'ondes intégrés au substrat (SIW en anglais) proposée dans les années 2000 a réduit la taille des guides d'ondes volumiques en combinant deux technologies : les guides d'ondes métalliques et les PCBs. Elle permet d'obtenir des pertes d'insertion relativement faibles, un blindage intrinsèque et de faibles dimensions. Le SIW simplifie l'intégration des dispositifs passifs basés sur des guides d'ondes avec les dispositifs actifs sur PCB. Afin d'optimiser ces performances, la technologie SIW a évolué avec l'introduction du guide d'ondes intégré au substrat rempli d'air (AFSIW en anglais). La cavité d'air à l'intérieur de l'AFSIW permet de réduire considérablement les pertes diélectriques. L'AFSIW a alors été appliquée à la conception de dispositifs passifs tels que des filtres, antennes ou déphaseurs.

Ces dispositifs sont conçus sur un plan unique et leurs interconnexions pour concevoir un système, tel qu'un émetteur ou récepteur radiofréquence (RF) nécessitant l'association de composants, se fait également sur le même plan. Toutefois, la structure multicouche de l'AFSIW offre de nouvelles possibilités de conceptions en utilisant ses couches inférieure et supérieure. Les composants peuvent être empilés et connectés par des transitions verticales. Le travail de cette thèse exploite la structure multicouche de l'AFSIW pour « verticaliser » un système. L'exploitation des couches inférieure et supérieure est étudiée d'une part pour la connexion de composants et d'autre part pour leur conception individuelle.

Pour la connexion de composants, la plupart des transitions entre SIW, AFSIW et lignes micro ruban sont réalisées sur le même plan mais cela augmente considérablement la longueur des circuits. Au contraire, la transition entre la cavité de l'AFSIW et la ligne

micro ruban proposée dans cette thèse peut être utilisée pour superposer des composants passifs et actifs sur le plan vertical en utilisant le substrat de la couche supérieure de l'AFSIW pour réduire le volume occupé.

Pour la conception de composants, les couches inférieure et supérieure de l'AFSIW sont utiles pour réaliser des composants multi-cavités comme des filtres d'ordre élevé. Le couplage inter cavité d'un filtre se faisant classiquement sur le même plan, l'ordre du filtre augmentant, sa longueur augmente aussi. La transition entre cavités empilées proposée dans cette thèse offre une autre possibilité pour la conception de tels composants quand l'espace horizontal alloué est insuffisant.

L'objectif global de cette thèse est de fournir une nouvelle possibilité pour l'organisation spatiale d'un émetteur-récepteur RF. Afin de fournir une preuve de concept, la conception d'une antenne est aussi proposée permettant d'aboutir à un système comprenant l'ensemble : antenne, filtre et amplificateur. Chaque composant et cavités résonantes du filtre sont situés sur des couches différentes. Comparés à l'état de l'art où les composants sont connectés sur un même plan horizontal, les résultats obtenus démontrent la possibilité de connecter verticalement des composants. Ces deux approches de connexion de composants (exploitant le plan horizontal et vertical) offrent plus de liberté pour une utilisation optimale de l'espace 3D, particulièrement critique pour les communications spatiales en raison des contraintes sur le volume occupé dans les satellites.

## ABSTRACT

Waveguide technology and printed circuit board (PCB) technology are two milestones in the engineering history of microwave technology. Waveguides are at the origin of different types of passive devices such as antennas or filters while PCB technology has made it possible to integrate today's active components such as amplifiers or mixers on very small volumes. Passive components based on waveguide technology have advantages such as low insertion losses, high power handling capability and auto-blind. Substrate-integrated waveguide (SIW) technology proposed in the early 2000s reduced the size of volume waveguides by combining two technologies: metallic waveguides and PCBs. It allows for relatively low insertion losses, auto-blind and small dimensions. The introduction of SIW technology simplifies the integration of passive waveguide-based devices with active PCB-based devices. To further optimize its performance, SIW technology has evolved with the introduction in 2014 of the air-filled substrate integrated waveguide (AFSIW). The cavity placed inside the AFSIW significantly reduces dielectric losses. Since 2014, this technology has been applied to the design of various passive devices such as filters, antennas or phase shifters.

These devices are individually designed on a single plane and their connections to each other to design a system, such as a radio frequency transmitter or receiver which requires the association of several components, is also done on the same plane. However, the multilayer structure of AFSIW offers new possibilities to design these systems using its lower and upper layers. Components can be stacked and connected using vertical transitions. The work of this thesis exploits the multilayer structure of AFSIW to “verticalize” a system. The use of the lower and upper layers is studied on the one hand for the connection of the different components of a system and on the other hand for the design of components individually.

For connecting different components, most of the transitions between SIW, AFSIW and various microstrip lines are made on the same plane but this significantly increases the circuit length. On the contrary, the transition between the AFSIW cavity and the micro strip line proposed in this thesis can be used to achieve the

superposition of passive and active components on the vertical plane using the substrate of the upper layer of the AFSIW allowing to reduce the occupied volume.

For designing individual components, the bottom and top layers of AFSIW are useful for making multi-cavity components such as high-order filters. The coupling between each cavity of a filter classically taking place on the same plane, as the order of the filter increases, its length also increases. The transition between stacked cavities proposed in this thesis offers another possibility for the design of such components in the case where the allocated horizontal space is insufficient.

The overall objective of this thesis is to provide a new possibility for the spatial organization of a radio frequency transceiver. In order to provide a proof of concept, the design of an antenna is also proposed in this thesis leading to a system comprising the assembly: antenna, filter and amplifier. Each component is located on a different layer and the filter's resonant cavities are also positioned on different layers. Compared to the state of the art where the components are connected on the same horizontal plane, the results obtained demonstrate the possibility to connect components vertically. These two approaches to connect components (exploiting both the horizontal and vertical plane) thus offer more degrees of freedom for optimal use of 3D space, which is particularly critical for spatial communications due to occupied volume constraints at satellite level.

# CONTENTS

ACKNOWLEDGEMENTS	1
INTRODUCTION	21
CHAPTER 1: STATE OF THE ART	27
<b>1.1 Satellite communication and antenna system</b>	<b>27</b>
1.1.1 History of satellite communication	27
1.1.2 Antenna system	32
<b>1.2 Transmission lines</b>	<b>35</b>
1.2.1 History of transmission lines	35
1.2.2 Air-filled substrate integrated waveguide	38
<b>1.3 Conclusion</b>	<b>43</b>
CHAPTER 2: TRANSITION AFSIW - MSL	45
<b>2.1 Overview</b>	<b>45</b>
<b>2.2 Transition design</b>	<b>51</b>
2.2.1 Microstrip	52
2.2.2 AFSIW geometry	53
2.2.3 Transition design process	55
2.2.4 Back-to-back transition	62
<b>2.3 Experimental Results</b>	<b>64</b>
<b>2.4 Conclusion</b>	<b>65</b>
CHAPTER 3: AFSIW ANTENNAS	69
<b>3.1 Overview</b>	<b>69</b>
<b>3.2 Cavity-backed slot antenna</b>	<b>72</b>
3.2.1 AFSIW CBSA design	73
3.2.2 Simulation results and comparison	76
3.2.3 Fabrication and measurement	77
	7

<b>3.3 Patch antenna fed by AFSIW</b>	<b>79</b>
3.3.1 AFSIW fed patch antenna design	80
3.3.2 Fabrication and measurement	84
<b>3.4 Conclusion</b>	<b>86</b>
<b>CHAPTER 4: MULTILAYER FILTER</b>	<b>89</b>
<b>4.1 Overview</b>	<b>89</b>
<b>4.2 Filter synthesis</b>	<b>93</b>
4.2.1 Vertical coupling structure	94
4.2.2 Input/Output coupling structure	98
4.2.3 Simulation and manufacture	101
<b>4.3 Conclusion</b>	<b>107</b>
<b>CHAPTER 5: SIMPLIFIED TRANSCEIVER</b>	<b>109</b>
<b>5.1 Assembly design</b>	<b>109</b>
<b>5.2 Fabrication and measurement</b>	<b>112</b>
<b>5.3 Conclusion</b>	<b>115</b>
<b>CONCLUSION AND PERSPECTIVES</b>	<b>117</b>

## LIST OF FIGURES

Fig. 1 The number of in-orbit spacecraft. Source: G Curzi, Aerospace Magazine, 2020. .....	21
Fig. 2 History of the invention of SIW.....	22
Fig. 3 SIW's applications. ....	22
Fig. 4 Evolution from SIW to AFSIW. ....	23
Fig. 5 (a) SIW filter, (b) AFISW filter and (c) performance comparisons. ....	23
Fig. 1.1 Different applications for satellite communication.....	27
Fig. 1.2 First concept of satellite constellation to coverage of the globe [12]. ....	28
Fig. 1.3 Diagram of different orbits. ....	29
Fig. 1.4 Spectrum of satellite application. ....	30
Fig. 1.5 Schematic of the transmission path.....	31
Fig. 1.6 Schematic of satellite architecture. ....	32
Fig. 1.7 Schematic of transponder.....	32
Fig. 1.8 Earth station diagram. ....	33
Fig. 1.9 (a) Receiver and (b) transmitter.....	33
Fig. 1.10 Different technologies for antenna system.....	34
Fig. 1.11 Complete line of Ka-band and Q-band components of Microwave Components and Systems Inc (MCS).....	35
Fig. 1.12 Early transmission line models.....	36
Fig. 1.13 Cross-sectional view of different types of planar transmission line: (a) stripline; (b) suspended stripline; (c) microstrip; (d) coplanar waveguide and (d) slotline.....	37
Fig. 1.14 Pictures of (a) SIW; (b) SISW; (c) SINRD; (d) SIIDG; (e) RSIW; (f) SW-SIW....	39
Fig. 1.15 The first concept of AFSIW.....	40

Fig. 1.16 Pictures of the (a) structure of AFSIW and (b) fabrication. ....	40
Fig. 1.17 Different components based on AFSIW technology.....	42
Fig. 2.1 E-Plane and H-Plane for a rectangular waveguide where $a > b$ .....	45
Fig. 2.2 Some in-line transitions between the waveguide and the microstrip line by: (a) stepped ridged waveguides [51]; (b) fin-line arrays [53]; (c) radial probes [54] and (d) coaxial probes [55]. ....	46
Fig. 2.3 Some E-Plane transitions between the waveguide and the microstrip line by: (a) probe feeding and [57] and (b) slot coupling [59]. ....	47
Fig. 2.4 SIW-Microstrip transition structure [62] in (a) simulation and (b) fabrication. ....	47
Fig. 2.5 SIW-Microstrip transition multilayer structure [63]. ....	48
Fig. 2.6 Some ESIW-Microstrip transitions structure: (a) original transition [64] and (b) improved version [65]. ....	48
Fig. 2.7 The structure of the transition SIW to microstrip with probe [66], [67]: (a) 3-D view, (b) top view, and (c) side view. ....	49
Fig. 2.8 Structure of the microstrip to ESIW version transition [68]: (a) Upper layer top; (b) Upper layer bottom; (c) Middle layer; (d) Transverse section. ....	50
Fig. 2.9 The structure of the transition SIW to microstrip [69] with (a) slot; (b) H-shape slot and (c) U-shape slot. ....	50
Fig. 2.10 The structure of the transition between AFSIW and microstrip with slot [70]: (a) 3-D view and (b) side view. ....	51
Fig. 2.11 Schematic diagram of transition. ....	52
Fig. 2.12 Basic structure of microstrip: (a) geometry; (b) electric and magnetic field lines. ....	52
Fig. 2.13 Simulated results for determining microstrip line width. ....	53
Fig. 2.14 Air-filled SIW (a)3D view and (b) cross sectional view. ....	54

Fig. 2.15 S-parameters and the E-field simulation results. ....	55
Fig. 2.16 Transition structure: (a) 3D view and (b) top and bottom view of layer S3. ....	56
Fig. 2.17 Cross-sectional view of the proposed transition: (a) without the copper patch; (b) with the copper patch.....	57
Fig. 2.18 Simplified top view of the slot coupling problem. ....	57
Fig. 2.19 Lg parameter analysis. ....	58
Fig. 2.20 Ld parameter analysis. ....	59
Fig. 2.21 I2 parameter analysis.....	60
Fig. 2.22 lcover parameter analysis. ....	60
Fig. 2.23 Parameter analysis of second round for the parameter (a) Ld; (b) I2 and (c) lcover. ....	61
Fig. 2.24 Simulated S-parameters results of the single transition. ....	62
Fig. 2.25 Simulated back-to-back transition. ....	63
Fig. 2.26 Fabricated back-to-back transition. ....	63
Fig. 2.27 Measured and simulated S-parameters results for the proposed back-to-back transition.....	64
Fig. 2.28 Proposed vertical transition design approach.....	66
Fig. 3.1 Pictures of (a) cavity-backed antenna [76]; (b) slot antenna [77]; (c) antipodal tapered slot antenna [78] and (d) dielectric resonator antenna [79]; (e) horn antenna [80] and (f) Yagi-Uda antenna [81]. ....	70
Fig. 3.2 Antipodal linearly tapered slot antennas with the technology (a) SIW and (b) AFSIW. ....	71
Fig. 3.3 Horn antennas with the technology (a) SIW and (b) AFSIW.....	71
Fig. 3.4 Simplified diagram of the transition structure.....	72
Fig. 3.5 Photo of the SIW CBSA in [88]. ....	73

Fig. 3.6 AFSIW CBSA structure.....	73
Fig. 3.7 (a) Top copper layer and (b) bottom copper layer of substrate 2 of AFSIW CBSA .....	74
Fig. 3.8 DFSIW CBSA structure.....	75
Fig. 3.9 Geometry of CBSA. ....	75
Fig. 3.10 Simulated S-parameters results of AFSIW and SIW CBSA. ....	76
Fig. 3.11 Simulated 3D view radiation result of AFSIW CBSA. ....	77
Fig. 3.12 Photos of the (a) front and (b) back of the fabricated CBSA. ....	77
Fig. 3.13 CBSA S-parameter measured result. ....	78
Fig. 3.14 CBSA measurement environment: (a) view in the anechoic chamber; (b) zoom view on the antenna. ....	78
Fig. 3.15 Simulated and measured CBSA radiation pattern in (a) H-plane and (b) E-plane at 27.92 GHz.....	79
Fig. 3.16 Patch antenna fed by waveguide rectangular in [90]: (a) rectangular microstrip patch antenna; (b) cut-away view.....	80
Fig. 3.17 3D view of the patch antenna using AFSIW feeding structure in [91]. ....	80
Fig. 3.18 3D view of proposed patch antenna for the system. ....	81
Fig. 3.19 (a) Symmetrical inductive and (b) equivalent circuit.....	82
Fig. 3.20 3D view of proposed patch antenna for the system. ....	82
Fig. 3.21 Simulated S-parameter result for the patch antenna. ....	83
Fig. 3.22 Simulated far-field result for the patch antenna.....	83
Fig. 3.23 (a) Top view and (b) bottom view of the patch antenna fabrication model.	84
Fig. 3.24 Photos of the (a) front and (b) back of the fabricated CBSA. ....	84
Fig. 3.25 Measured and simulated S-parameter result for the patch antenna.....	85

Fig. 3.26 patch antenna measurement environment: (a) view in the anechoic chamber; (b) zoom view on the antenna. ....	85
Fig. 3.27 Simulated and measured patch antenna radiation pattern in (a) H-plane and (b) E-plane at 28 GHz.....	86
Fig. 3.28 The impact of the size of the ground for: (a) CBSA AFSIW; (b) patch antenna. .....	87
Fig. 3.29 Different organizations of antenna system.....	88
Fig. 4.1 Pictures of filters with different technologies: (a) lumped element filter [15]; (b) microstrip filter [18]; (c) dielectric filter [98]; (d) cavity filter [100] and (e) waveguide filter [19]. ....	89
Fig. 4.2 Picture of the air-filled SIW (a) third-order [8] and (b) fifth-order [110] band-pass filter. ....	90
Fig. 4.3 Pictures of filters proposed to overcome the problem of oversize: (a) Partially Air-Filled Substrate Integrated Waveguide Filters [112]; (b) Dielectric Slab Air-Filled Substrate Integrated Waveguide (SAFSIW) [115]; (c) AFSIW Filter with Multilayer Cross-Coupling [116] and (d) Vertically Stacked SIW Filter [117]. ....	91
Fig. 4.4 Configuration of the alternative four-cavity filter [118].....	92
Fig. 4.5 3D view of cross-coupled AFSIW filter [116]. ....	92
Fig. 4.6 Coupling topology.....	94
Fig. 4.7 Proposed vertical transition design approach.....	94
Fig. 4.8 Equivalent T-network for a thick iris. ....	96
Fig. 4.9 Variation of Ks for the parameter (a) Ls; (b) Ws; (c) Wl; (d) Ll; (e) Lg and (f) Lc. .....	97
Fig. 4.10 Input/output iris structure.....	99
Fig. 4.11 Inverter model (center) for an inductive window in waveguide technology. .....	100

Fig. 4.12 Variation of $K_s$ for $w_1$ . .....	100
Fig. 4.13 Detailed view of proposed vertical filter. ....	101
Fig. 4.14 Electric field in the cavity. ....	102
Fig. 4.15 Simulated S-parameters of proposed filter. ....	102
Fig. 4.16 Simulated structure for measurement of proposed filter. ....	103
Fig. 4.17 Fabrication of proposed filter. ....	103
Fig. 4.18 (a) Simulated S-parameters and (b) comparisons of simulated and measured S-parameters of proposed filter. ....	104
Fig. 4.19 Proposed filter with the correction. ....	105
Fig. 4.20 Comparisons of simulated and measured results with S-parameters of (a) $S_{11}$ ; (b) $S_{21}$ ; (c) $S_{22}$ of proposed filter. ....	106
Fig. 4.21 Proposed multilayer filter design approach. ....	107
Fig. 5.1 System schematic. ....	109
Fig. 5.2 (a) 3D view; (b) top view and (c) bottom view of the system's simulated model. ....	110
Fig. 5.3 E-field simulation result of the antenna circuit (cross section according to $XX'$ ). ....	111
Fig. 5.4 Far field simulation result of the antenna circuit. ....	111
Fig. 5.5 Photos of the (a) front and (b) back of the fabricated antenna circuit. ....	112
Fig. 5.6 Antenna circuit measurement environment: (a) view in the anechoic chamber; (b) zoom view on the antenna circuit and (c) S-parameters measurement. ....	112
Fig. 5.7 Measured and simulated S-parameter results. ....	113
Fig. 5.8 Simulated and measured antenna circuit radiation pattern at their respective resonant frequency (28 GHz and 27.3 GHz) in (a) H-plane and (b) E-plane. ....	113
Fig. 5.9 Measurement with the LNA. ....	114

Fig. 5.10 Measured S-parameters results with the LNA. ....115

Fig 6. Schematic of the ideal integration circuit. ....120



## LIST OF TABLES

Tab. 1.1 Satellite communication frequency band .....	31
Tab. 1.2 Earth station types .....	33
Tab. 1.3 Performances comparisons of waveguide and planar transmission lines....	38
Tab. 1.4 Performances comparisons of different waveguide-based technologies ....	41
Tab. 2.1 Geometry of the waveguide with technology AFSIW .....	55
Tab. 2.2 Dimensions of proposed transition .....	62
Tab. 2.3 Comparison with other vertical transitions .....	66
Tab. 3.1 Dimensions of CBSA in millimeter .....	76
Tab. 3.2 Dimensions of patch antenna in millimeter.....	83
Tab. 3.3 Radiation center frequency and variation .....	87
Tab. 4.1 Coupling matrix setup.....	95
Tab. 4.2 Variation of $K_s$ .....	98
Tab. 4.3 Geometry of coupling inter-cavity .....	98
Tab. 4.4 Geometry of input/output iris. ....	101

## LIST OF SYMBOLS AND ABBREVIATIONS

$f_0$	Center Frequency
$f_c$	Cutoff Frequency
$k_0$	Wave Number in Free-Space
$\lambda_g$	Guide Wavelengths
$c$	Light Velocity (M/S)
$f$	Frequency
$\tan\delta$	Loss Tangent
A/D	Analogue To Digital Converter
AFSIW	Air-Filled Substrate Integrated Waveguide
ALTSA	Antipodal Linearly Tapered Slot Antenna
ALTSA	Antipodal Linearly Tapered Slot Antenna
BPF	Bandpass Filter
BSS	Broadcasting Satellite Service
CBSA	Cavity-Backed Slot Antenna
CPW	Coplanar Waveguide
D/A	Digital To Analogue Converter
DFSIW	Dielectric-Filled Substrate Integrated Waveguide
DSP	Digital Signal Processor
E-field	Electric Field
FR-4	Flame Resistant 4
FSS	Fixed Satellite Service
GCPW	Grounded Coplanar Waveguide
GCPW	Grounded Coplanar Waveguide
GEO	Geosynchronous Orbit
GPS	Global Positioning System
HEO	High Earth Orbit
H-field	Magnetic Field
IoT	Internet Of Thing
ITU	International Telecommunication Union

LEO	Low Earth Orbit
LNA	Low Noise Amplifier
LTCC	Low Temperature Co-Fired Ceramics
LTSA	Linearly Tapered Slot Antenna
MEO	Medium Altitude Earth Orbit
MICs	Microwave Integrated Circuits
MSS	Mobile Satellite Service
PCB	Printed Circuit Board
SAFSIW	Dielectric Slab Air-Filled Substrate Integrated Waveguide
SIC	Substrate Integrated Circuit
SICs	Substrate Integrated Circuit Concepts
SINRD	Substrate Integrated Non-Radiating Dielectric Waveguide
SISW	Substrate Integrated Slab Waveguide
TE	Transverse Electric
TEM	Transverse Electric Magnetic
TM	Transverse Magnetic
TRL	Thru-Reflect-Line
USAT	Ultra-Small Aperture Terminal
VCO	Voltage Controlled Oscillator
VNA	Vector Network Analyzer
VSAT	Very Small Aperture
W	Width Of the Structure



# INTRODUCTION

In daily life, satellite communication provides a lot of convenience for human beings. With the development of satellite communication technology, satellites in space are becoming increasingly crowded, which can be seen from the curve of the explosive growth of spacecraft shown as Fig. 1.

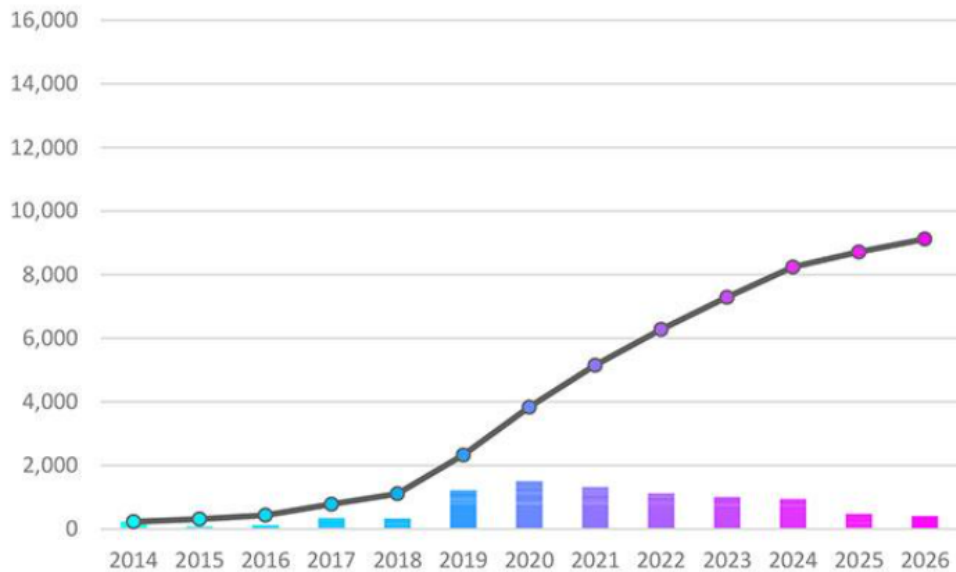


Fig. 1 The number of in-orbit spacecraft. Source: G Curzi, Aerospace Magazine, 2020.

Due to limited space resources, the number and quality of payload carried by a satellite is very important. Therefore, this allows researchers and industries to continuously optimize the performance and volume of the system. The minimization of electronic system volume starts from the proposal of printed circuit board (PCB) technology in 1929 [1]. Due to the development of communication technology, the low frequency band is becoming more and more saturated. With the development of high-frequency bands, the loss of PCB is becoming more and more important. Therefore, in high-frequency bands, although the volume of the waveguide is large, it still has advantages for PCBs. Therefore, in order to reduce the high-frequency loss and reduce the system volume at the same time, the substrate integrated waveguide (SIW) was proposed in 2001 [2]. SIW is a structure manufactured by PCB as shown in Fig. 2.

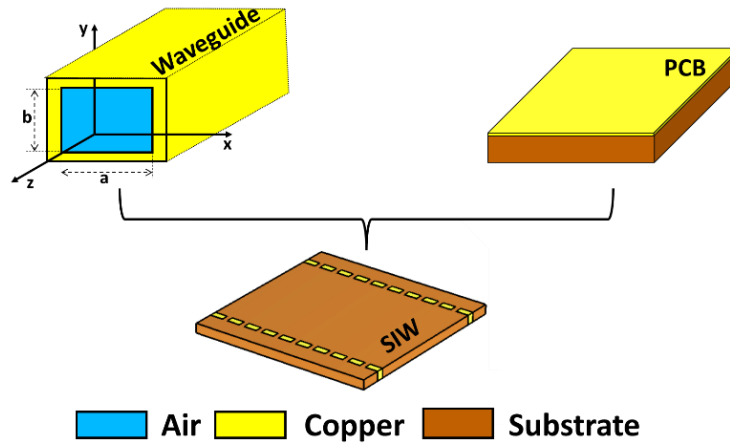
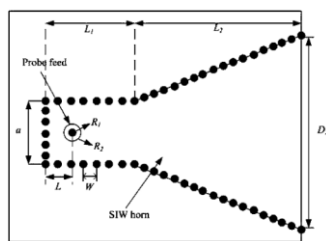


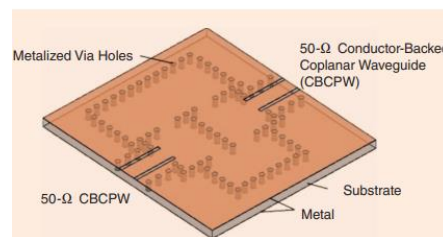
Fig. 2 History of the invention of SIW.

The SIW's waveguide-based structure also makes SIW's components that have low insertion loss, higher power handling capability, enhanced isolation and wider bandwidth.

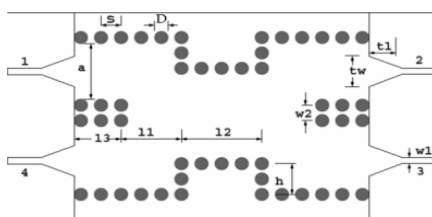
Since then, SIW has been widely used in the design of passive devices such as antenna, filter, coupler and the complex electric circuits as VCO (Voltage Controlled Oscillator), sensor as shown in Fig. 3. However, the medium between the two rows of vias still makes the loss of the SIW greater than that of the waveguide.



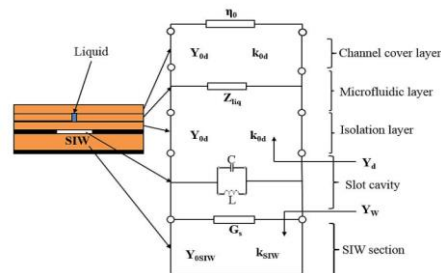
(a) H - Plane Horn Antennas [3].



(b) Fourth-order cross-coupled SIW filter[4].



(c) Coupler [5].



(d) Sensor [6].

Fig. 3 SIW's applications.

In order to further improve the performance of SIW, especially to reduce the insertion loss and power handling, in 2014, Air-Filled SIW (AFSIW) was proposed. Compared with SIW, AFSIW is characterized by an air cavity between the two rows of vias. This structure has been proven to reduce the insertion loss and improve power handling capabilities in [7] as shown in Fig. 4.

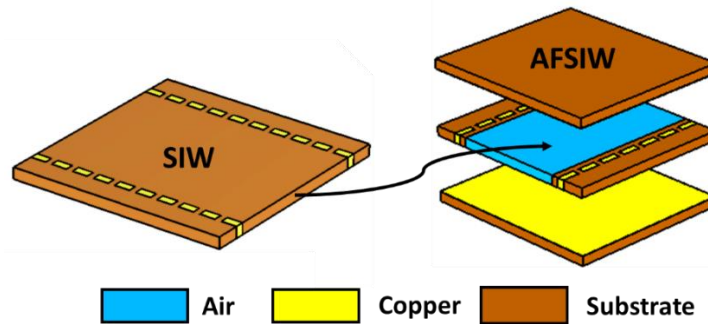
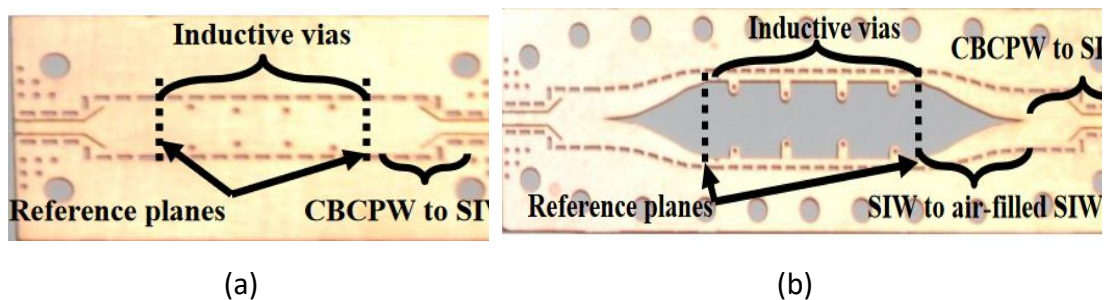


Fig. 4 Evolution from SIW to AFSIW.

Since AFSIW was proposed, many devices realized by SIW have been optimized on AFSIW such as filters on SIW and AFSIW compared in [8] as shown in Fig. 5.a and Fig. 5.b. This literature proved that proposed filter on AFSIW had a lower insertion loss and higher Q-factor than SIW counterpart. The comparison listed in this literature is shown in Fig. 5.c.



COMPARISON OF THE TWO FILTERS IN BOTH TECHNOLOGIES

	Dimensions $W*L$ (mm)	IL (dB)	Bandwidth (%)	Center frequency (GHz)	Q Factor (Sim./Meas/ @ $f_0$ )
<i>Air-filled</i>	7.04*16.64	0.18±0.17	15.04	31.65	908/706
<i>Dielectric-filled</i>	4.099*9.73	0.56±0.24	15.8	31.83	269/157

(c)

Fig. 5 (a) SIW filter, (b) AFSIW filter and (c) performance comparisons.

Currently, there are some antenna systems proposed in SIW technology [9] to minimize the size of the system. Therefore, in order to further improve system performance, the antenna system can be designed using AFSIW technology.

Current systems based on SIW/AFSIW technology are limited to a horizontal layout, which means that all components are on the same plane. This design solution is limited if the allocated space is not sufficient for all components to be on the same plane.

In this context, the thesis provides a possibility to organize a system such as a transceiver (transmitter and receiver) in the vertical plane. The main purpose of this Ph.D. thesis is to provide more possibilities for the placement and connection of components so as to efficiently use the three-dimensional space of a satellite. For the demonstration, a part of the transceiver of an antenna system consisting of an antenna, a filter and a LNA is developed using the AFSIW technology. In order to reflect the advantages of AFSIW in the high frequency band, the system designed in this thesis works in the Ka frequency band.

In order to achieve this objective, first of all, in chapter 1, the AFSIW technology and the structure of a transceiver are presented. This chapter presents the structure of AFSIW and its advantages compared to other technologies in one part and introduces the important influence of satellites in human life, and clarifies the components required for an antenna system in satellites in another part. In a transceiver of an antenna system, there are active devices based on microstrip line power supply and there are also passive devices based on AFSIW structure. Therefore, a transition from microstrip line for active devices to AFSIW for passive devices is particularly important.

The transition between the AFSIW structure and the microstrip lines in the vertical plane was designed and fabricated in chapter 2. This transition can transfer signals from one layer to another. This transition structure that transmits signals on different planes is an important design to form the transceiver circuit in this thesis on the vertical plane.

In this thesis, this transition structure has three main functions:

The first function is to connect components based on different technologies (AFSIW technology and microstrip technology). Therefore, in chapter 3, two antenna structures are proposed in response to different requirements (because the proposed transition has two different ports: AFSIW port and microstrip line port), one is the antenna fed by the AFSIW structure, and the other is the antenna fed by the microstrip. The second function is to provide measurement ports for AFSIW based structures. Since the current measuring instruments are usually based on the coaxial cable interface, the transition from AFSIW to microstrip is required, and then the coaxial connector is used to realize the measurement.

The third function is to design the passive device in vertical structure. In chapter 4, using the same transition structure, a third-order passband filter was proposed in this thesis. The cavities of this third-order filter are on 3 different substrate layers for demonstration.

From chapters 2 to 4, at the beginning an overview is given to have a global view of each component in literature and identify the need. Furthermore, at the end, a conclusion is provided to summarize the procedure of the design or shows the advantages and disadvantages of the device.

In the previous chapters, the components that make up the simplified transceiver: antenna, filter and transition are designed and measured. In chapter 5, the proposed antenna, filter and LNA (Low Noise Amplifier) are integrated to form a system in the vertical plane through the vertical transition. The simulation and measurement results show the possibility of this re-organization in vertical plane.

In the final conclusion, all of the research activities over this thesis are summarized, this chapter also gives some ideas for improvement and some perspectives for the next work.



# CHAPTER 1: STATE OF THE ART

The purpose of this thesis is to build a circuit in a vertical plane for a satellite antenna system in AFSIW. Therefore, in this chapter, first, a short history of satellite development and the structure of its antenna system will be introduced. Secondly, a state of the art of the planar transmission lines technology will be developed in order to bring out the advantages of AFSIW technology.

## 1.1 Satellite communication and antenna system

### 1.1.1 History of satellite communication

Satellite communications are everywhere in our lives. The most historic device in everyone's mind is the 'big dish' on the balcony for satellite television. In addition, they are vital to global communication, such as weather forecast, radio and television broadcasting, military satellites, navigation satellites, global telephone, connecting remote areas, and global mobile communication [10]. Some applications are illustrated in Fig. 1.1 [11].

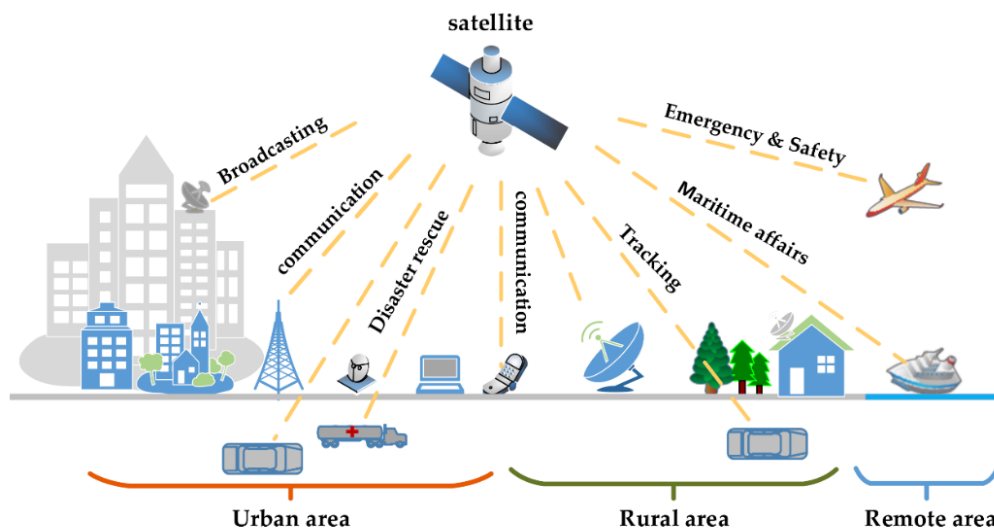


Fig. 1.1 Different applications for satellite communication.

Satellite communication has characteristics that cannot be replaced by other communication methods. The cost of satellite communication doesn't depend on distance so it is extra-suitable for long distance communication. Since each satellite

can cover 42.4% of the earth's surface, and three geosynchronous orbit satellites can cover the whole earth, the satellite is also suitable for large-scale coverage. Satellite communications has a large frequency band and high capacity. Because satellites are in space, their communications are more resistant to natural disasters [11].

The development of satellite communication started in 1945. The first article that marked the beginning of the satellite communication described the spacecraft and space station in geosynchronous orbit, as shown in Fig. 1.2 [12]. After that, the microwave is mainly transmitted between towers, or transmitted by high frequency or short wave reflected by ionosphere. Long-distance transmission began to develop rapidly in the 1960s thanks to the launch of satellites by USSR and USA in the late 1950s. In 1974, the International Telecommunication Union (ITU) proposed a process for the first time to allocate the RF spectrum for satellite communication [13].

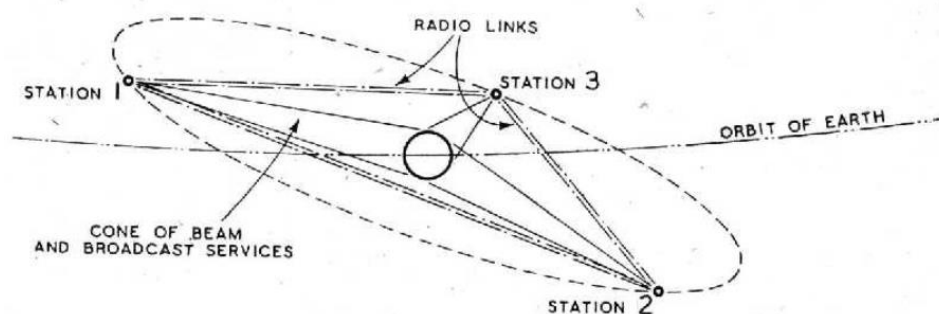


Fig. 1.2 First concept of satellite constellation to coverage of the globe [12].

Satellites can provide different communication services according to different types of orbits. ITU classifies these services into three categories: FSS (Fixed Satellite Service), BSS (Broadcasting Satellite Service) and MSS (Mobile Satellite Service). FSS is a kind of service between satellites and fixed antenna, and it is also the first service supported by satellites. FSS usually provides real-time interactive communication. BSS is used for broadcast and TV transmission. BSS satellites usually have high power. MSS provides service between the satellite and mobile end-user antennas. For example, ships, planes and broadcasting satellite send the signal directly to terminals.

An important criterion for a satellite service is to reach into a defined orbit and maintain itself in its orbit. There are some common different orbits: "Far" Geosynchronous Orbit (GEO), "Near" Low Earth Orbit (LEO) and the so-called Medium Earth Orbit (MEO) between these two orbits. The last one is called high earth orbit (HEO) beyond geosynchronous orbit. The schematic diagram of different orbits is illustrated in Fig. 1.3 [15].

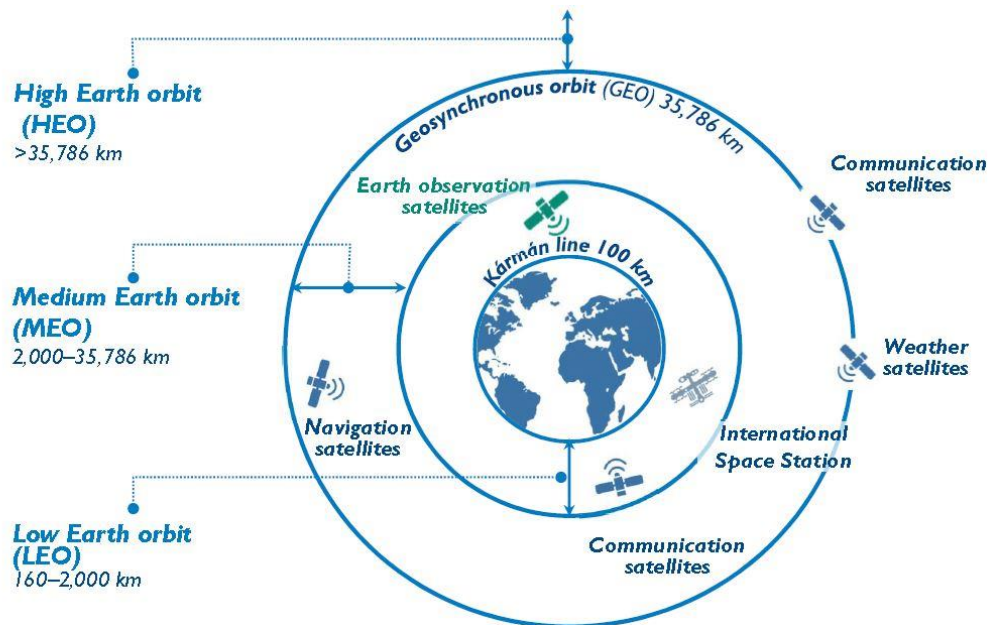


Fig. 1.3 Diagram of different orbits.

Three GEO satellites can cover nearly the whole earth. In addition, the GEO satellite's orbital period is similar to Earth's rotation therefore it is relatively stationary to a certain point on the ground. Given this feature, it is suitable for meteorology to monitor the weather in particular regions or always-on communication services like television, for example. LEO satellite is usually used for scientific research, remote sensing or applications that require fast data transmission. MEO satellite is located between the LEO and GEO, so this type of satellite provides the agreement between transmission rates and coverage. MEO satellites are usually used for navigation, such as the Global Positioning System (GPS) in the USA.

With the increasing number of satellites and the wide application of satellite communications, it is necessary to allocate frequency ranges for satellite

communication. Frequency allocation can provide a constant basis for different areas or applications to minimize interferences [14]. The spectrum is one of the most important treasures. The distributable frequency spectrum is limited, because the orbit's length is limited, and radio communication is applied to all aspects of life. The satellite communication spectrum is shown in Fig. 1.4. The satellite frequency band can be divided in L, S, C, X, Ku, Ka, etc.

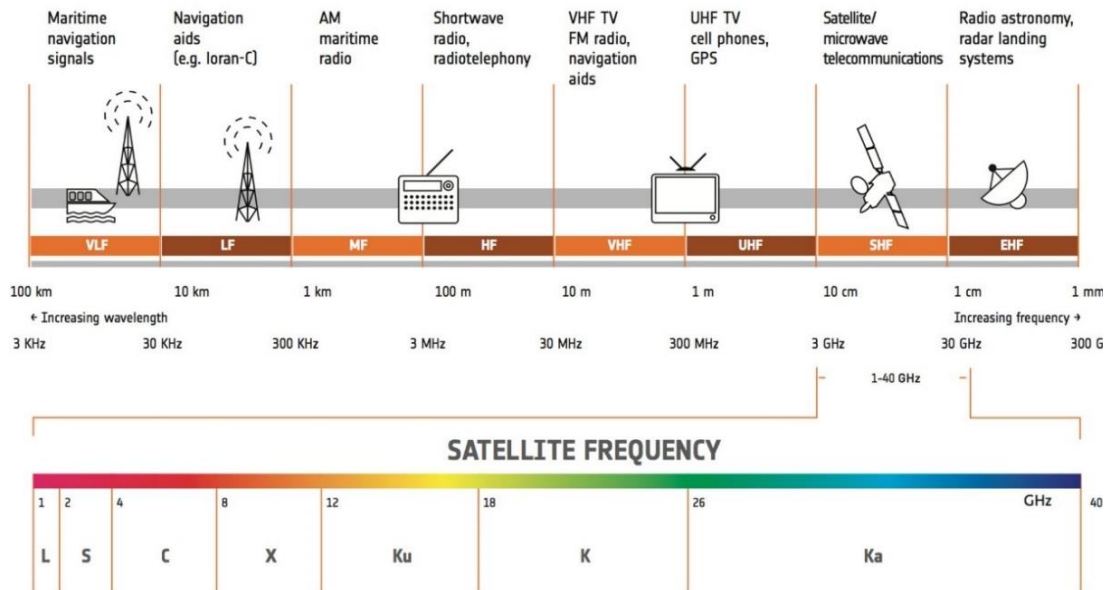


Fig. 1.4 Spectrum of satellite application.

Each frequency band is composed of uplink and downlink. The uplink represents the direction from the terminals to the satellite, while the downlink is the transmission from the satellite to the earth. A schematic diagram of the satellite transmission paths is shown in Fig. 1.5.

This separation of the uplink and downlink can avoid interference between the two communication directions, and at the same time allow two-way communication between the end users or the antenna and satellites. In addition, the characteristics of different frequency bands have different performances in atmospheric attenuation, interface and so on, so it is very useful to choose different frequency bands in different directions. Tab. 1.1 summarizes different frequency bands and their main service and applications.

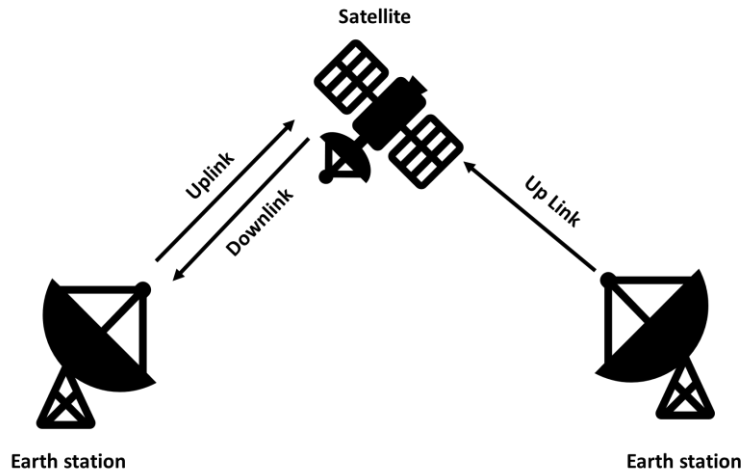


Fig. 1.5 Schematic of the transmission path.

Tab. 1.1 Satellite communication frequency band

Band Spectrum	Frequency Range (GHz)	Satellite Service	Application
L	1 - 2	MSS	GPS; Satellite Mobile Phones
S	2 - 4	MSS	Satellite Tv; Mobile Broadband Services; Radio Broadcasting
C	4 - 8	FSS	Data Services; Full-Time Satellite Tv Networks; Raw Satellite Feeds
X	8 - 12	FSS, MSS	Non-Line-Of-Sight Satellite Communication; Ship Based Satellite Communications
Ku	12 - 18	FSS, BSS	Television, Radio, And Internet Services, Mobile Phone
K	18 - 26	FSS, BSS	Direct Broadcast; Earth Observation; Remote Sensing
Ka	26 - 40	FSS, BSS	Satellite Internet Access; 5th Generation Mobile Networks

*\*Source: The European Space Agency (ESA) and RF Wireless World website*

### 1.1.2 Antenna system

A satellite system consists of two parts: satellite and earth station. The structure of a satellite is complex, and what it carries depends on its applications, but it also has some basic structures as shown in Fig. 1.6: antenna, transponder, housing, command and data handling, guidance and stabilization, thermal control and power supply. The antenna system for the satellite part is mainly a transponder. The schematic of the transponder is shown in Fig. 1.7. The basic structure of the transponder consists of antennas, filters, LNAs, mixers and oscillators.

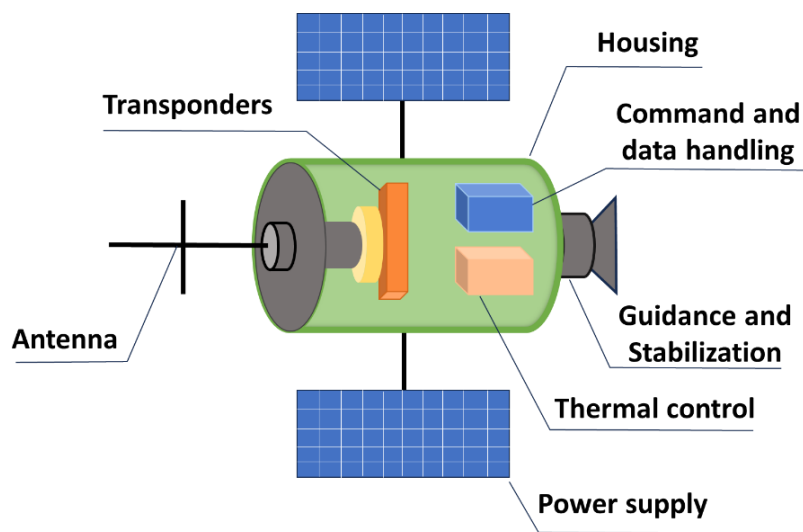


Fig. 1.6 Schematic of satellite architecture.

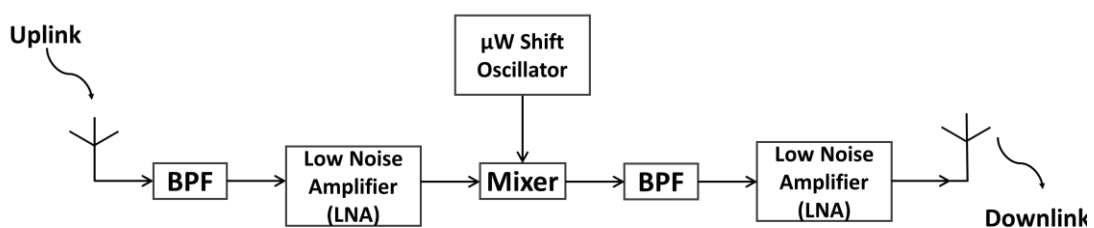


Fig. 1.7 Schematic of transponder.

For the earth station, its type can be divided into long earth station, short earth station, very small aperture (VSAT) earth station and ultra-small aperture terminal (USAT). The corresponding antenna sizes for different earth station types are listed in Tab. 1.2.

Tab. 1.2 Earth station types

Earth Station Types	Long Earth Station	Short Earth Station	Very Small Aperture (VSAT) Earth Station	Ultra-Small Aperture Terminal (USAT)
Antenna Diameter (m)	10 - 60	1 - 10	0.3 – 0.9	< 0.3

The structure of an earth station includes an antenna, and possibly a tracking system, transceiver (transmitter and receiver), multiplexer and modem or codec. The basic structure is shown in Fig. 1.8.

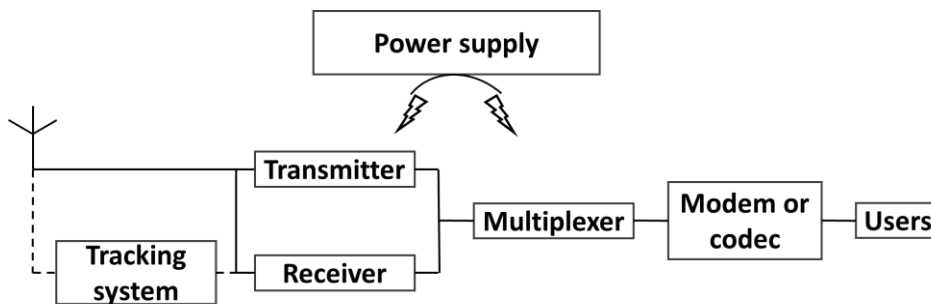


Fig. 1.8 Earth station diagram.

The antenna system of the earth station is mainly the transceiver. The structure of a transceiver is as shown in Fig. 1.9.

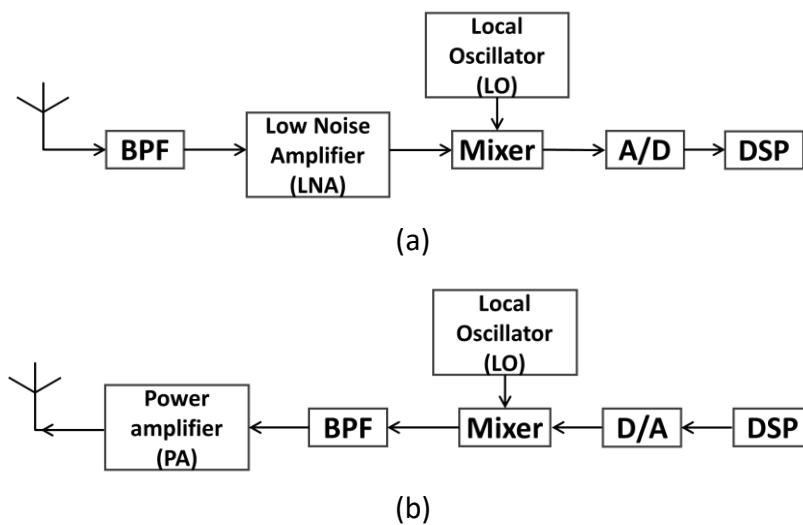
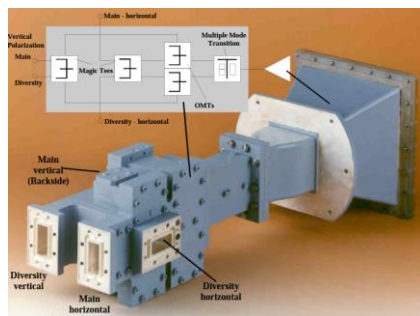


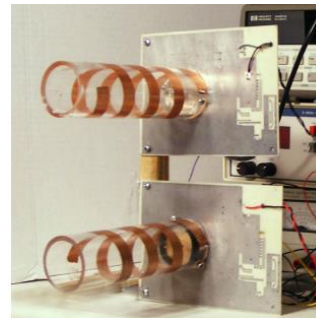
Fig. 1.9 (a) Receiver and (b) transmitter.

The basic components are the bandpass filter, amplifier (low noise amplifier for the receiver and power amplifier for the transmitter), mixer, local oscillator, analogue to digital converter (A/D or digital to analogue converter D/A) and digital signal processor (DSP).

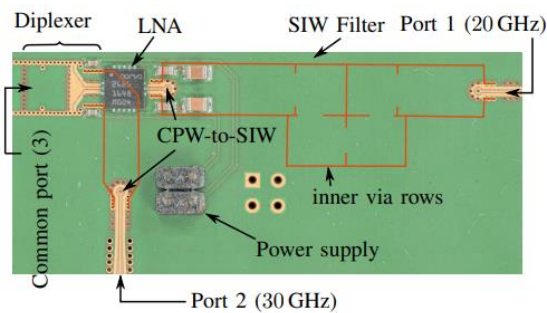
In the implementation of the antenna system, many technologies are adopted, such as waveguide [15] (Fig. 1.10.a), PCB [16] (Fig. 1.10.b), and SIW [9] (Fig. 1.10.c).



(a)[15]



(b)[16]



(c)[9]

Fig. 1.10 Different technologies for antenna system.

The waveguide antenna system is the earliest antenna system technology. It has the advantages of a waveguide, for example, low insertion loss, high power handling and low interference. In satellite communication, the waveguide technology is often used in high frequency operations, but it is inherently big and heavy. Due to its compact size, the antenna system based on PCB is mainly used for small satellites, CubeSats and satellite navigation systems. However, it cannot be used in applications that are exposed to high levels of interference and require high gain. Since SIW technology is waveguide-based technology, passive components (such as filter, antenna) in the

system have lower insertion loss than PCB technology. However, the loss of dielectric makes it have the same shortcomings as PCB technology, such as narrow bandwidth. Therefore, the alternative technology AFSIW is a good candidate for an antenna system. The part of the antenna system in this thesis is designed by AFSIW technology and in the next section, the detail of the AFSIW technology will be presented.

## 1.2 Transmission lines

### 1.2.1 History of transmission lines

Waveguide technology is one of the milestones in the history of microwave engineering at high frequencies thanks to its low loss, auto shield, high power-handling capability etc. In 1897, the first waveguide was proved mathematically [17], but no experimental results were available at that time. In 1936, the first experimental results were presented [18]. Two researchers confirmed the propagation of the electromagnetic wave in the hollow tube waveguide. As one of the earliest transmission line technologies, the utilization of waveguide is still very active. It is not only used as a signal transmission line, but also widely used to form other components, such as filters [19], couplers [20], etc. as shown in Fig. 1.11.

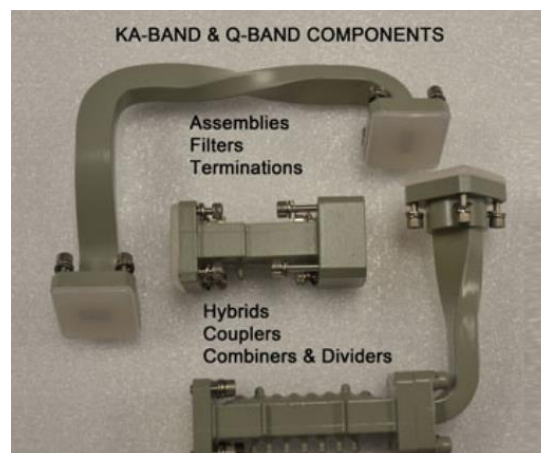


Fig. 1.11 Complete line of Ka-band and Q-band components of Microwave Components and Systems Inc (MCS).

However, a waveguide is bulky, and metal is expensive. At the beginning of the development of radio frequency and microwave systems, instead of the expensive waveguides, the transmission was also realized by double-wire lines and coaxial lines.

Structures of these transmission lines are shown in Fig. 1.12. However, they also have their own shortcomings: two-wire lines cannot be isolated from surrounding component, and coaxial lines are not suitable for complex RF components [21].

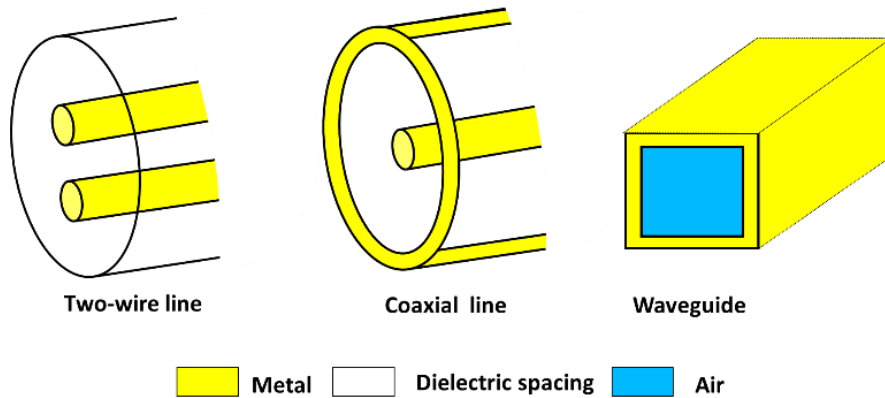


Fig. 1.12 Early transmission line models.

In this condition, planar transmission lines were invented as a compromise technology, because they are low-cost and easy to integrate even though they have a higher insertion loss than the waveguides. Planar transmission lines can be divided into several types: stripline [22], suspended stripline [23], microstrip [24], coplanar waveguide [25], slotline [26] and so on.

The first planar transmission line was proposed for power divider networks in World War II, and then the first stripline analysis was published in 1950 [27]. Next, the microstrip lines were studied, and the report was published in 1952 two years later. Soon, microstrip showed its advantages because it could use thinner substrates. Until now, microstrip lines are widely used in integrated circuits because their fields are quasi-TEM, which is the same as the DC (direct current) solution. However, the stripline or the microstrip line can't supply the circularly polarized magnetic fields and also for some active microstrip components, their ground planes situated on the opposite side pose problems for mounting. The surface-strip transmission lines like coplanar waveguide (CPW) and slotline were proposed for overcoming these disadvantages. The first coplanar waveguide and slotline were reported both in 1969. The characteristics of CPW, such as impedance, phase velocity and attenuation were calculated and the experimental results have also been reported. It was proved that

CPW is suitable for external elements' shunt connections and monolithic integrated circuits. [28]. The same kind of results have been reported for the slotline [29]. In addition, the comparison of the slotline to the microstrip line was realized in terms of characteristic impedance and effective dielectric constant.

Since the development of the microwave integrated circuits (MICs) technology, the planar transmission line has become a world representative with low cost, light weight and easy manufacturing. However, compared with the non-planar waveguide-based technology, the planar transmission line has a higher insertion loss and lower power handling capability owing to its thin dielectric substrate. Moreover, the sensitivity of its manufacturing process has brought more difficulties to the application of higher frequencies. Comparisons of the waveguide and the planar transmission lines are listed in Tab. 1.3 and the illustrations of each planar transmission line are demonstrated in Fig. 1.13. Therefore, for components requiring high power handling capability, low insertion loss, wide bandwidth, waveguides were still the best choice and those devices that didn't have high requirements for the above conditions were realized by planar transmission lines technology especially for the active component. This type of system has both 3D and 2D components and the connections between them often cause problems not only in terms of RF performance but also fabrication complexity. Therefore, it is necessary to find a technology trade between previous technologies, which is why the concept of substrate integrated circuits (SICs) was put forward [30].

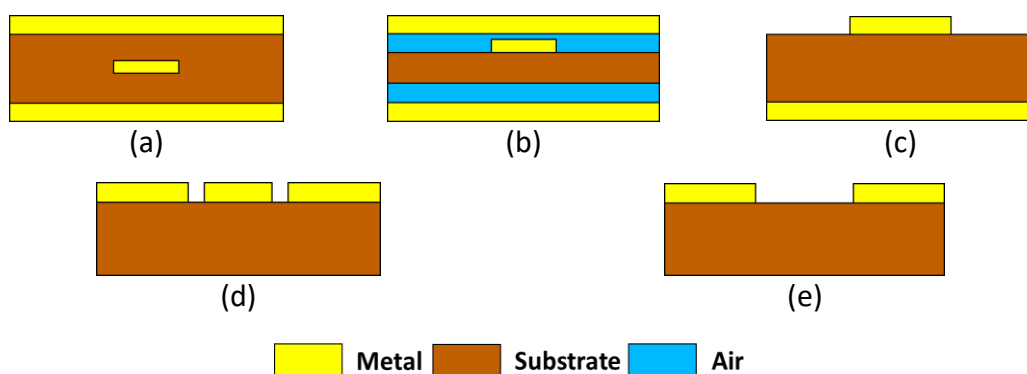


Fig. 1.13 Cross-sectional view of different types of planar transmission line: (a) stripline; (b) suspended stripline; (c) microstrip; (d) coplanar waveguide and (e) slotline.

Tab. 1.3 Performances comparisons of waveguide and planar transmission lines

Transmission line	Metallic waveguide	Stripline or Suspended Stripline	Microstrip	Coplanar Waveguide	Slotline
Structure	3D	Planar			
Fundamental mode	TE, TM	TEM	Quasi-TEM		TE
Size	Larger	Moderate	Compact		
Losses	Low	Moderate			Low
Bandwidth	Large	Moderate	Limited	Moderate	
Power handling	High		Moderate		
Fabrication complexity	Complex	Moderate	Simple		

### 1.2.2 Air-filled substrate integrated waveguide

The main concept of SICs is to create a waveguide by synthesizing a non-planar structure with a dielectric substrate and converting it into a planar form to be compatible with other planar structures [31]. SICs include (listed in proposition's chronological order): SIW (shown in Fig. 1.14.a)[2]; SISW (Integrated Slab Waveguide, shown in Fig. 1.14.b) [32], SINRD (Substrate Integrated Non-Radiating Dielectric guide shown in Fig. 1.14.c) [33], SIIDG (Substrate Integrated Image Dielectric Guide shown in Fig. 1.14.d) [34], RSIW (Ridge Substrate Integrated Waveguide shown in Fig. 1.14.e) [35], SW-SIW (Slow-Wave Substrate Integrated Waveguide shown in Fig. 1.14.f) [36] and etc. Among the various structures of SICs, SIW is the most popular technology thanks to its easy fabrication. SIW was invented in 2001 [2]. As seen in the Fig. 1.14.a, the SIW consists of two rows of metal holes which imitate the waveguide and provide the necessary shielding. The electromagnetic wave propagates mainly in the middle of the substrate. Therefore, in the high frequency band, SIW has a more significant dielectric loss and a lower power handling capacity [37]. So, for several applications, these disadvantages have limited the utilization of SIW technology.

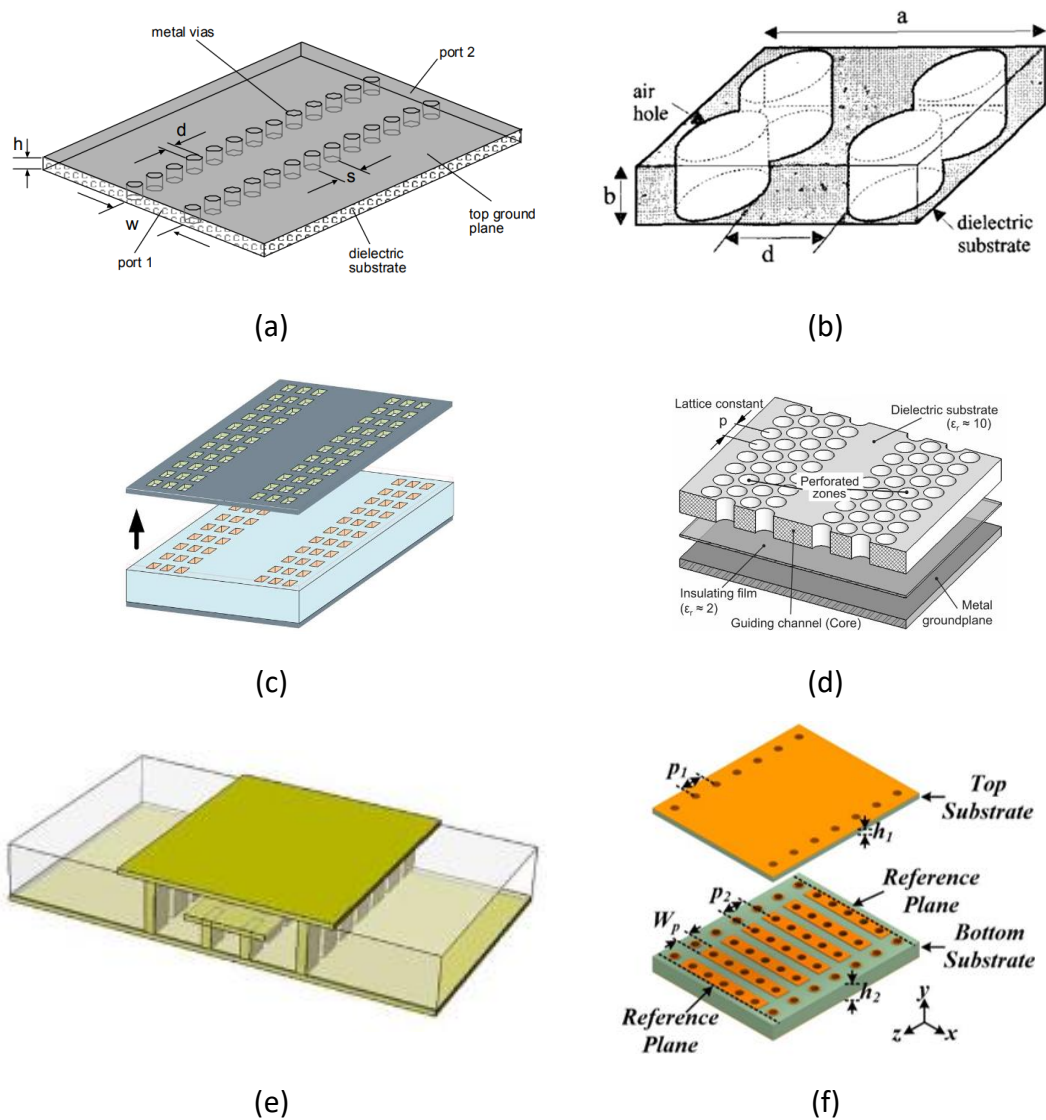


Fig. 1.14 Pictures of (a) SIW; (b) SISW; (c) SINRD; (d) SIIDG; (e) RSIW; (f) SW-SIW.

To overcome the disadvantages such as high dielectric loss and poor power handling capability, the first concept of the AFSIW (Air-Filled Substrate Integrated Waveguide) technology was proposed in [38]. As shown in Fig. 1.15, this structure is realized in multilayer PCB technology. In order to reduce the dielectric loss, the substrate in the middle is removed. The top and bottom layers support the conducting boundaries for the air cavity in the middle substrate. Therefore, this type of structure needs a three-layer PCB fabrication process. In this paper [38], the analysis of the attenuation constant and cut-off frequency was reported.

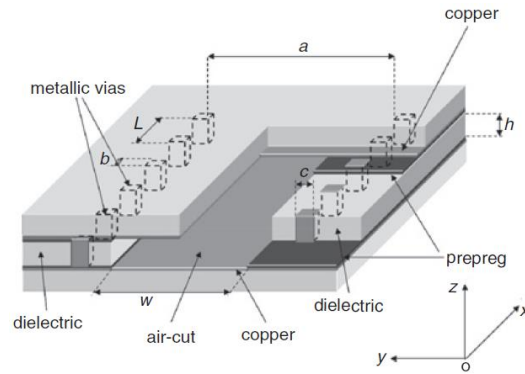
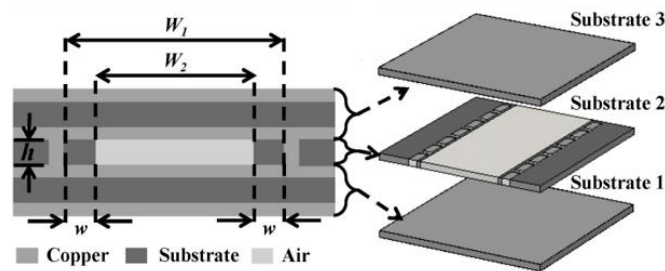
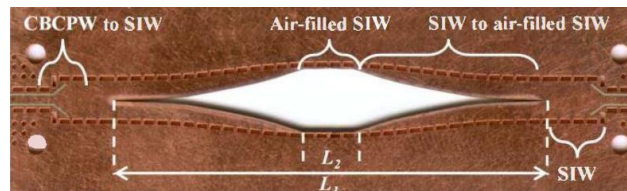


Fig. 1.15 The first concept of AFSIW.

In order to further study the performance of the AFSIW technology, in [7], the structure of the Fig. 1.16.a was proposed and analyzed.



(a)



(b)

Fig. 1.16 Pictures of the (a) structure of AFSIW and (b) fabrication.

This structure is utilized for this thesis. This structure is also based on a three-layer PCB fabrication process. The air cut is on the substrate. The conducting boundaries are ensured by the copper layers of substrate 1 and 3 and two rows of metallic vias on the substrate 2.

The cutoff frequencies can be calculated approximately by (1.2.1), if the two dielectric slabs (marked with  $w$  in Fig. 1.16.a) are negligible. The condition negligible means that

the E-field of the mode TE<sub>10</sub> is not important near to the dielectric slabs. If not, the cutoff frequency with the dimensions of the slabs can be calculated by (1.2.2).

$$f_{c_{mn}} = \frac{c}{2\pi\sqrt{\epsilon_r}} \sqrt{\left(\frac{m\pi}{W}\right)^2 + \left(\frac{n\pi}{h}\right)^2} \quad (1.2.1)$$

$$\tan\left(\frac{\sqrt{\epsilon_r} * (W_1 - W_2) * \pi * f_{c_{1,0}}}{c}\right) = \sqrt{\epsilon_r} * \cot\left(\frac{W_2 * \pi f_{c_{1,0}}}{c}\right) \quad (1.2.2)$$

The analysis of the total transmission loss, surface roughness effects, and the cut off frequency were also reported in [7] according to its geometries marked in the Fig. 1.16.a. In addition, comparisons of the SIW and AFSIW in terms of transmission loss (dielectric loss, ohmic loss, surface roughness loss), Q-factor, power-handling capability (average power handling capability and peak power-handling capability) and the width of the structure are presented in Tab. 1.4.

Tab. 1.4 Performances comparisons of between waveguide-based technologies

Technology	Metallic waveguide	Planar transmission line	SIW	AFSIW	
Transmission loss	Low	High	Moderate	<b>Low</b>	
Power handling	High	Low		Moderate	<b>High</b>
Q-factor					<b>High</b>
Size	Bulky	Compact	Compact	<b>Large</b>	
Fabrication complexity	High	Low	Low	<b>Moderate</b>	

Based on these comparisons, it can be noted that AFSIW has better results than SIW in terms of Q-factor, transmission loss and average power handling capability. For a fixed cutoff frequency ( $f_{c_{mn}}$ ) and substrate thickness  $h$ , the smaller  $\epsilon_r$ , the wider the width  $W$  of the structure according to equation (1.2.1). Therefore, the footprint of AFSIW is bigger than that of SIW. This is not entirely a disadvantage. From the point of view of system integration, this is a disadvantage, but from the point of view of

manufacturing, the larger volume makes manufacturing more fault-tolerant. Comparisons between different waveguide-based technologies including metallic waveguide, planar transmission line, SIW and AFSIW are summarized in Tab. 1.4. Comparisons show that in the case of ensuring planar structure and low manufacturing complexity, AFSIW technology has lower transmission loss, higher power handling and Q-factor and no dramatic increase in size.

Since then, the performance analysis of AFSIW has gradually improved and with its advantages, a lot of components of radiofrequency has been designed based on AFSIW technology such as antenna [39], filter [40], coupler [41], power divider [42], phase shifter [43] and transition [7]. These different components are shown in Fig. 1.17.

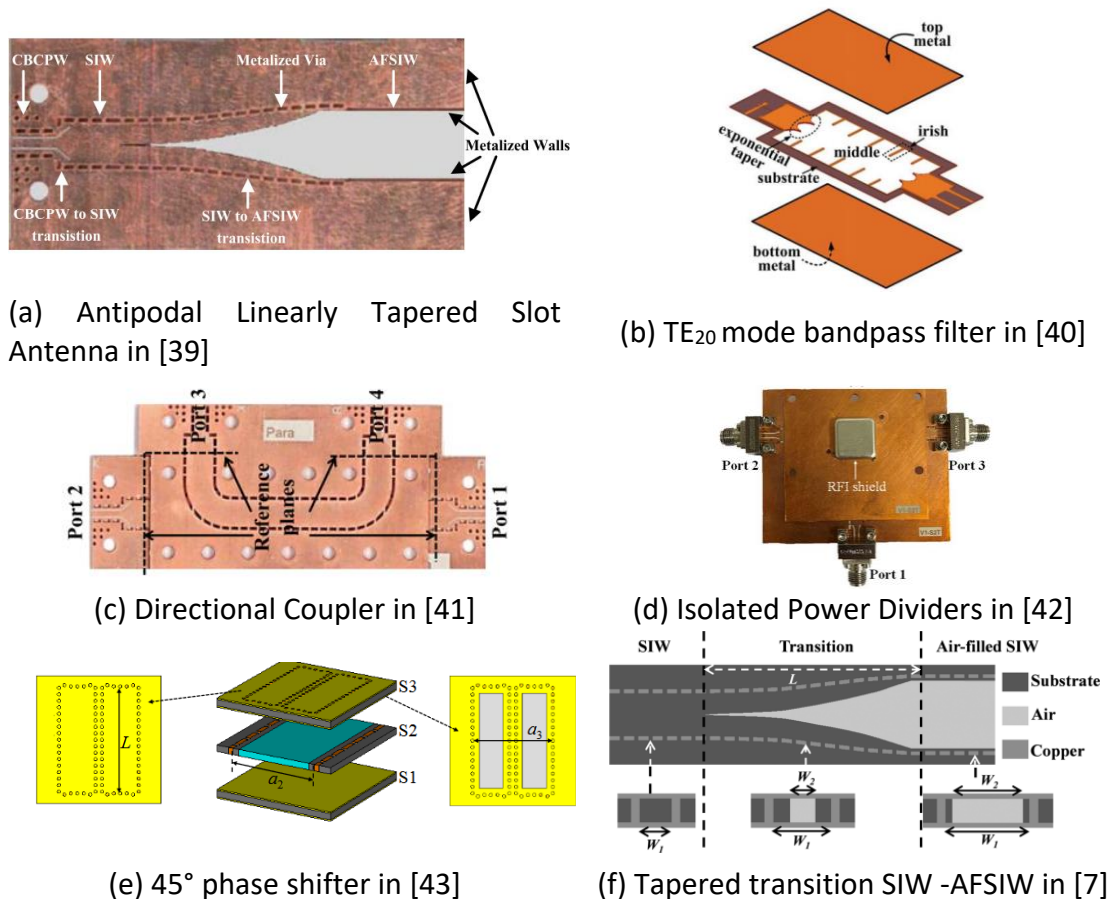


Fig. 1.17 Different components based on AFSIW technology.

AFSIW technology has its own advantages in various types of components. Taking the antenna as an example, the waveguide structure and cavity of AFSIW enable the antenna of AFSIW to have good radiation efficiency and bandwidth. Combining its

performance and multi-layer structure advantages, this thesis will design the part of the transceiver in AFSIW technology.

### **1.3 Conclusion**

In this chapter, overviews of satellite communication and the AFSIW technology were presented. The history of satellite communication has been detailed chronologically with different types of satellite orbits. In order to make full use of orbital space and frequencies, satellite communications are divided into frequency bands. Band frequencies and applications are shown in Tab. 1.1. The simple model of a satellite, the satellite antenna system and the earth station antenna system are introduced. The common structure of the satellite and earth station antenna system is the transceiver. Therefore, in this thesis, researches are based on the design of the simplified transceiver which consists of an antenna, a filter, a LNA and transitions between each other, due to the limit of the time. Different technologies including waveguide, PCB, SIW are applied for antenna systems. After analyzing the advantages and disadvantages of each technology, AFSIW technology is proposed as a combination of waveguide and PCB technology and a derivative version of SIW technology. Comparisons between different transmission lines in terms of transmission loss, power handling, Q-factor, size and fabrication complexity are shown in Tab. 1.4. Based on the study of the state of the art on AFSIW, it can be seen that AFSIW technology can have a significant use in satellite antenna communication systems with its low insertion loss and high-power handling capability. Therefore, the simplified transceiver in this thesis will be designed using AFSIW technology.



## CHAPTER 2: TRANSITION AFSIW - MSL

To design a circuit in a vertical plane, a simplified transceiver is used as an example in this thesis. The essential point to realize vertical plane stacking of components is to design a transition that can couple signals between different layers. In most designs, the transition from waveguide to active devices based on PCB technology is a difficult part, which increases the length of the circuit. In this chapter, a transition between the AFSIW technology and the microstrip line is designed, fabricated and experimentally measured. The design is optimized using the CST Studio Suite 2020 software. The transition organizes the system on vertical plane in order to decrease the length of the circuit.

### 2.1 Overview

Modern technology allows the integration of planar elements and three-dimensional elements in the multi-layer space. This is of great significance for optimizing the radio frequency performances or size of electronic systems [44]–[47]. For some systems, the transmission lines and the components in 2-D or 3-D are adapted to minimize insertion losses, reflection losses, etc. In addition, some of the transitions can limit the DC (direct current) coupling, filter the signals [48], etc.

The transitions can be divided into 2 types [49]: in-line transitions and E-plane transitions (E-plane correspond to the plane which is parallel to the E-field in rectangular waveguides for the fundamental mode [50] as shown in Fig. 2.1).

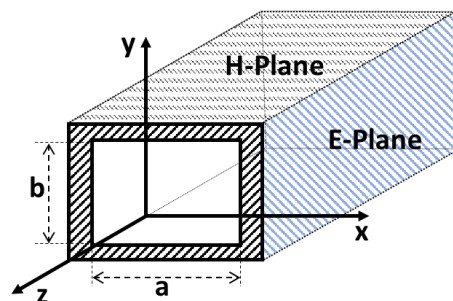


Fig. 2.1 E-Plane and H-Plane for a rectangular waveguide where  $a > b$ .

For in-line type transitions, the direction of field propagation in the waveguide and the microstrip line is the same. These transitions can achieve impedance matching by stepped ridged waveguides [51], [52], fin-line arrays [53], different types of probes such as radial probes [54] and coaxial probes [55] as shown in Fig. 2.2.

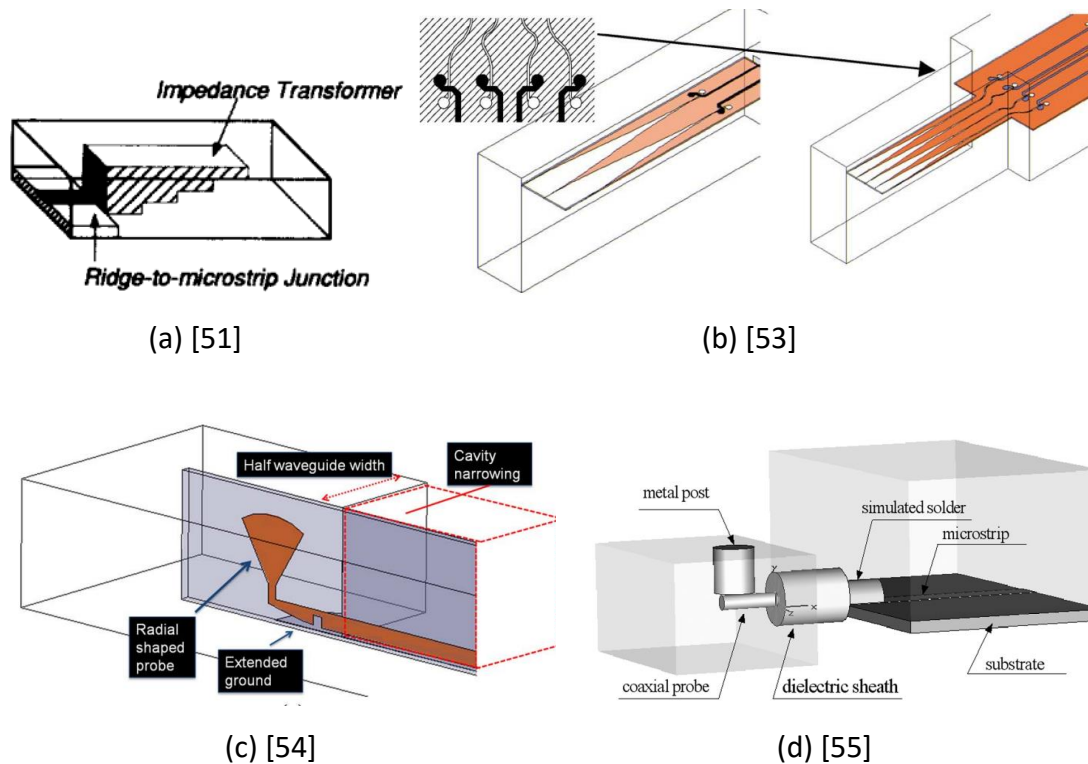


Fig. 2.2 Some in-line transitions between the waveguide and the microstrip line by: (a) stepped ridged waveguides [51]; (b) fin-line arrays [53]; (c) radial probes [54] and (d) coaxial probes [55].

For the second type of transitions called E-plane transitions, refer to as vertical transitions. There are two main methods [56]: probe feeding [57], [58] and slot coupling [59], [60] as shown in Fig. 2.3. Probe feeding transitions compared to other types show the best performances in terms of insertion and reflection losses. However, this type manufacture is very complicated, especially for high frequency, where a metal post is tiny and sensitive to fabricate. The slot coupling type transition can simplify fabrication through micromachining but it has poor return loss and radiation from the coupling slots [61].

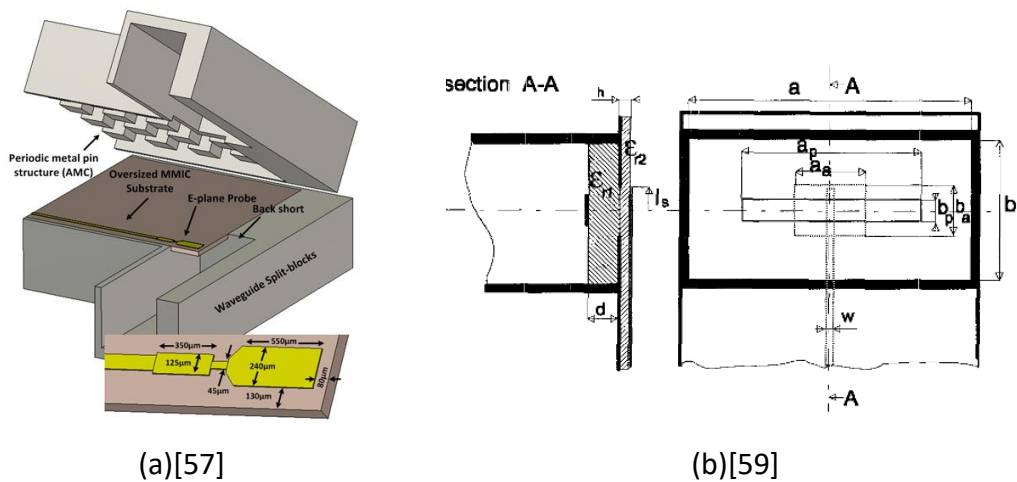


Fig. 2.3 Some E-Plane transitions between the waveguide and the microstrip line by: (a) probe feeding [57] and (b) slot coupling [59].

Since the SIW technology was put forward, people have invented many transitions for reference. The first in-line transition between SIW and microstrip lines was proposed in 2005 [62]. The transition has been realized by via-holes on the substrate (shown in Fig. 2.4). These two via-holes connect the ground of the microstrip and the part of the waveguide where its electric field reaches the maximum.

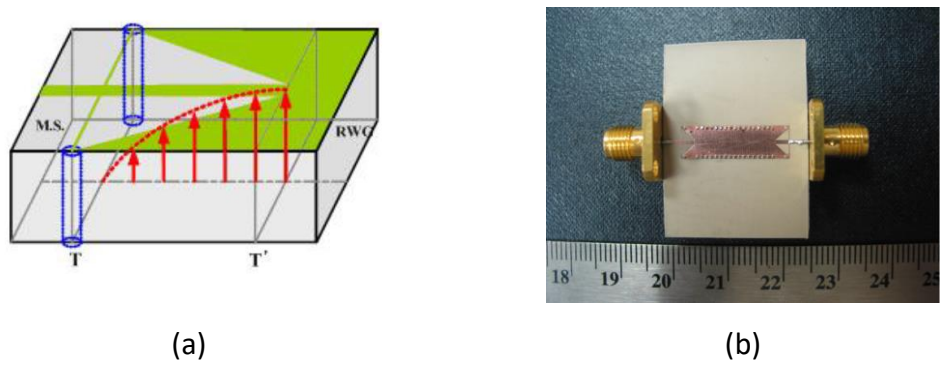


Fig. 2.4 SIW-Microstrip transition structure [62] in (a) simulation and (b) fabrication.

Then the first transition in a multilayer structure was proposed to reduce the radiation loss due to the thin substrate [63] (shown in Fig. 2.5). The principle of this transition is based on the similarity of the distribution of electric field lines in the ridged waveguide and the microstrip.

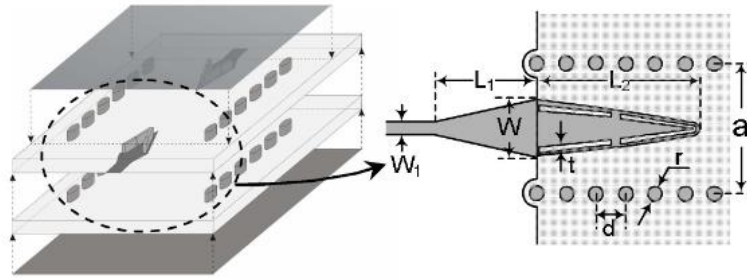


Fig. 2.5 SIW-Microstrip transition multilayer structure [63].

This tapered transition provides the inspiration for the transition of AFSIW to microstrip because the structure of AFSIW is also based on a multilayer structure like the transition between empty substrate integrated waveguide and microstrip presented in [64] as shown in Fig. 2.6.a. Then, it was proposed to add taper and through hole in the microstrip line to improve reflection loss and avoid power leakage [65] as shown in Fig. 2.6.b.

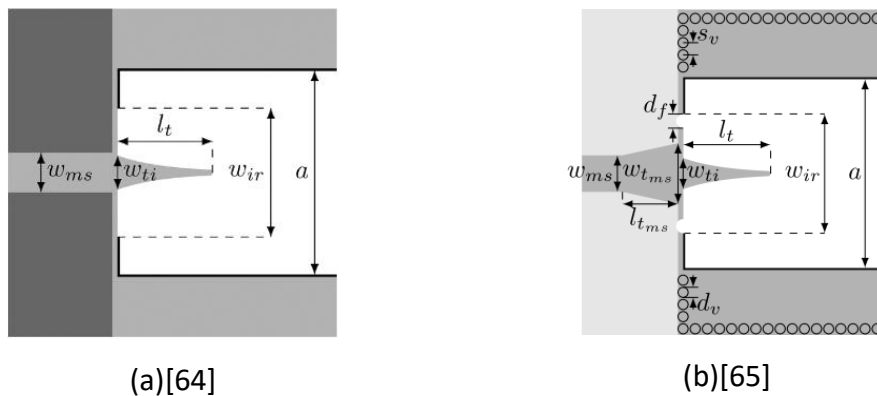


Fig. 2.6 Some ESIW-Microstrip transitions structure: (a) original transition [64] and (b) improved version [65].

But all these previous transitions are designed in the same plane, that is to say, the structure of the microstrip is on the same layer as the structure of SIW or ESIW. This leads to a longer length of the entire assembly. Therefore, the multi-layer structure of AFSIW can be used to solve this problem. The upper or lower substrate of the AFSIW for supporting a copper layer can be shared with the substrate of the microstrip to realize the vertical transition.

The vertical transition of SIW or AFSIW to microstrip can be realized in two methods like the waveguide transitions: one is with a probe, and the other is with a slot.

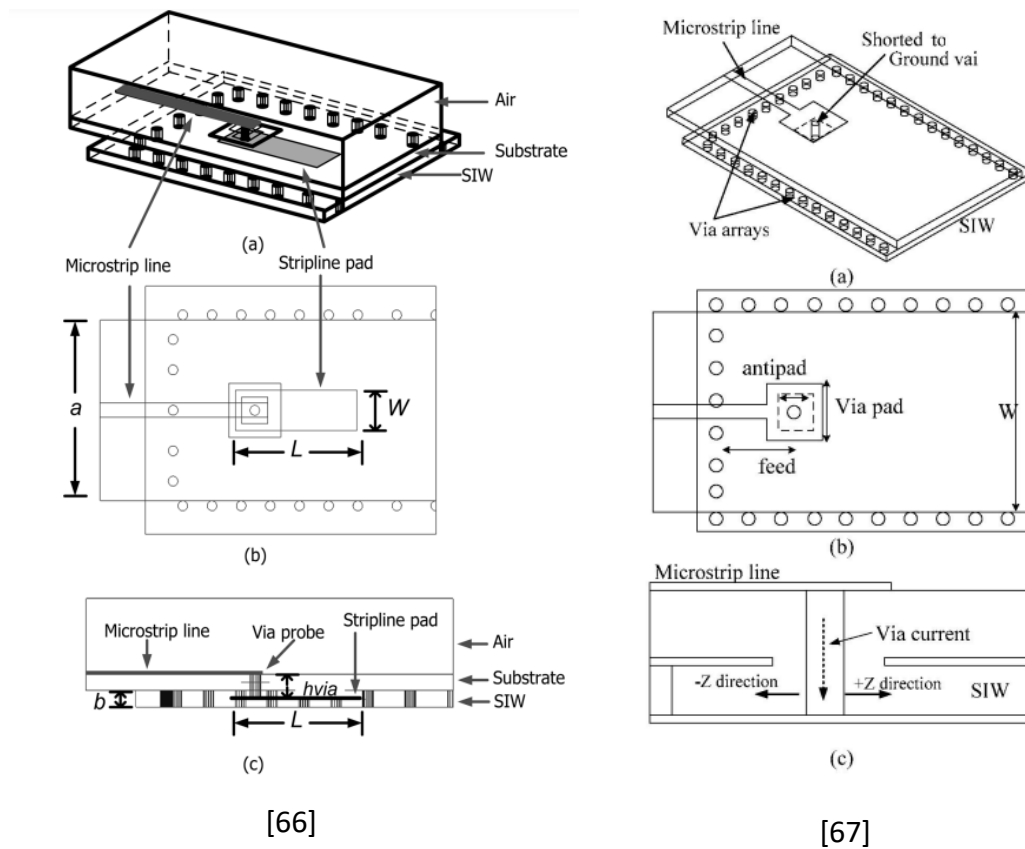


Fig. 2.7 The structure of the transition SIW to microstrip with probe [66], [67]: (a) 3-D view, (b) top view, and (c) side view.

The first vertical transition of SIW to microstrip with a probe was invented in 2005 in technology LTCC (Low Temperature Co-fire Ceramic) [66]. The coupling is realized with a probe and tuned with a stripline pad inside the substrate of SIW. However, the insertion position and depth of the probe and the relative position of the stripline increase the difficulty of manufacturing. So in [67], shorted-via between microstrip line and bottom of waveguide is used to excite  $TE_{10}$  mode in waveguide. The probe is connected from the upper wall to the lower wall of the waveguide, so it is relatively stable. The configuration of via pad and antipad realize the adaptation as shown in Fig. 2.7. On the same principle, this design refers to the ESIW technology [68] as shown in Fig. 2.8.

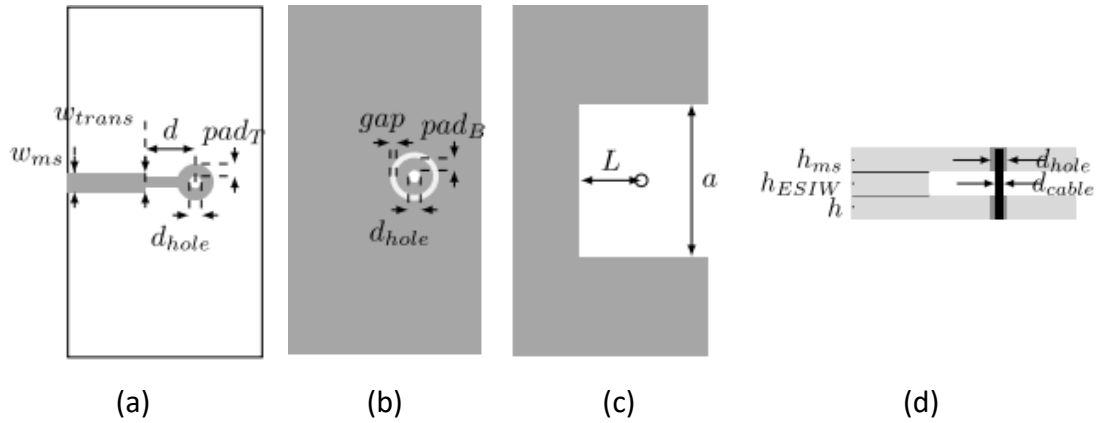


Fig. 2.8 Structure of the microstrip to ESIW version transition [68]: (a) Upper layer top; (b) Upper layer bottom; (c) Middle layer; (d) Transverse section.

In 2010, the vertical transition between SIW and microstrip with slot was first proposed [69]. The slot is opened as close as possible to the end of the SIW to transmit the maximum power, also the length and shape of the slot can indirectly change the input conductance as shown in Fig. 2.9.

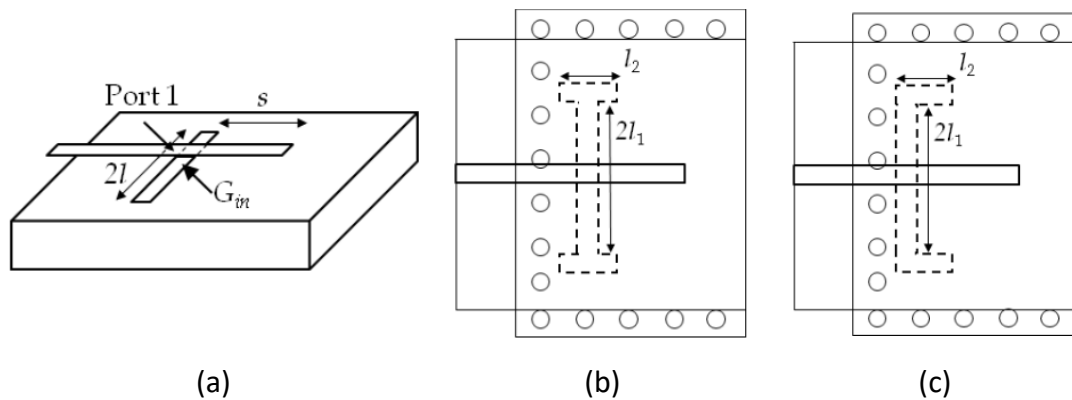


Fig. 2.9 The structure of the transition SIW to microstrip [69] with (a) slot; (b) H-shape slot and (c) U-shape slot.

However, the impedance between the microstrip substrate and the air cavity of the AFSIW is quite different due to the differences in the dielectric permittivity of the substrate and the air. It is generally difficult to achieve impedance matching for a single slot. In [70], the transition between AFSIW and microstrip with slot realized by printed circuit board (PCB) technology was proposed for the first time [70] as shown in Fig. 2.10. The signal is coupled through the slot and the impedance matching is

realized by a dielectric step in the air cavity and two vias in the substrate of the microstrip.

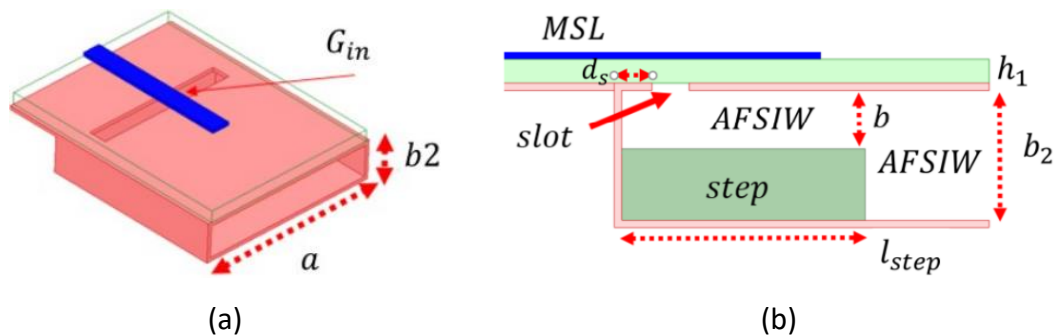


Fig. 2.10 The structure of the transition between AFSIW and microstrip with slot [70]: (a) 3-D view and (b) side view.

According to the state of the art, the two coupling methods, probes and slots, have their own advantages and disadvantages. For the method of coupling with a probe, the dielectric loss is relatively low, but it is difficult to manufacture. On the contrary, for the method of coupling with slot, the manufacturing based on PCB technology is relatively simple, but other settings are required to achieve impedance matching and it also increases the dielectric loss, because of the dielectric step and vias [70].

In the study of the state of the art, the slot coupling is easier to fabricate and takes full advantage of the multilayer substrate structure of AFSIW and the copper surface, associated to each substrate, to achieve coupling and impedance matching without adding any equipment.

Due to its easier manufacturing, the slot coupling method for the transition between AFSIW and microstrip is selected for the design of the transition. Its study is developed in the next subsection. The innovation for this transition consists of a thin substrate which is inserted between the AFSIW structure and the microstrip structure to achieve impedance matching.

## 2.2 Transition design

The design of the transition is divided into three parts (shown in Fig. 2.11): the microstrip line (MSL), the air-filled substrate integrated waveguide (AFSIW), the

coupling structure design and impedance adaptation between the two structures. The transition is designed on the substrate Rogers RT6002 which has a dielectric constant of  $2.94 \pm 0.04$ .

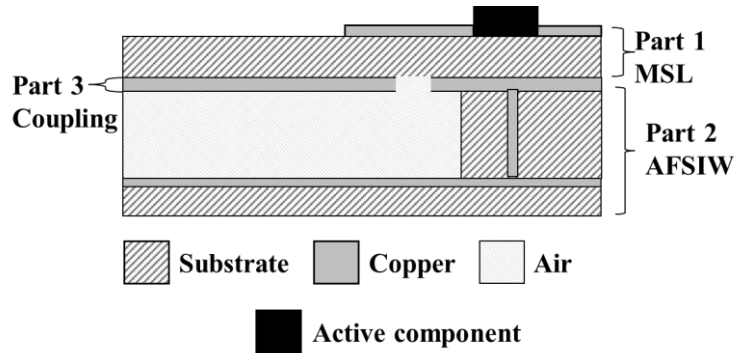


Fig. 2.11 Schematic diagram of transition.

### 2.2.1 Microstrip

Firstly, the geometry of microstrip line has to be computed. The basic structure of the microstrip is shown in the Fig. 2.12. A copper line of width  $W$  is printed on the thin dielectric substrate of thickness  $H$  with a ground on the bottom.

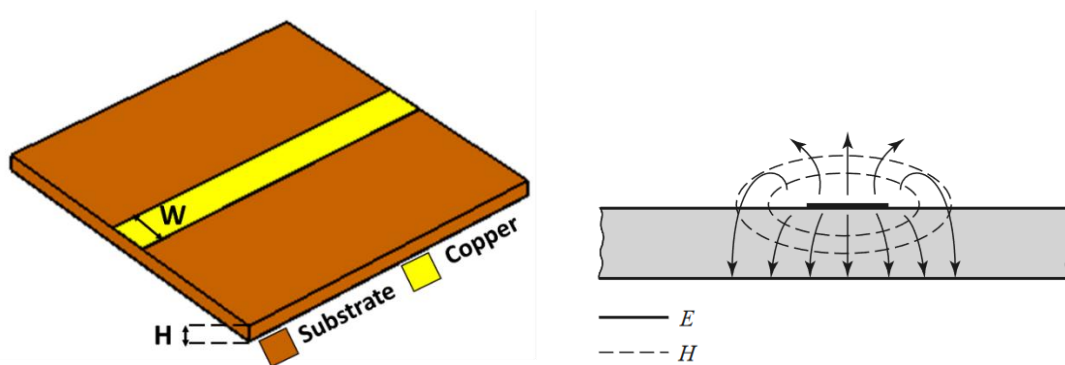


Fig. 2.12 Basic structure of microstrip: (a) geometry; (b) electric and magnetic field lines.

In this proposed microstrip line, the substrate is designed with Rogers RT6002 ( $\epsilon_r = 2.94$ ,  $\tan\delta = 0.0012$ ) of 0.508 mm thickness. The propagation mode in the microstrip structure is quasi-TEM [71]. The width of the line of copper can be calculated as follows [72]:

$$\epsilon_e = \frac{\epsilon_r + 1}{2} + \frac{\epsilon_r - 1}{2} \left( 1 + 12 \left( \frac{H}{W} \right) \right)^{-\frac{1}{2}} \quad (2.2.1)$$

$$Z_0 = \frac{120\pi}{\sqrt{\epsilon_e} \times \left[ \frac{W}{H} + 1.393 + \frac{2}{3} \ln \left( \frac{W}{H} + 1.444 \right) \right]} \Omega \quad (2.2.2)$$

where H is the thickness of the substrate,  $\epsilon_r$  is the relative permittivity and  $Z_0$  is the characteristic impedance.

In order to reach 50 ohms at 28 GHz for the characteristic impedance, the final line width W is determined to be 1.24 mm (instead of 1.3 mm in theory calculated by equations (2.2.1) and (2.2.2)) by optimization (see in Fig. 2.13).

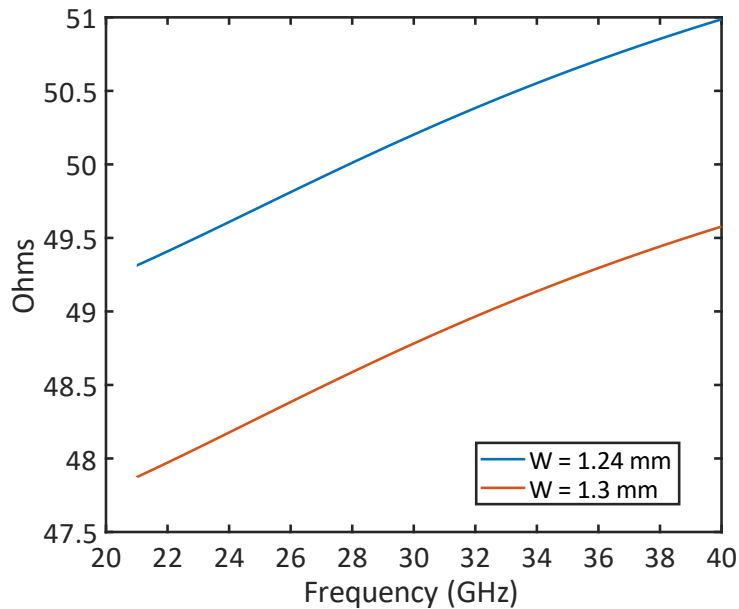


Fig. 2.13 Simulated results for determining microstrip line width.

## 2.2.2 AFSIW geometry

Secondly, the geometry of AFSIW will be computed in this subsection. The basic structure of AFSIW based on multilayer PCB process is shown in Fig. 2.14.a. The AFSIW structure consists of three layers of substrate.

The medium layer, the substrate 2, as shown in Fig. 2.14.b, is filled with air. The two layers, substrate 1 and substrate 3, support the copper layers. The waveguide is closed by vias on both sides and the copper layers to ensure the conductive boundaries.

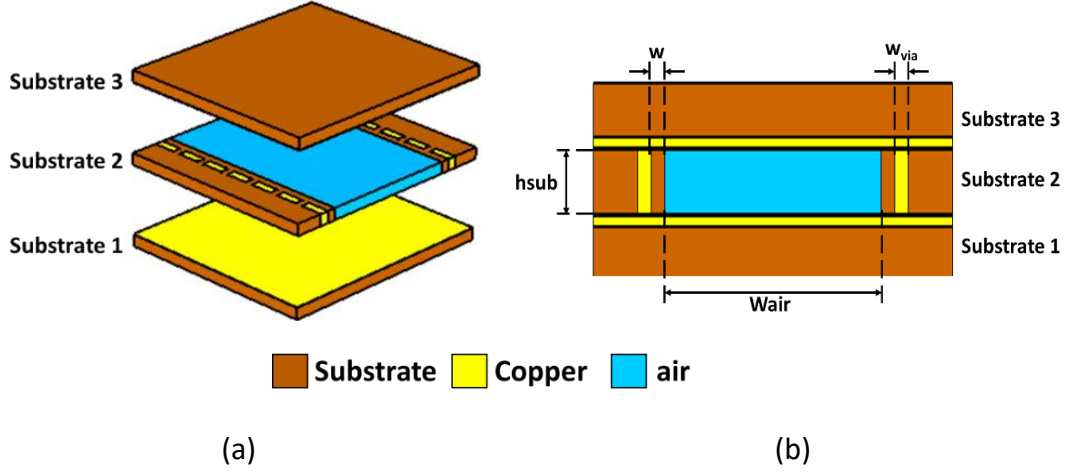


Fig. 2.14 Air-filled SIW (a)3D view and (b) cross sectional view.

The fundamental propagation mode  $TE_{10}$  is considered in this thesis. The cutoff frequencies for  $TE_{10}$  mode for the AFSIW can be calculated approximately by (2.2.3) if two dielectric slabs  $w$  are small enough to ignore. More generally, equation (2.2.4) can be used for any provided slab width  $w$ . The geometry of the AFSIW structure can be determined by equation (2.2.4) [73].

$$f_{c_{m,n}} = \frac{c}{2\pi\sqrt{\epsilon_r}} \sqrt{\left(\frac{\pi m}{W_{air} + 2 * w}\right)^2 + \left(\frac{\pi n}{h_{sub}}\right)^2} \quad (2.2.3)$$

$$\tan\left(\frac{\sqrt{\epsilon_r} * 2w * \pi * f_{c_{1,0}}}{c}\right) = \sqrt{\epsilon_r} * \cot\left(\frac{W_{air} * \pi f_{c_{1,0}}}{c}\right) \quad (2.2.4)$$

For the Ka-band (from 21 GHz to 40 GHz) and considering the limitation of fabrication, the geometry of the waveguide with technology AFSIW is illustrated in Tab. 2.1. The results of the S-parameters and the E-field simulation are illustrated in Fig. 2.15. According to these configurations, the cutoff frequency of mode  $TE_{10}$  is fixed at 21.17 GHz.

Tab. 2.1 Geometry of the waveguide with technology AFSIW

Parameters	hsub	w	Wair	wvia
Dimensions (mm)	0.508	0.508	6.024	0.381

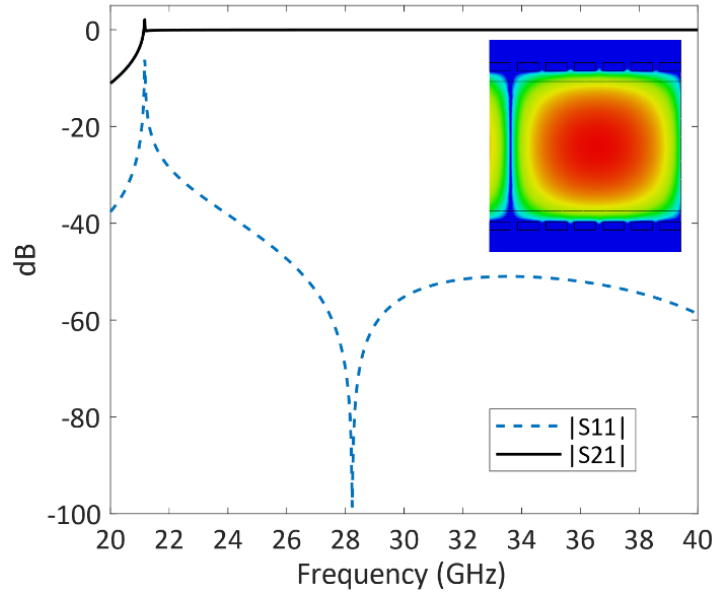


Fig. 2.15 S-parameters and the E-field simulation results.

### 2.2.3 Transition design process

The final step is to connect the structure of microstrip line and AFSIW. The coupling structure and its geometries will be presented and calculated in this subsection.

The overall transition structure is illustrated in Fig. 2.16.a. The proposed transition consists of four layers named from S1 to S4. All of the substrate is RT/Duroid 6002 because this type of substrate has lots of benefits like a low loss for high frequency performance, low out-gassing and good dimensional stability.

Substrate thickness of S1, S2 and S4 is 0.508 mm to improve robustness and that of S3 is 0.254 mm to reduce the dielectric loss.

To obtain the signal transmission between the microstrip and the AFSIW waveguide, the top and bottom views of the coupling structure are shown in Fig. 2.16.b. The slot on the upper copper layer of S3 can couple electric fields of microstrip and AFSIW. The

copper patch (the central copper rectangle) on the lower copper layer of S3 completes the slot to reach impedance matching.

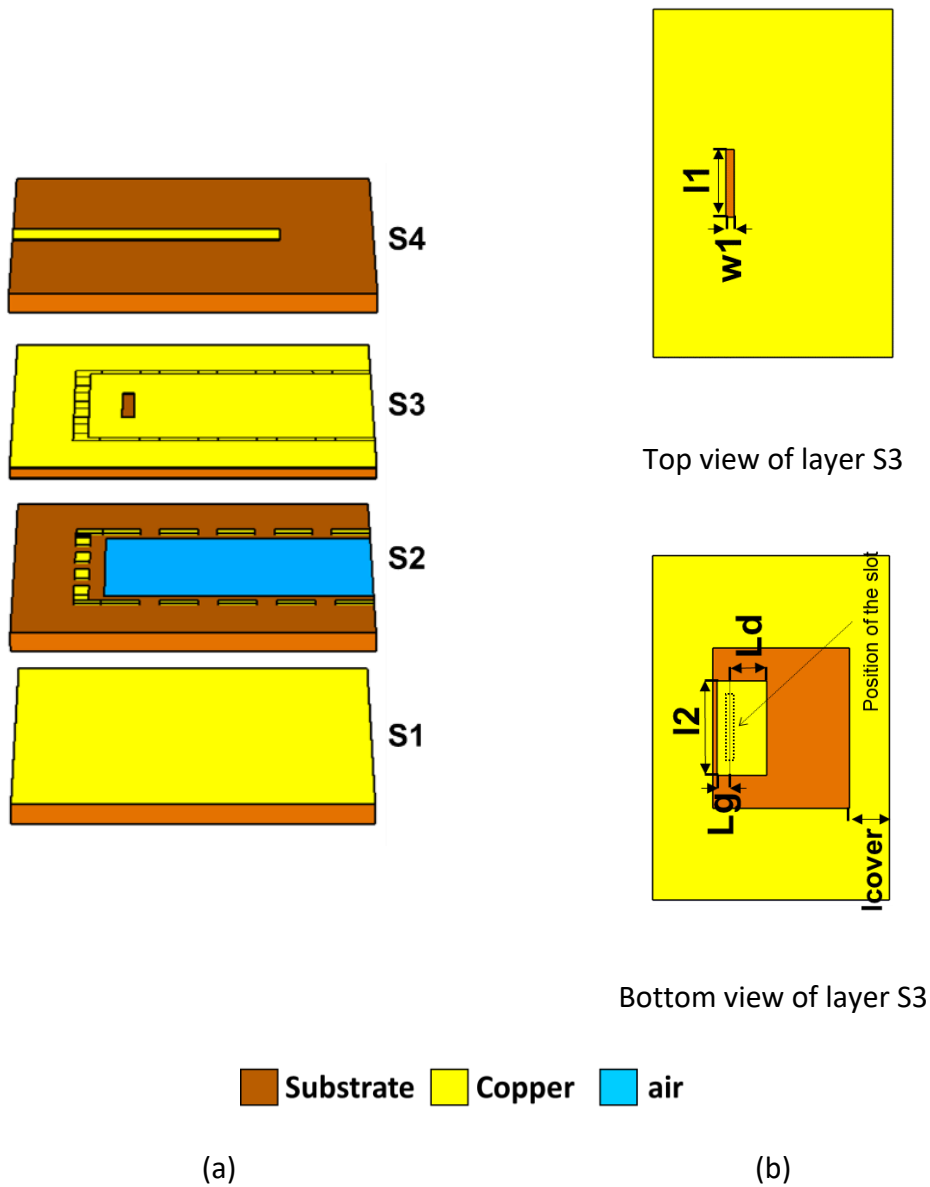


Fig. 2.16 Transition structure: (a) 3D view and (b) top and bottom views of layer S3.

This copper patch can also enhance the electric field in the structure of AFSIW so that the E-field is like the one illustrated in Fig. 2.17.b.

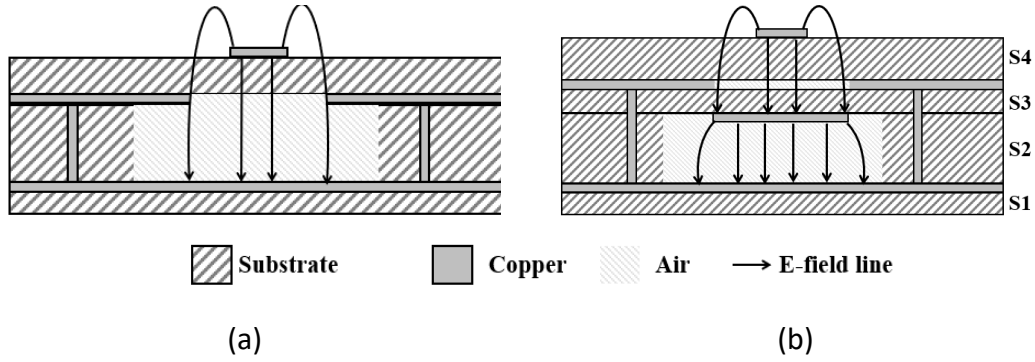


Fig. 2.17 Cross-sectional view of the proposed transition: (a) without the copper patch; (b) with the copper patch.

To determine the dimensions of the coupling structure, the first step is to find out the size and the position of the slot.

### 2.2.3.1 Position and size of the slot

The electric field excited by the slot is in opposite directions for forward and backward waves. As a result, the slot should be opened as close as possible to the short-circuited end of the AFSIW to ensure maximum energy transfer in the forward direction [69].

Fig. 2.18 shows a simplified diagram of the slot structure used for the transition.

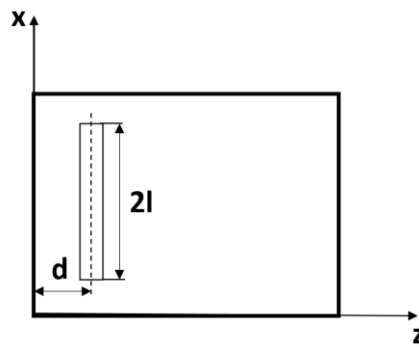


Fig. 2.18 Simplified top view of the slot coupling problem.

The phenomenon of maximum energy transfer at the short-circuited end of the AFSIW can be demonstrated as

$$P = |V_0|^2 \frac{2k}{ab\eta\beta_{10}^3} (\cos k_{c,10}l - \cos kl)^2 \cos^2 \beta_{10}d \quad (2.2.5)$$

where  $P$  is the power flows through waveguide cross section,  $V_0$  is the input voltage,  $k$  is the propagation constant,  $\beta_{10}$  is the phase constant,  $k_{c,10}$  is the cutoff wavenumber.

When  $d = 0$ , the power reaches its maximum value. Therefore, this slot should be opened at the closest position to the end of the AFSIW air cavity, considering the limitations of fabrication technology. The length of the slot is chosen to be near half-wavelength at 28 GHz for the maximum amount of radiating energy.

Once the theoretical size and the position of the slot have been determined, the next step is to find out the size and position of the insert copper patch.

### 2.2.3.2 Position and size of the copper patch

For this patch, there are 4 dimensions which can influence the impedance matching between the substrate of the microstrip and the air cavity of the AFSIW (shown in Fig. 2.16.b):  $L_g$ ,  $L_d$ ,  $l_2$ ,  $l_{cover}$ . For the whole analysis, the port 1 is the AFSIW side and the port 2 is the microstrip line side.

First, the initial size of the copper patch is set equal to the slot. Next, the first parameter to be determined by parameter analysis is  $L_g$ . Because the boundary value of the parameter  $L_g$  is clear, that is, in the range of 0 to 0.559 mm. As a result of technical manufacturing conditions, the copper patch cannot be too close to the via. The value of the parameter  $L_g$  is determined by parameter analysis shown in Fig. 2.19.

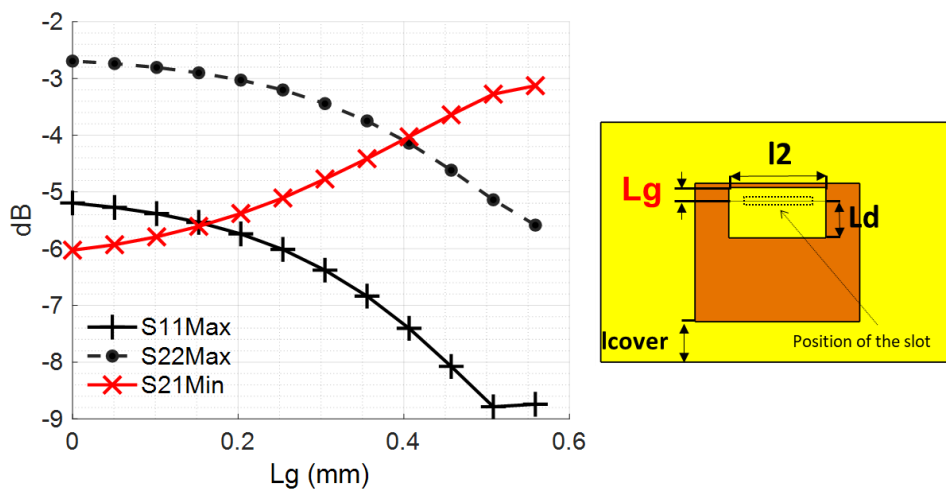


Fig. 2.19  $L_g$  parameter analysis.

When the value of  $L_g$  increases, the minimum value of the parameter  $S_{21}$  ( $S_{21min}$  will be used in the following and the maximum value of the parameter  $S_{11}$  or  $S_{22}$  will be replaced by  $S_{11max}$  or  $S_{22max}$  in the following text) of the transition increases, that is to say, when the value of  $L_g$  increases, the insertion loss of the transition decreases. And for the parameter  $S_{11max}$  and  $S_{22max}$ , when the value of  $L_g$  increases, the value of these two parameters decreases. In other words, the return loss of the transition is better. So, the value of  $L_g$  is selected as the maximum value within the limit of the manufacture.

The parameter  $L_d$  can vary between 0 and the length of the substrate. The value of the parameter  $L_g$  is determined by parameter analysis shown in Fig. 2.20.

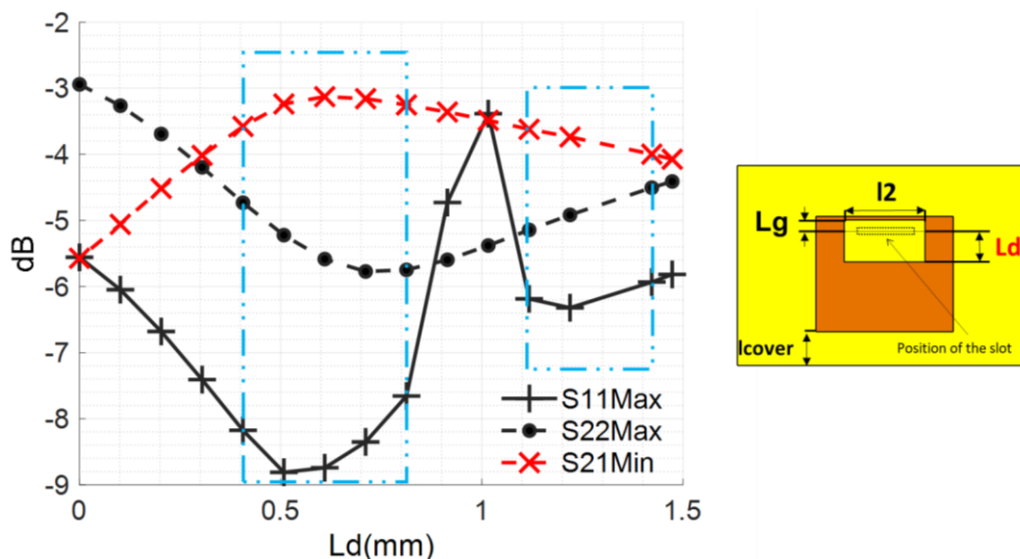


Fig. 2.20  $L_d$  parameter analysis.

It can be seen from the analysis that  $S_{11max}$  parameter has two relative minimum values (the area at the blue rectangular). Therefore, the following parameter optimization can be carried out in these two areas. During the first round of parameter analysis, the minimum value of the blue box on the left is used to analyze the remaining parameters.

The parameter  $l_2$  can vary between 0 and the width of the air cavity of AFSIW. The value of the parameter  $l_2$  is determined by parameter analysis shown in Fig. 2.21. According to the simulated results, in the area at the blue rectangular,  $S_{11max}$  and  $S_{22max}$

have the minimum values and  $S_{21min}$  reaches its maximum. Therefore, during this round of parameter analysis, the minimum value of the blue rectangular is used to analyze the remaining parameter  $l_{cover}$ .

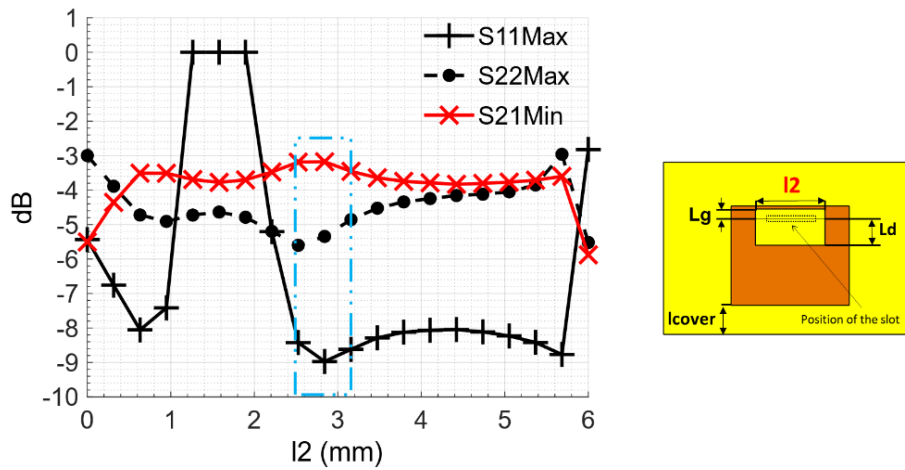


Fig. 2.21  $l_2$  parameter analysis.

The parameter  $l_{cover}$  can vary between the end of the structure and the end of the copper patch, but it can't touch the patch so the  $l_{cover}$  is limited by the minimum gap in the fabrication between the copper patch and the copper cover. Here when  $L_d$  is fixed at 0.61 mm for the first round of analysis, the parameter  $l_{cover}$  vary between 0.15 mm and 4.77 mm. It can be seen from the analysis as shown in Fig. 2.22 that it exists an area marked in the blue rectangular where these three parameters have good results. So, for this round,  $l_{cover}$  is fixed at the value that  $S_{11max}$  and  $S_{22max}$  have the minimum values.

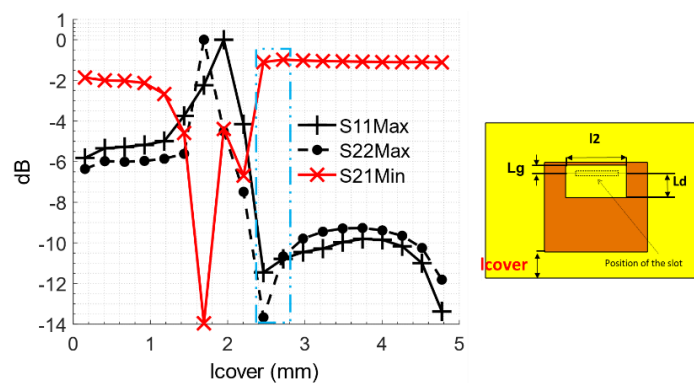


Fig. 2.22  $l_{cover}$  parameter analysis.

Until now, all of parameters for the copper patch are determined for the first time. The value of  $L_g$  is fixed within the limit of the manufacture so it doesn't participate in further parameters analysis. In subsequent rounds of parameter analysis, repeat the steps of the first round to change the values of parameters  $L_d, L_2, l_{cover}$ , to continuously optimize the results. For example, for the second round,  $L_2, l_{cover}$  have values which are fixed by the first round, and  $L_d$  vary between 0 and the length of the substrate like the first round. The result of the simulation has changed as shown in Fig. 2.23.a. According to the simulation results, the value of the parameter  $L_d$  is updated to 0.81 mm. In the same way,  $L_2$  and  $l_{cover}$  are also updated to the values within the area of the blue rectangular according to simulation results as shown in Fig. 2.23.

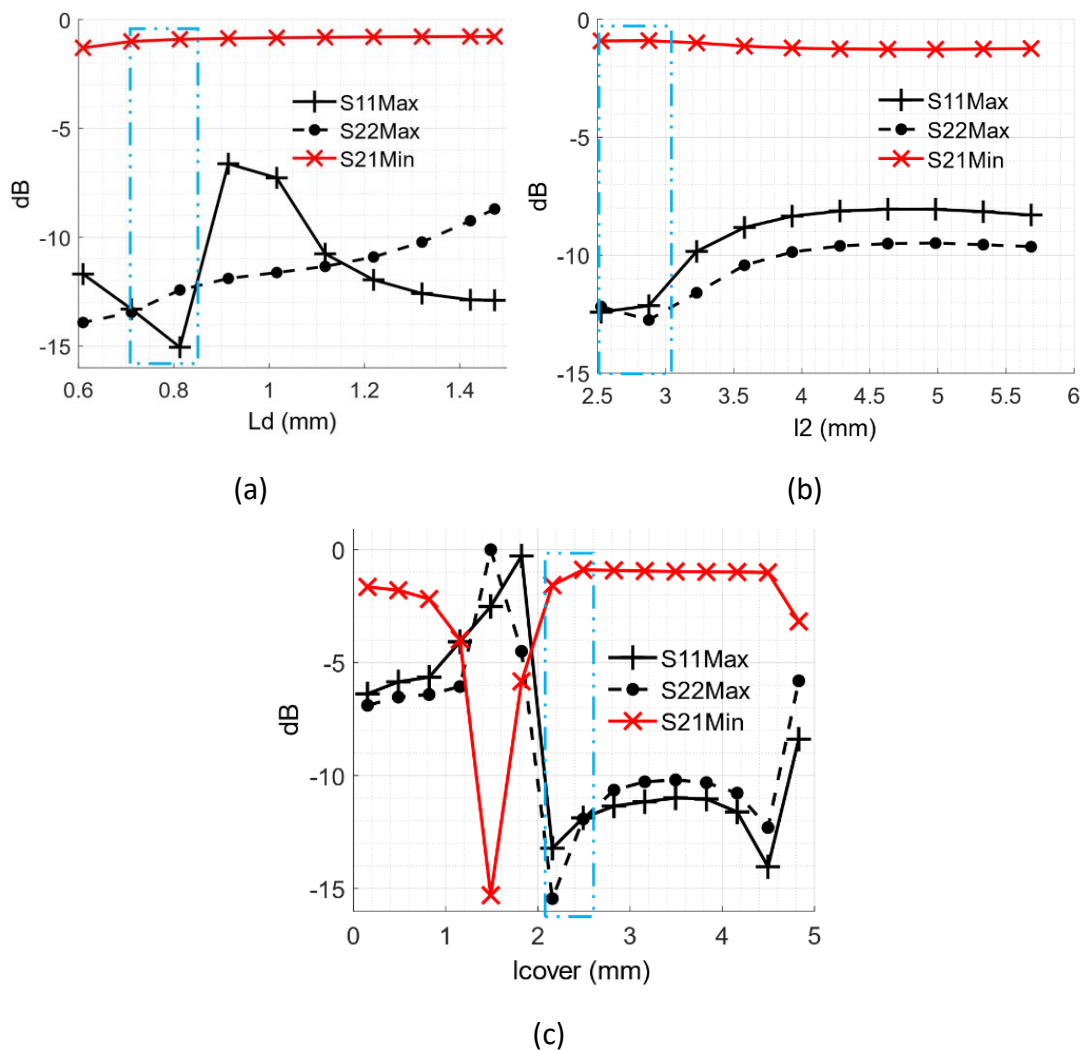


Fig. 2.23 Parameter analysis of second round for the parameter (a)  $L_d$ ; (b)  $l_2$  and (c)  $l_{cover}$ .

With all of the parameter analysis and the optimization, the final dimensions are shown in the Tab. 2.2. With the determined dimensions, the simulated S-parameters results are shown in Fig. 2.24. For a single transition, the return loss is less than -13 dB, and the insertion loss is less than 0.76 dB within the operating frequency bandwidth.

Tab. 2.2 Dimensions of proposed transition

Parameter	$l_1$	$w_1$	$L_g$	$L_d$	$l_2$	$L_{cover}$
Dimensions (mm)	2.70	0.36	0.44	1.48	1.93	1.06

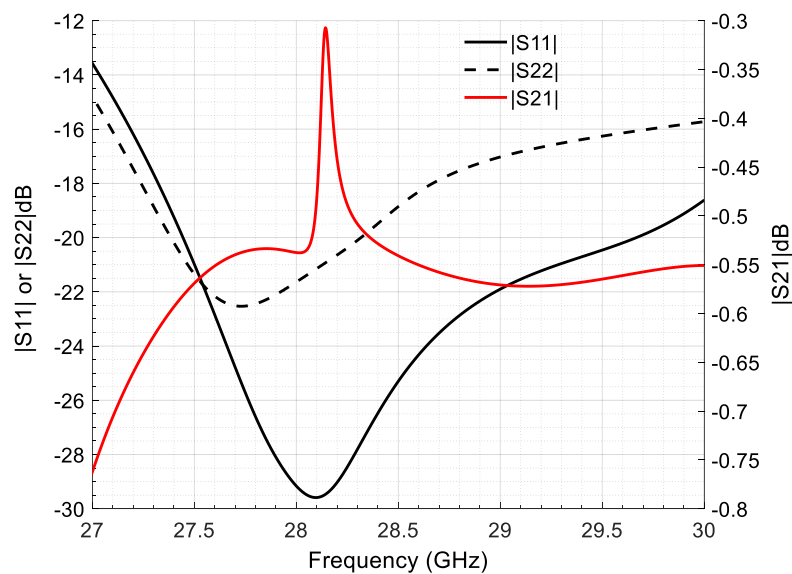


Fig. 2.24 Simulated S-parameters results of the single transition.

#### 2.2.4 Back-to-back transition

For measurement and for connection with the coaxial cables, a back-to-back transition is designed and optimized. The back-to-back transition is formed by connecting two proposed transitions as shown in Fig. 2.25. The distance between two microstrip lines ( $L_3$ ) is optimized to reduce the effect of coupling between the two lines.

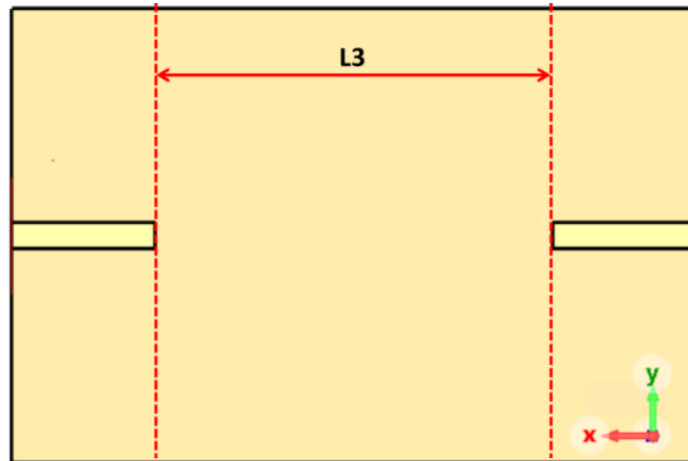


Fig. 2.25 Simulated back-to-back transition.

The picture of the fabricated back-to-back transition is shown in Fig. 2.26.a. In order to improve the accuracy of the measurement, a microstrip type TRL (for Thru or open-Reflect-Line) calibration kit is designed and fabricated as shown in Fig. 2.26.b. It allows the reference plane to be set to the same position as the simulation, so as to eliminate the influence of the extension of the connector microstrip line.

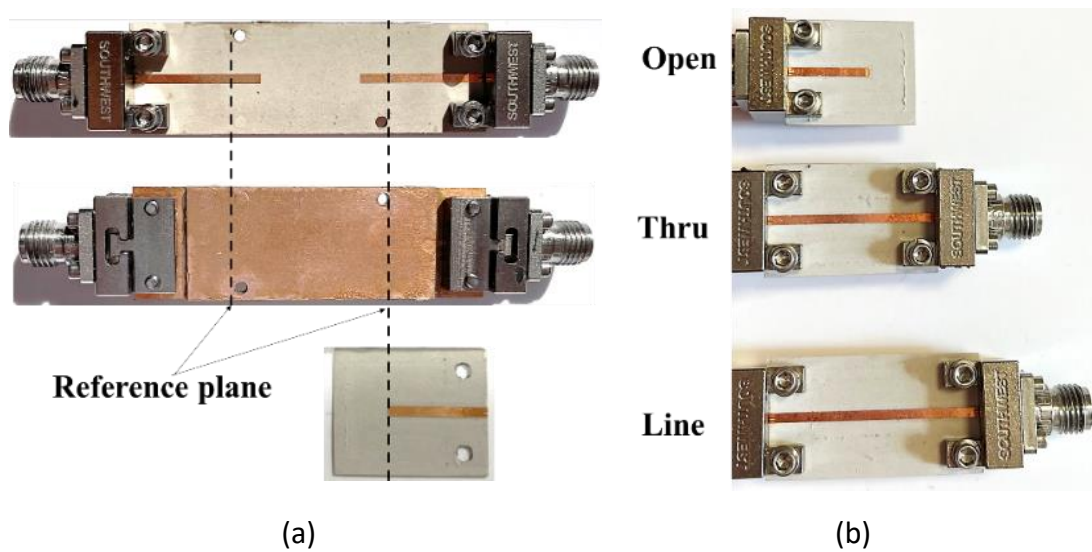


Fig. 2.26 Fabricated back-to-back transition.

## 2.3 Experimental Results

In the simulations, for a proposed transition, its return loss is higher than 13 dB and its insertion loss is below 0.76 dB over its operating frequency band (27 GHz - 30 GHz).

In the experiment, the proposed back-to-back transition is measured with the VNA (Vector Network Analyzer AGILENT 8720ES). The experimental and simulated S-parameters results is shown in Fig. 2.27. Over the frequency range of 27.40 GHz to 29.88 GHz, the reflection coefficient is between -8.2 dB and -20.6 dB, and the insertion losses are between 1.56 dB and 3.3. dB. It can be inferred from the results of back-to-back transition, for each side of transition MSL-AFSIW (as shown in Fig. 2.16), the insertion losses are between 0.78 dB and 1.65 dB. Compared with simulations, due to manufacturing errors and assembly qualities, the maximum difference in insertion loss between simulation and measurement is 1.3 dB (the maximum difference is at 27.8 GHz).

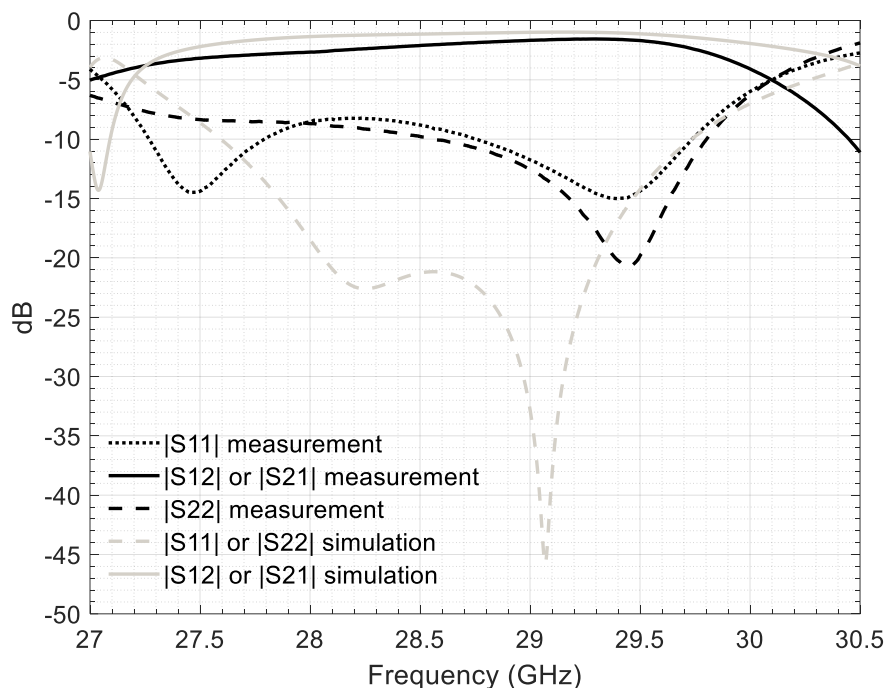


Fig. 2.27 Measured and simulated S-parameters results for the proposed back-to-back transition.

In [73], with the substrate Rogers RT/Duroid 6002, the AFSIW has a transmission loss of 0.03 dB/cm. The length of the back-to-back transition is 3.27 cm, it can be calculated that the transmission loss for the AFSIW part is 0.10 dB. It can be deduced, by considering the AFSIW losses, that the transition achieves  $1.16 \pm 0.43$  dB over the frequency range of 27.40 GHz to 29.88 GHz.

It can be seen from the experimental results that the measured back-to-back  $S_{12}$  parameters and  $S_{21}$  parameters do not coincide. This error mainly comes from the assembly qualities.

## 2.4 Conclusion

In this chapter, a vertical transition between AFSIW and microstrip is proposed, designed, analyzed and measured and a design approach has been synthesized

The design approach can be summarized in five steps. The flow chart is shown in Fig. 2.28 and the design steps are as follows:

*Step 1:* Calculate the geometries of microstrip line and AFSIW by the working frequency.

*Step 2:* Calculate the length of the coupling slot by central frequency.

*Step 3:* Fix the parameter  $L_g$  by limit of fabrication between 2 copper parts.

*Step 4:* The parameter sweep is performed one by one on parameters:  $L_d$ ,  $l_2$ ,  $l_{cover}$ .

After each round of parameter sweep, the optimal value of the parameter in this round is fixed, and then the next parameter sweep is performed, and the cycle repeats until the S-parameter is close to the required value.

*Step 5:* Optimize all the parameters with CST Studio Suite 2020. The goal of the optimization is to reduce the modulus of  $S_{11}$  and  $S_{22}$  and increase the modulus of  $S_{12}$  or  $S_{21}$  in all the working bandwidth.

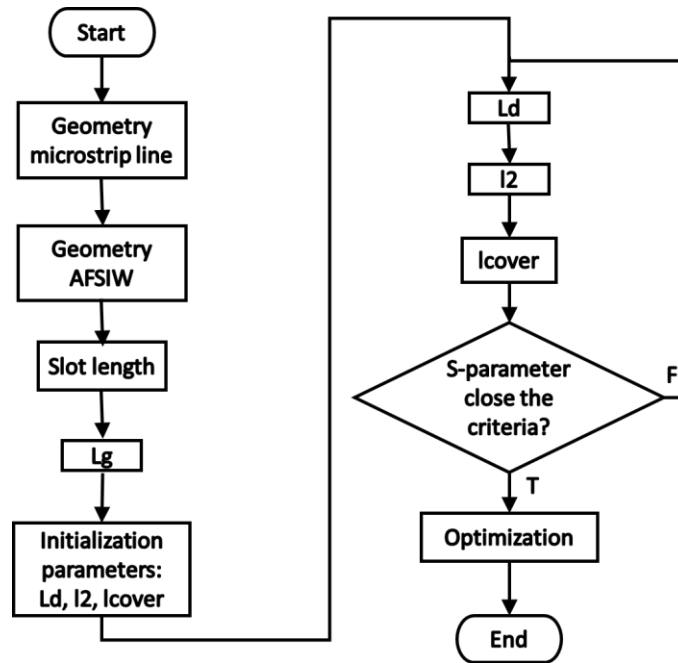


Fig. 2.28 Proposed vertical transition design approach.

This transition is compared to some vertical transitions found in the literature in Tab. 2.3. It can be seen from the table that the proposed transition is the first transition from AFSIW to microstrip working in Ka-band. Compared with the probe type transition, it is completely based on the PCB process, so the manufacturing is relatively simpler and the structure is more stable. Compared with the same type of slot transition, it has less insertion loss in its working frequency.

Tab. 2.3 Comparison with other vertical transitions

Reference	Frequency (GHz)	Coupling method	Insertion loss (dB)	Return loss(dB)
[68]	8.0 - 12.0	Probe	0.9	12
[66]	57 - 64	Probe	2*	15*
[70]	60.6 - 64.5	Slot	2.4	15
This work	27.5 - 29.8	Slot	1.16	8

\*Simulation results

However, in the experimental results, it can be found that its return loss is higher than the simulated value and  $S_{11}$  and  $S_{22}$  are different. This error mainly comes from the assembly quality, and a small amount of error comes from the operation of calibration and measurement in the experiment. Therefore, improving assembly skills can reduce errors and improve experimental results.



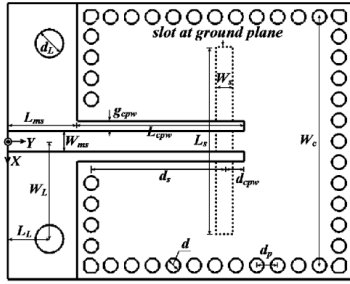
## CHAPTER 3: AFSIW ANTENNAS

Once the transition is proposed, the next step is to design the parts of the simplified transceiver in the vertical plane. Therefore, the purpose of this chapter is to design the antenna as a part of the vertical simplified transceiver. Also, in order to prove the variety of the system using the transition proposed in the previous chapter, two kinds of antennas are proposed and integrated with the transition in simulation.

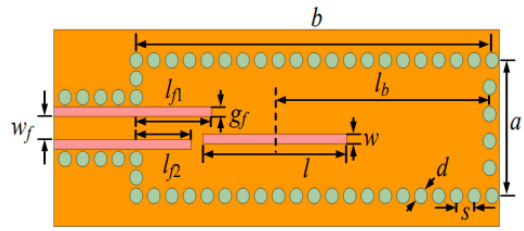
### 3.1 Overview

As a key component of the antenna system, the millimeter wave antenna is expected to have characteristics of compactness and low profile [74]. In order to obtain the antenna system with high quality factor, low insertion loss and high compactness, the SIW based antenna is a good candidate. With the SIW technology, active and passive components like antennas can be integrated on the same substrate. Compared to the patch antenna, which also has high compactness, the SIW antenna provides high gain when the number of slots increases and a lower cost system [75].

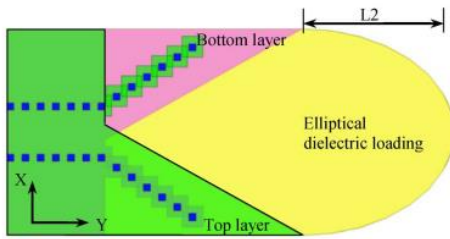
SIW technology can be applied to different types of antennas such as cavity-backed antenna [76], slot antenna [77], antipodal tapered slot antenna [78], dielectric resonator antenna [79], horn antenna [80], Yagi-Uda antenna [81], etc. The example pictures are shown in Fig. 3.1. However, the biggest drawback of SIW technology is the high dielectric loss, which leads to low radiation efficiency, thus reducing the gain of the antenna [82]. AFSIW technology which has a lower dielectric loss is implemented in different types of antennas to improve their performances.



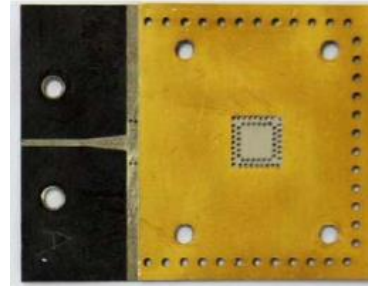
(a) [76]



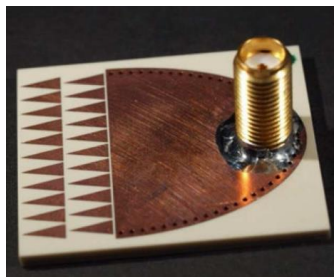
(b) [77]



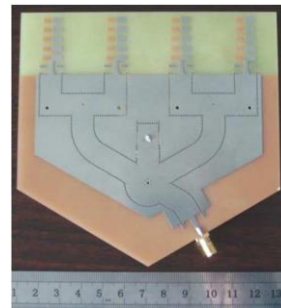
(c) [78]



(d) [79]



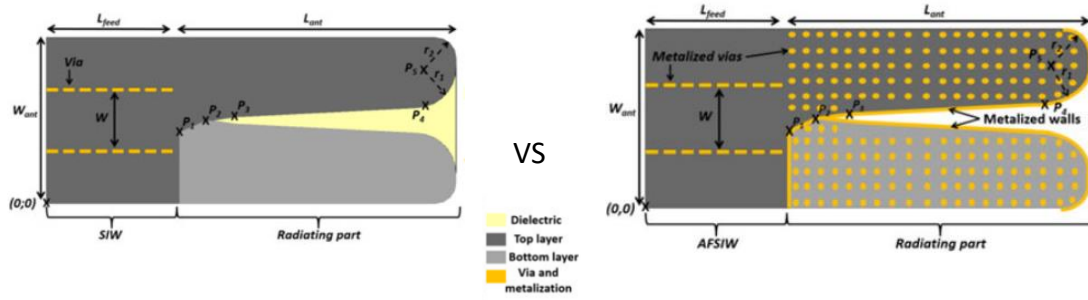
(e) [80]



(f) [81]

Fig. 3.1 Pictures of (a) cavity-backed antenna [76]; (b) slot antenna [77]; (c) antipodal tapered slot antenna [78] and (d) dielectric resonator antenna [79]; (e) horn antenna [80] and (f) Yagi-Uda antenna [81].

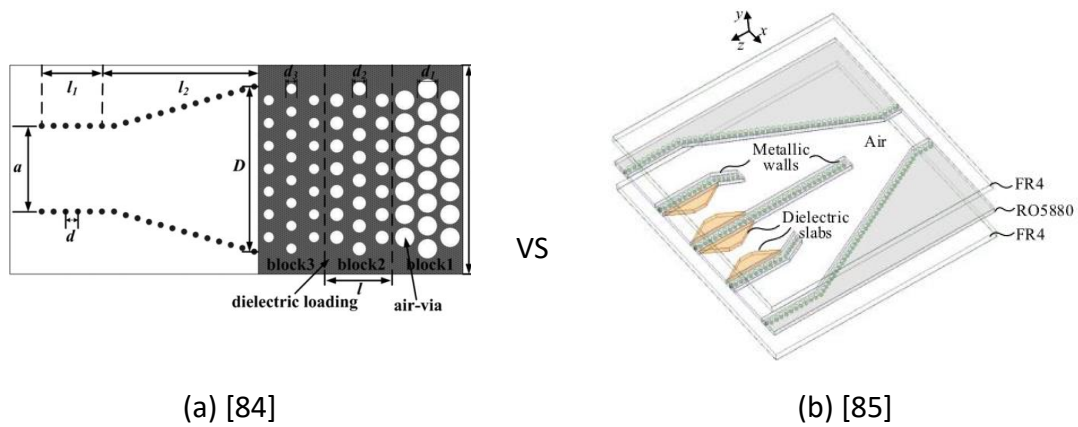
An example was given in [83], for antipodal linearly tapered slot antenna (AL TSA), over Ka-band, the gain of AFSIW AL TSA is improved by  $3.5 \pm 0.5$  dB compared to its dielectric-filled (SIW) counterpart. The structures of these two antennas are shown in Fig. 3.2. The same conclusion can be applied to the horn antenna [84], [85] and the structures are shown in Fig. 3.3.



(a) SIW ALTSA

(b) AFSIW ALTSA

Fig. 3.2 Antipodal linearly tapered slot antennas with the technology (a) SIW and (b) AFSIW.



(a) [84]

(b) [85]

Fig. 3.3 Horn antennas with the technology (a) SIW and (b) AFSIW.

Therefore, for this thesis, the antenna with the AFSIW technology is chosen for the system. In order to achieve the goal, which is to reorganize the components of system in a vertical plane, the transition AFSIW to microstrip presented in the chapter 2 can be used. The transition has two sides to be connected: one is the side of the microstrip line (port 1) and another is the side of the waveguide AFSIW (port 2), as shown as Fig. 3.4. With this transition, there are two possibilities of antenna selection for the system: microstrip feed antenna or waveguide AFSIW-based antenna, so it provides more flexibility.

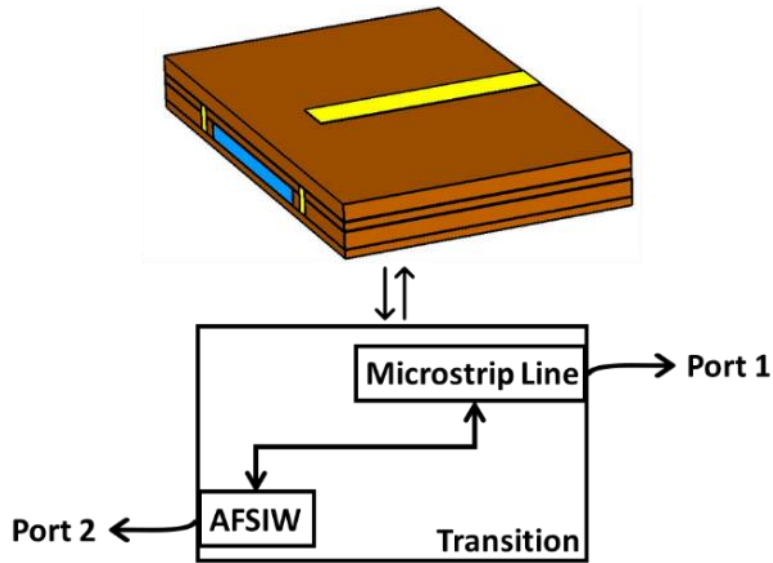


Fig. 3.4 Simplified diagram of the transition structure.

In order to prove the variety of the system using the transition proposed in the previous chapter, two kinds of antennas are proposed and integrated with the transition in simulation: cavity backed slot antenna which is fed by the microstrip line and patch antenna fed by AFSIW. The cavity backed slot antenna and patch antenna integrated with the transition are fabricated and experimentally measured.

### 3.2 Cavity-backed slot antenna

The purpose of this section aims to develop a cavity-backed slot antenna (CBSA) fed by microstrip line based on AFSIW technology, so as to connect to the proposed transition in the previous chapter on the microstrip line side.

In many applications, slot antenna is a good choice for the researchers because of its wideband, easy integration, low profile, good isolation from feeding network, etc. [86]. And cavity-backed slot antenna is a derivative type of slot antenna, it not only has the advantages of slot antenna but also reduces its backside radiation [87]. The first SIW CBSA was proposed in [88], the structure is shown in Fig. 3.5. Compared with the conventional CBSA with the metallic bulky cavity resonator drawback, the SIW CBSA shows a high gain of 5.3 dBi at 10 GHz while a planar configuration and low cost. Unfortunately, due to its low-profile configuration, unique responding mechanism and

dielectric loss, this SIW CBSA has a narrow bandwidth of 1.7% and a low radiation efficiency of 86%.

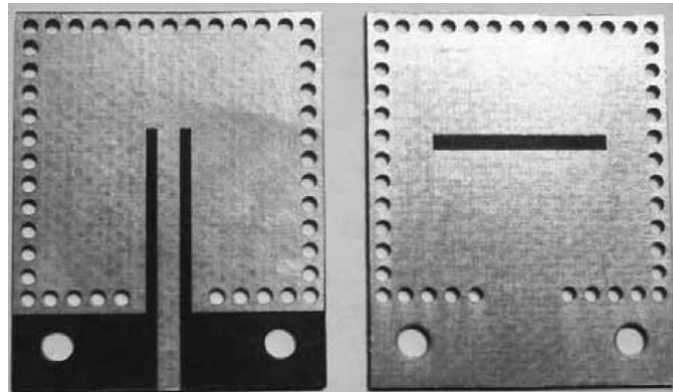


Fig. 3.5 Photo of the SIW CBSA in [88].

Therefore, the technology AFSIW is a good alternative technology to improve the bandwidth and the radiation efficiency by removing the dielectric and forming an air-cavity like conventional CBSA.

In the next section, an AFSIW CBSA is proposed, compared to its SIW counterpart, fabricated and measured.

### 3.2.1 AFSIW CBSA design

The design of the AFSIW CBSA at 28 GHz for the system is inspired by [88] which has presented a DFSIW CBSA at 10 GHz. The structure of the AFSIW is shown on Fig. 3.6.

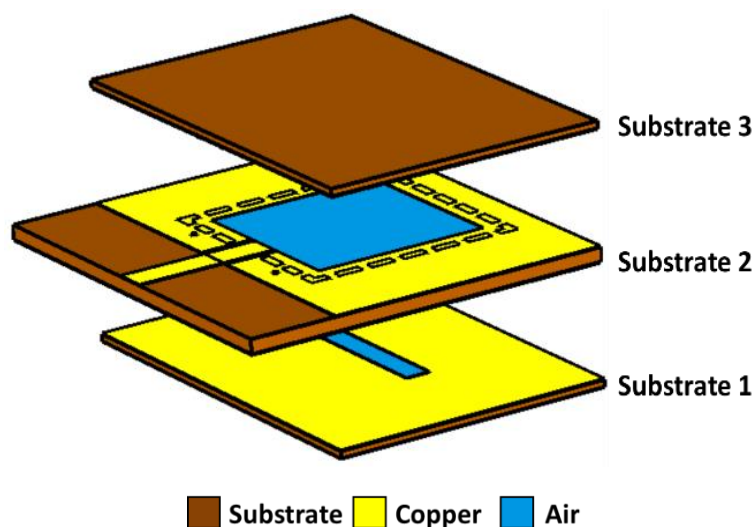


Fig. 3.6 AFSIW CBSA structure.

The AFSIW CBSA has three layers. The middle substrate (indicated as substrate 2 shown on Fig. 3.6.a) is filled with the air.

In order to place the cutoff frequency of TE<sub>10</sub> mode at 21 GHz, the width of the air cavity is approximately determined by equation (3.2.1).

$$f_{c_{1,0}} = \frac{c}{2\sqrt{\epsilon_r}} \sqrt{\left(\frac{1}{W_c}\right)^2} \quad (3.2.1)$$

where relative permittivity  $\epsilon_r$  for AFSIW equals to 1 approximately.

The length of the radiating slot (indicated as  $L_s$  in the Fig. 3.9) is chosen as  $0.5\lambda_g$  so that the antenna can resonate around 28 GHz for the system. The Grounded Coplanar Waveguide (GCPW) is used as the feed element to excite the air cavity. For measurement and connection with the system, at the end of the inside conductor of the GCPW, a 50  $\Omega$  microstrip line is added. The GCPW and the microstrip line situate on the top copper layer as shown in Fig. 3.7.a. The slot situate on the bottom copper layer given in Fig. 3.7.b.

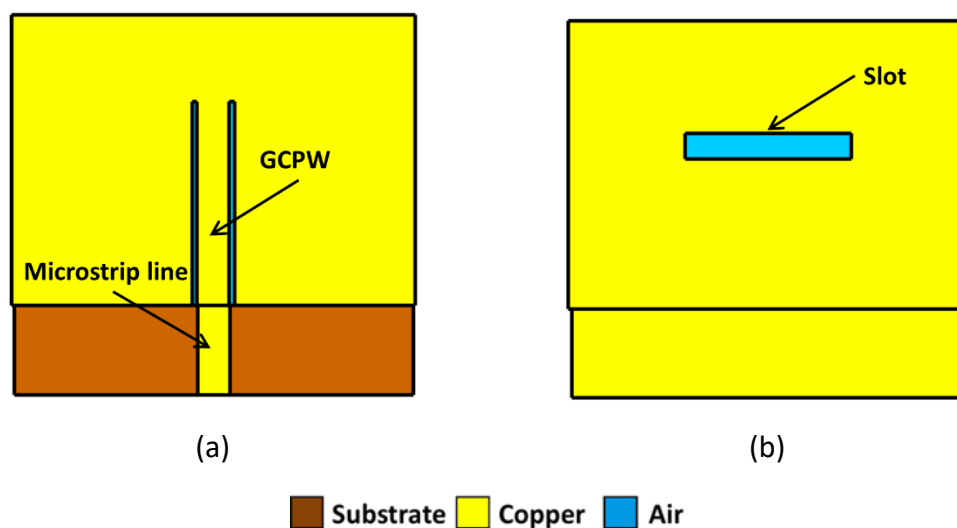


Fig. 3.7 (a) Top copper layer and (b) bottom copper layer of substrate 2 of AFSIW CBSA

In order to demonstrate the advantages of the AFSIW technology, a DFSIW CBSA has been designed with the same method for comparison. The structure of DFSIW CBSA is

shown in Fig. 3.8. Compared to the proposed AFSIW CBSA, this antenna has only one substrate, with copper layers on both sides.

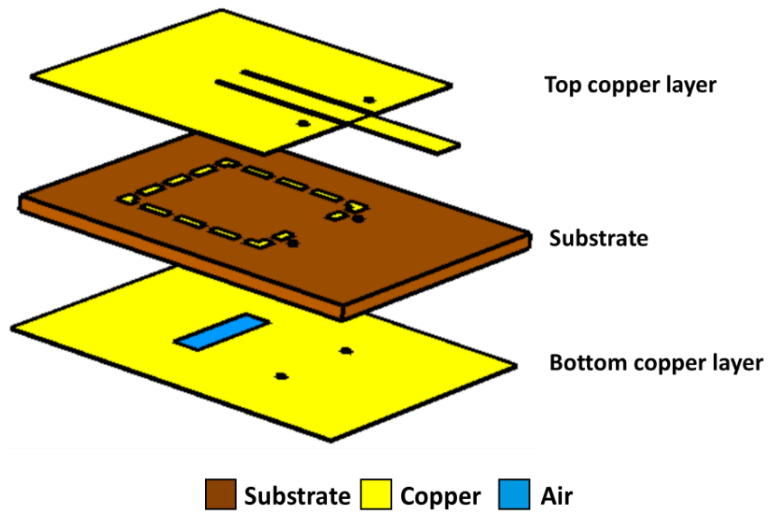


Fig. 3.8 DFSIW CBSA structure.

The geometric shapes of these two antennas are demonstrated in Fig. 3.9 and the dimensional details are recorded in Tab. 3.1. It can be noted that the DFSIW one is more compact than the AFSIW one.

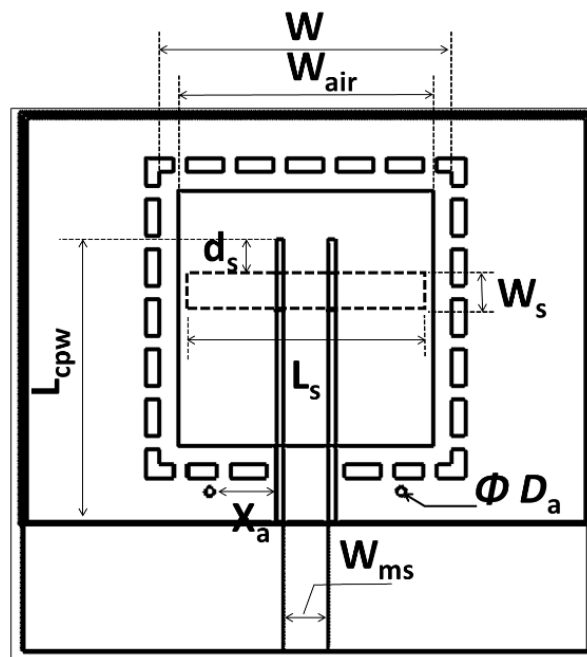


Fig. 3.9 Geometry of CBSA.

Tab. 3.1 Dimensions of CBSA in millimeter

Parameter (mm)	W	W <sub>air</sub>	W <sub>ms</sub>	W <sub>s</sub>	X <sub>a</sub>	D <sub>a</sub>	L <sub>cpw</sub>	L <sub>s</sub>	d <sub>s</sub>
AFSIW CBSA	7.96	6.94	1.24	1.00	1.70	0.25	8.05	6.50	1.20
DFSIW CBSA	4.37	0	1.24	1.00	0.70	0.28	4.14	3.65	-1.08*

\* -: L<sub>cpw</sub> is lower than the height of the slot.

### 3.2.2 Simulation results and comparison

The simulation results of the AFSIW and SIW CBSA are compared in Fig. 3.10.

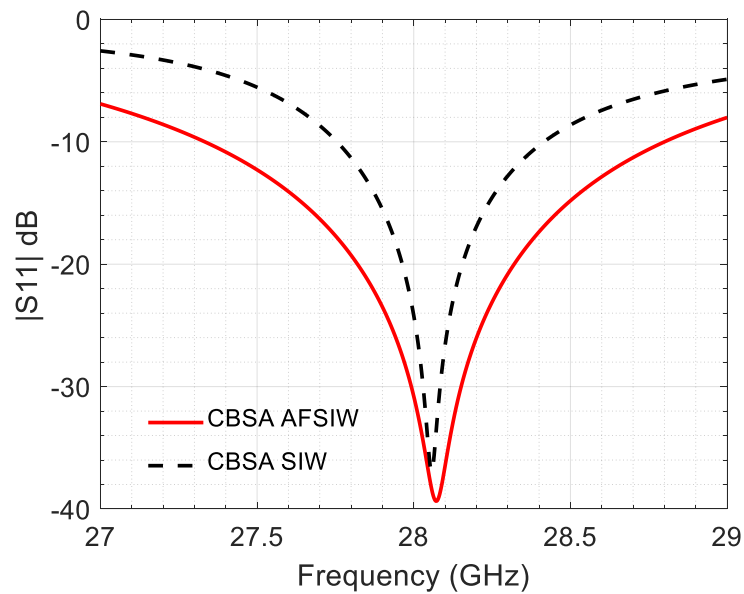


Fig. 3.10 Simulated S-parameters results of AFSIW and SIW CBSA.

The -10 dB bandwidth of AFSIW CBSA is 1.47 GHz (27.33 GHz to 28.80 GHz) and its counterpart SIW CBSA is 0.66 GHz (27.75 GHz to 28.41 GHz). It can be noted that with the same level of impedance adaptation, the AFSIW CBSA has larger bandwidth than SIW CBSA thanks to its low dielectric loss. The simulated radiation result of AFSIW CBSA is shown in Fig. 3.11. This single antenna has a gain of 8.76 dBi at 28.05 GHz and with its low loss, this antenna obtained a total efficiency of 98.3%.

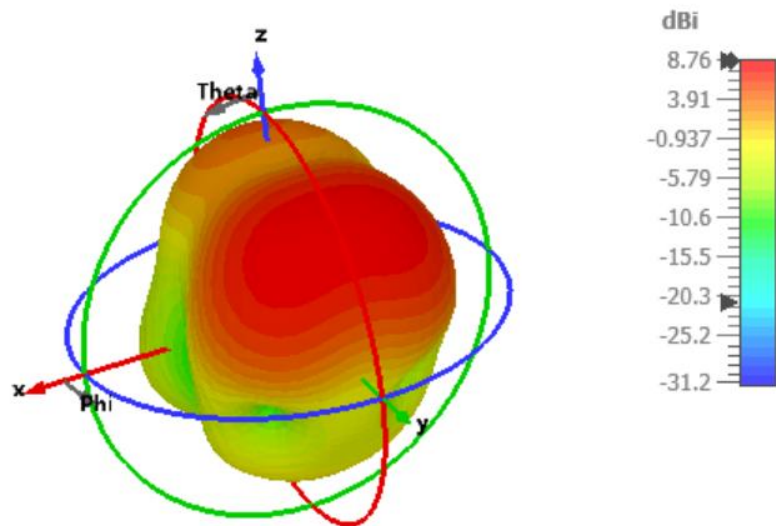


Fig. 3.11 Simulated 3D view radiation result of AFSIW CBSA.

### 3.2.3 Fabrication and measurement

For the fabrication, the dimensions of the AFSIW CBSA are optimized considering the influence of the 2.92 mm jack (female) end launch connector. The photo of the fabricated CBSA is shown in Fig. 3.12. It can be noted that there is no open slot on the surface in order to protect the antenna structure.

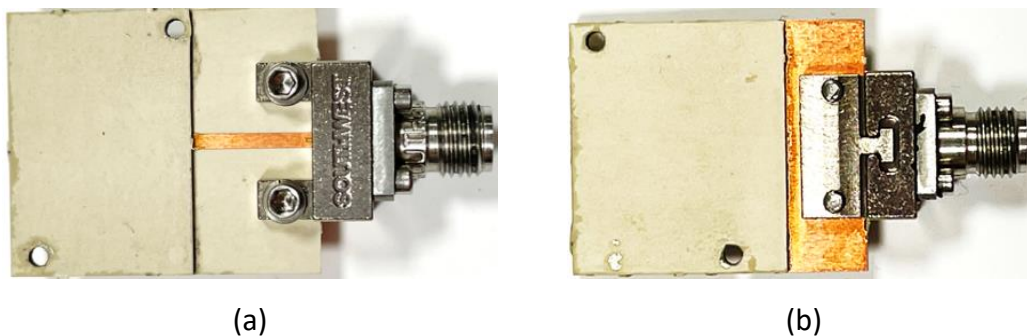


Fig. 3.12 Photos of the (a) front and (b) back of the fabricated CBSA.

The measured parameter-S result compared with the simulated parameter-S result is indicated in Fig. 3.13. It can be noted that, these two results have a good agreement. According to the measurement, the antenna has a -10dB bandwidth of 420 MHz.

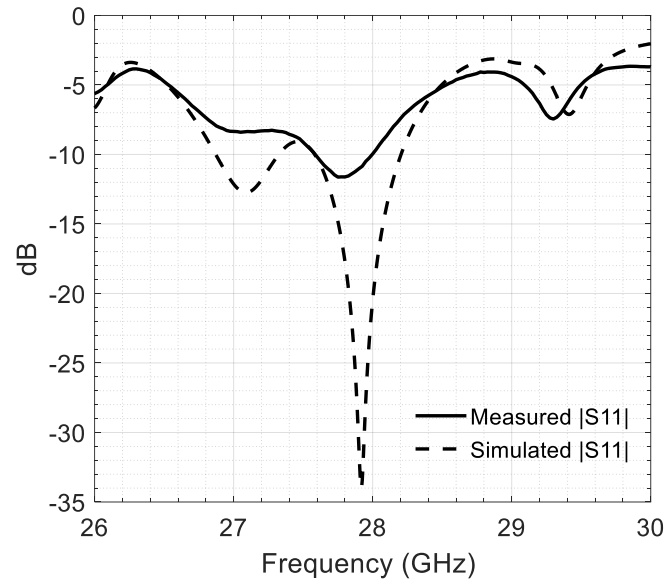


Fig. 3.13 CBSA S-parameter measured result.

The radiation patterns were measured in the anechoic chamber shown in Fig. 3.14.a. The proposed CBSA was located at the position of the reception ( $R_x$ ) and it was placed on a support as shown in Fig. 3.14.b.

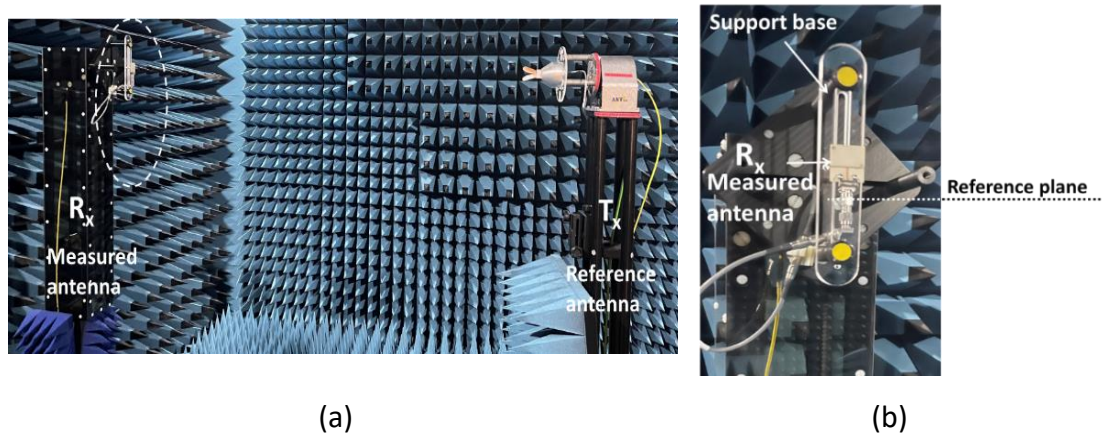


Fig. 3.14 CBSA measurement environment: (a) view in the anechoic chamber; (b) zoom view on the antenna.

The results of the simulated and the measured radiation patterns are shown in Fig. 3.15. It can be noted that there is a good match between simulated and measured results. On H-plane, the measured gain is 8 dBi and on E-plane, the measured gain is 9.3 dBi at 27.92 GHz where the antenna has the best impedance adaptation.

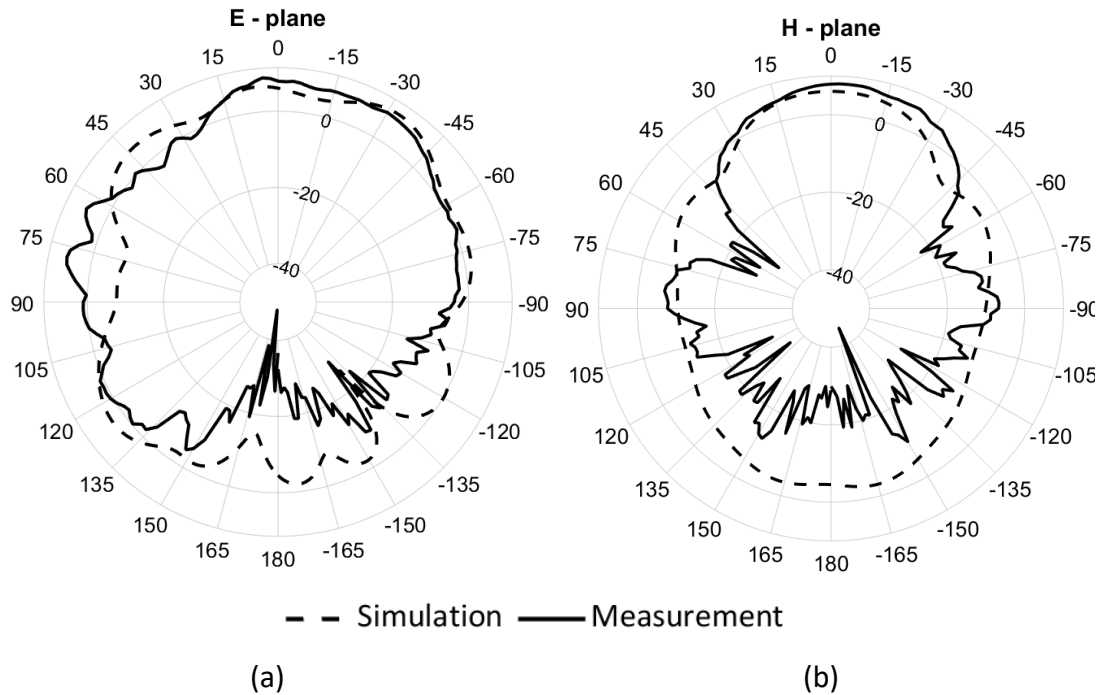


Fig. 3.15 Simulated and measured CBSA radiation pattern in (a) H-plane and (b) E-plane at 27.92 GHz.

### 3.3 Patch antenna fed by AFSIW

The second choice of antenna is the patch antenna fed by AFSIW in order to connect to the waveguide side of the proposed transition. As mentioned in overview, the patch antenna is well known for low cost, ease of fabrication and integration. The role of the feed structures is also very important. The losses of the microstrip is significant in millimeter-wave range [89]. Therefore, the indirect waveguide feed shows its advantages for millimeter-wave antenna and antenna arrays, for example, the patch antenna fed by a rectangular waveguide as shown in Fig. 3.16 [90] shows a lower loss than its counterpart fed by microstrip line or coaxial. To benefit the planar and the low loss characteristic of the AFSIW technology, the patch antenna using AFSIW feeding structure is firstly proposed in Fig. 3.17 [91]. A total efficiency of 92% is obtained thanks to the AFSIW technology. Therefore, the AFSIW feeding structure can preserve the planar structure of the system while improving the total efficiency of the antenna.

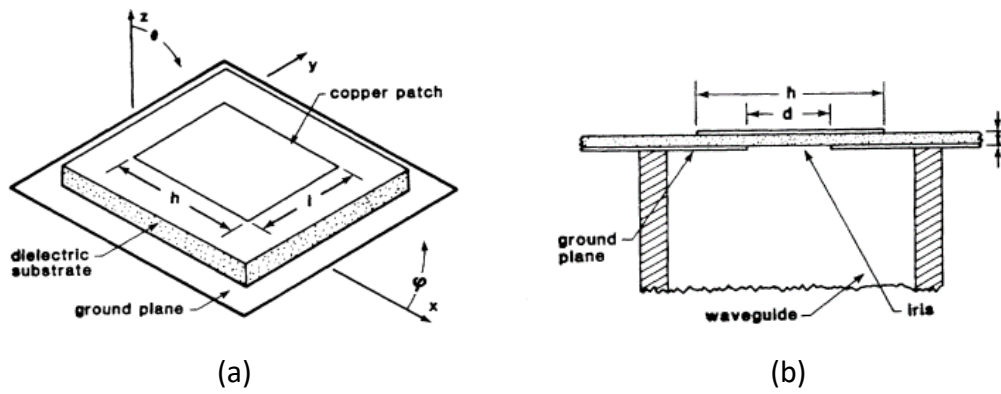


Fig. 3.16 Patch antenna fed by waveguide rectangular in [90]: (a) rectangular microstrip patch antenna; (b) cut-away view.

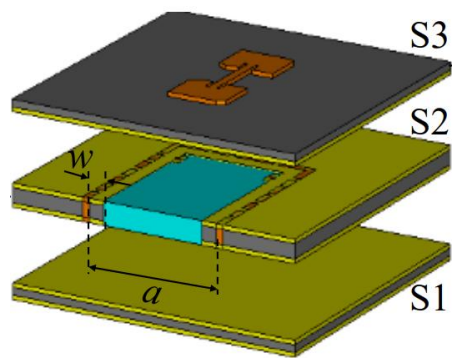


Fig. 3.17 3D view of the patch antenna using AFSIW feeding structure in [91].

In the next section, an AFSIW fed patch antenna is designed for this thesis's antenna system, adapted with the proposed transition, fabricated and measured.

### 3.3.1 AFSIW fed patch antenna design

The antenna connected with its AFSIW port to the rest of the system in this thesis is inspired by the AFSIW fed patch antenna [91]. The novelty lies with the connection to the transition proposed in the previous subsection. The entire measurable antenna, that is to say the antenna and its transition for connector of VNA, lies in a vertical plane. The 3D view of the proposed antenna is shown in Fig. 3.18. This antenna array consists of three substrates indicated S1, S2 and S3 in the right of the Fig. 3.18.

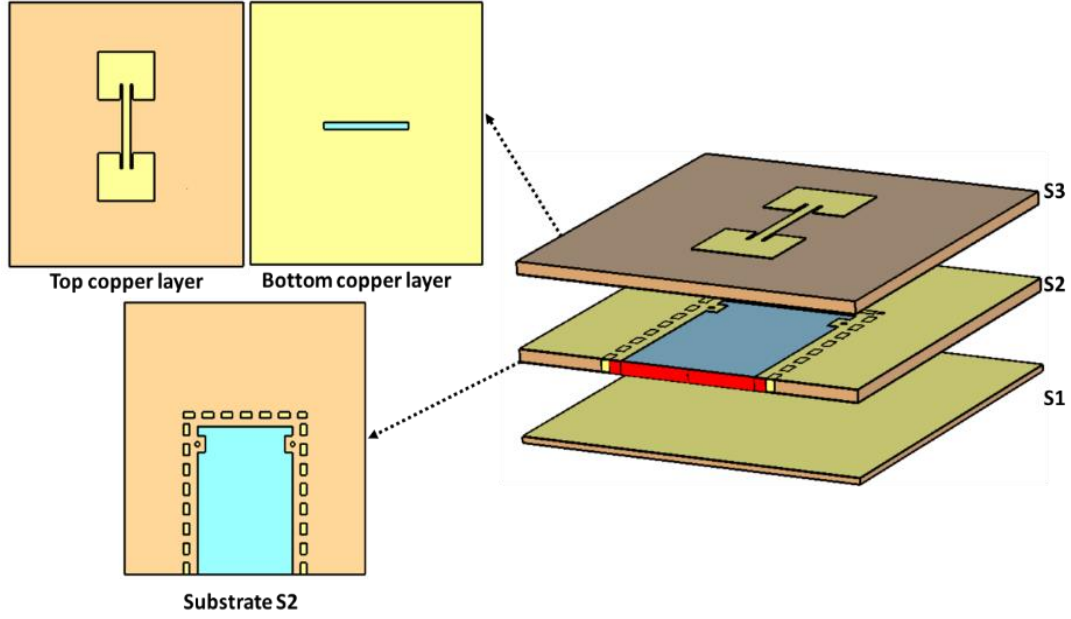


Fig. 3.18 3D view of proposed patch antenna for the system.

There are two patch antennas which are situated on the top layer of the substrate S3. These two antennas are in the opposite direction in order to generate a sum beam pattern to obtain a gain comparable to the slot antenna previously proposed. The dimensions of the patch antenna can be calculated by the following equations [92]:

$$W_p = \frac{c}{2f_c} \sqrt{\frac{2}{\epsilon_r + 1}} \quad (3.3.1)$$

$$\Delta L = 0.412h \frac{(\epsilon_e + 0.3) \left( \frac{W_p}{h} + 0.264 \right)}{(\epsilon_e - 0.258) \left( \frac{W_p}{h} + 0.8 \right)} \quad (3.3.2)$$

$$L_{eff} = \frac{c}{2f_c \sqrt{\epsilon_e}} \quad (3.3.3)$$

$$L_p = L_{eff} - 2\Delta L \quad (3.3.4)$$

$$\epsilon_e = \frac{\epsilon_r + 1}{2} + \frac{\epsilon_r - 1}{2} \left[ 1 + 12 \frac{h}{W_p} \right]^{-\frac{1}{2}} \quad (3.3.5)$$

Where  $f_c$  is 28 GHz,  $h$  is the thickness of the substrate S2 (0.508 mm for the proposed antenna).

The feeding of the patch antenna is realized by the slot on the bottom copper side of the substrate S3. The slot is opened at the end of the air cavity to couple the energy between the waveguide and the microstrip line of the patch antenna feeding. The vias on the substrate S2 can realize the inductive effect to reduce the capacitive effect which is created by the coupling slot [21]. The equivalent circuit of the via is shown in Fig. 3.19.



Fig. 3.19 (a) Symmetrical inductive and (b) equivalent circuit.

The geometric shapes of these two antennas are demonstrated in Fig. 3.20 and the dimensional details are recorded in Tab. 3.2.

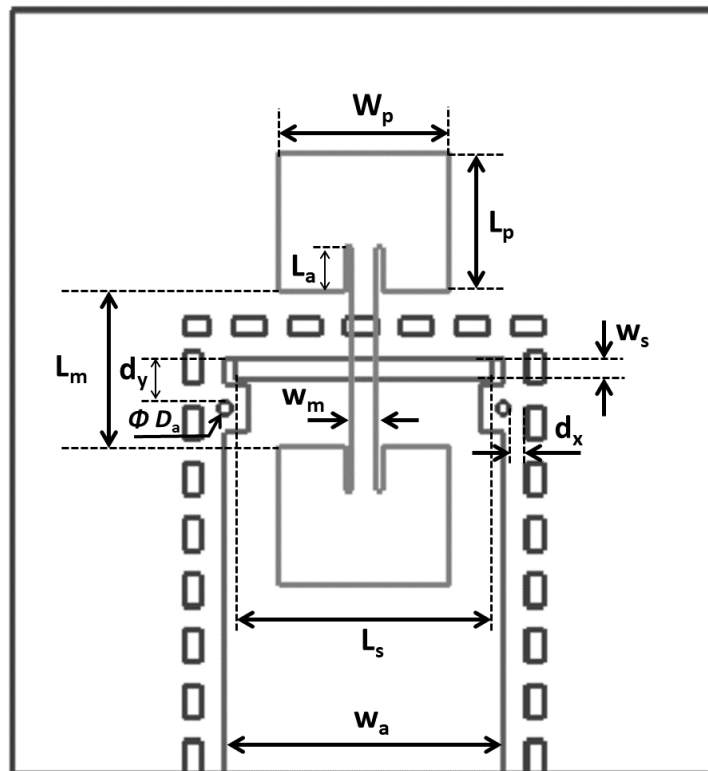


Fig. 3.20 3D view of proposed patch antenna for the system.

Tab. 3.2 Dimensions of patch antenna in millimeter

Parameter	$W_a$	$W_m$	$W_s$	$W_p$	$L_s$	$L_m$	$L_a$	$L_p$	$D_a$	$d_y$	$d_x$
Dimension (mm)	6.02	0.52	0.45	3.68	5.57	3.33	0.97	2.92	0.28	0.94	0.37

The S-parameter simulated result of the patch antenna model in the Fig. 3.18 is shown in Fig. 3.21. For the single patch antenna, that is to say, the transition and the connector for the coaxial line are not included; its radiation center frequency is at 27.93 GHz. Its -10 dB bandwidth is approximately 7% at 27.93 GHz (1.95 GHz between 27.16 GHz and 29.11 GHz). It's simulated far-field result is shown in Fig. 3.22. The patch antenna has achieved a gain of 9.98 dBi at its resonant frequency.

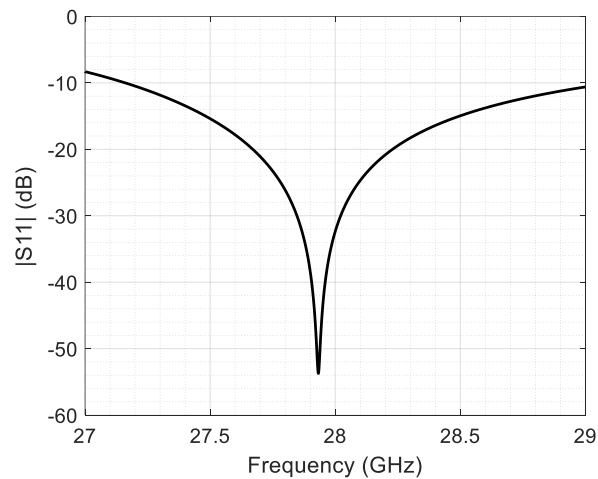


Fig. 3.21 Simulated S-parameter result for the patch antenna.

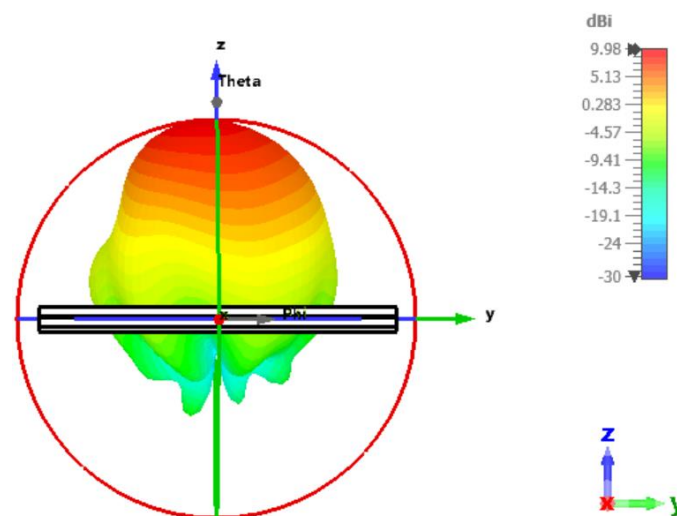


Fig. 3.22 Simulated far-field result for the patch antenna.

### 3.3.2 Fabrication and measurement

For fabrication and measurement, the transition between the AFSIW and microstrip is indispensable. Therefore, the transition AFSIW-MSL presented in chapter 2 is applied here to realize the fabrication. The prototype of the fabrication is shown in Fig. 3.23. The antenna is connected to the transition AFSIW-MSL through the waveguide side and the connector (End Launch Southwest 2.92 mm) is placed at the end of the microstrip line of the transition. The patch antenna radiates on the back of the device to minimize the impact of the microstrip line.

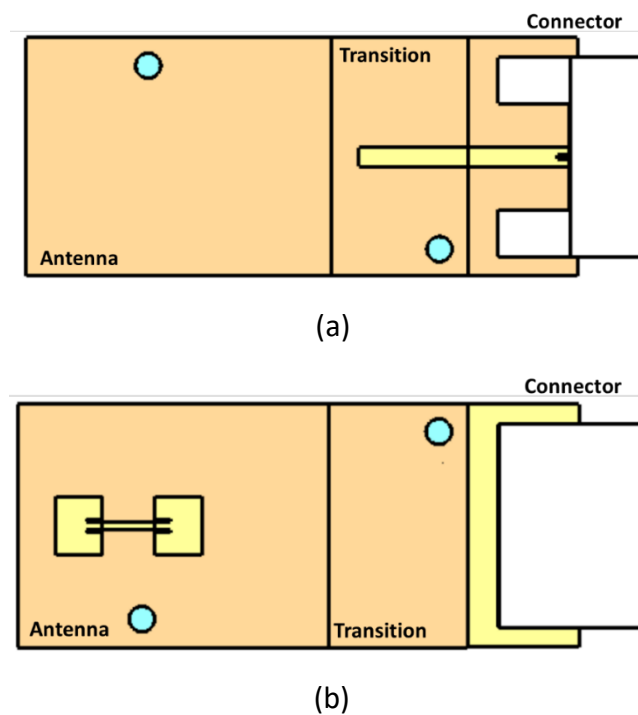


Fig. 3.23 (a) Top view and (b) bottom view of the patch antenna fabrication model.

The adaptation between the antenna and the transition is realized by optimization algorithm. The photo of the fabricated patch antenna is shown in Fig. 3.24.

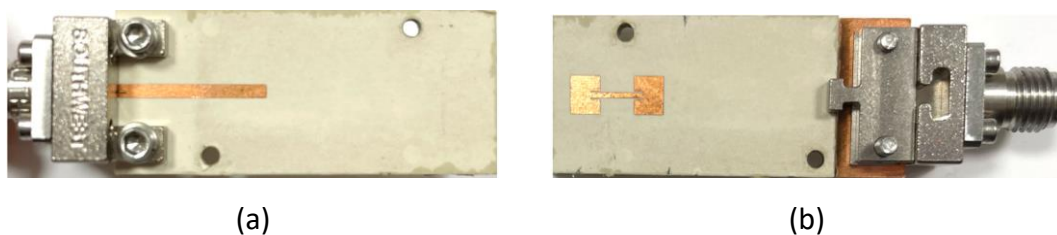


Fig. 3.24 Photos of the (a) front and (b) back of the fabricated CBSA.

The S-parameter measured result compared to the simulated result is shown in Fig. 3.25. It can be noted that the measurement and simulation results are very consistent. For the measurement, the proposed antenna with the transition radiation center frequency is at 28.05 GHz. Its -10 dB bandwidth is approximately 6.9% at 28.05 GHz (1.95 GHz between 27.02 GHz and 28.95 GHz).

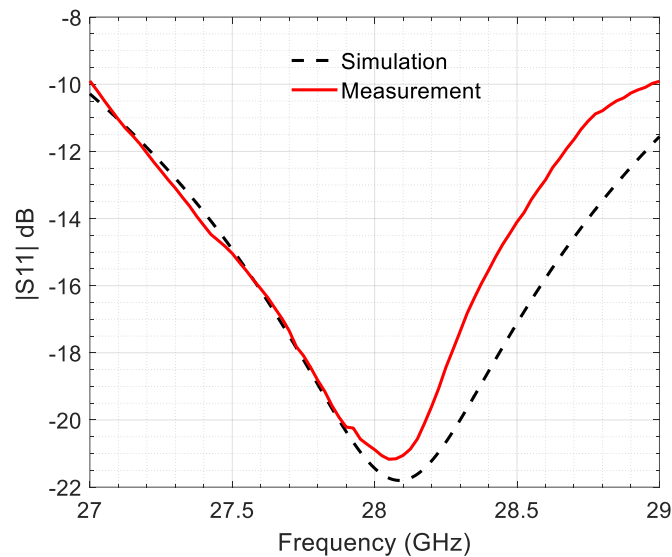


Fig. 3.25 Measured and simulated S-parameter result for the patch antenna.

The radiation patterns were measured in the anechoic chamber shown in Fig. 3.26.a. The proposed patch antenna was located at the position of the reception ( $R_x$ ) and it was placed on a support as shown in Fig. 3.26.b.

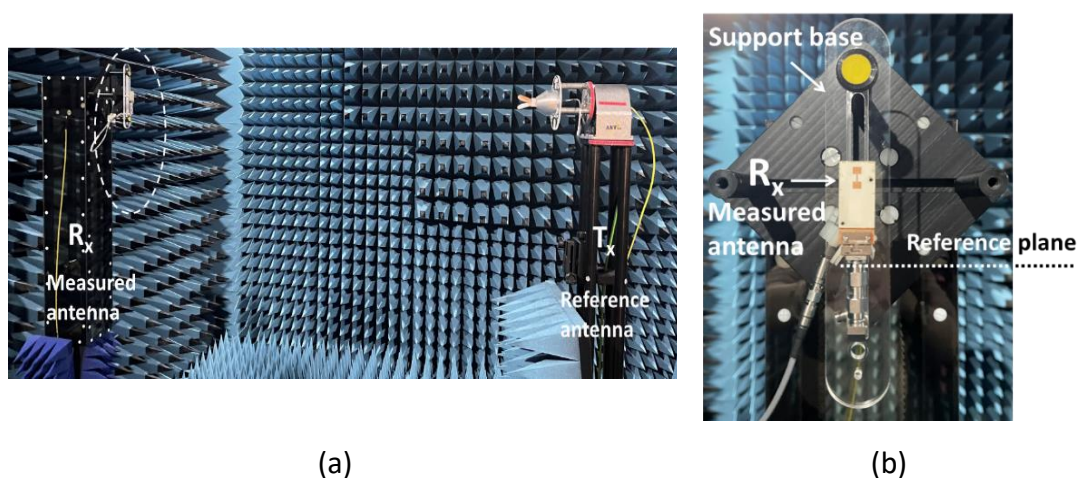


Fig. 3.26 patch antenna measurement environment: (a) view in the anechoic chamber; (b) zoom view on the antenna.

The results of the simulated and measured radiation patterns are shown in Fig. 3.27. It can be noted that there is a good match between simulated and measured results. On H-plane, the measured gain is 6.8 dBi and on E-plane, the measured gain is 7.8 dBi at 28 GHz.

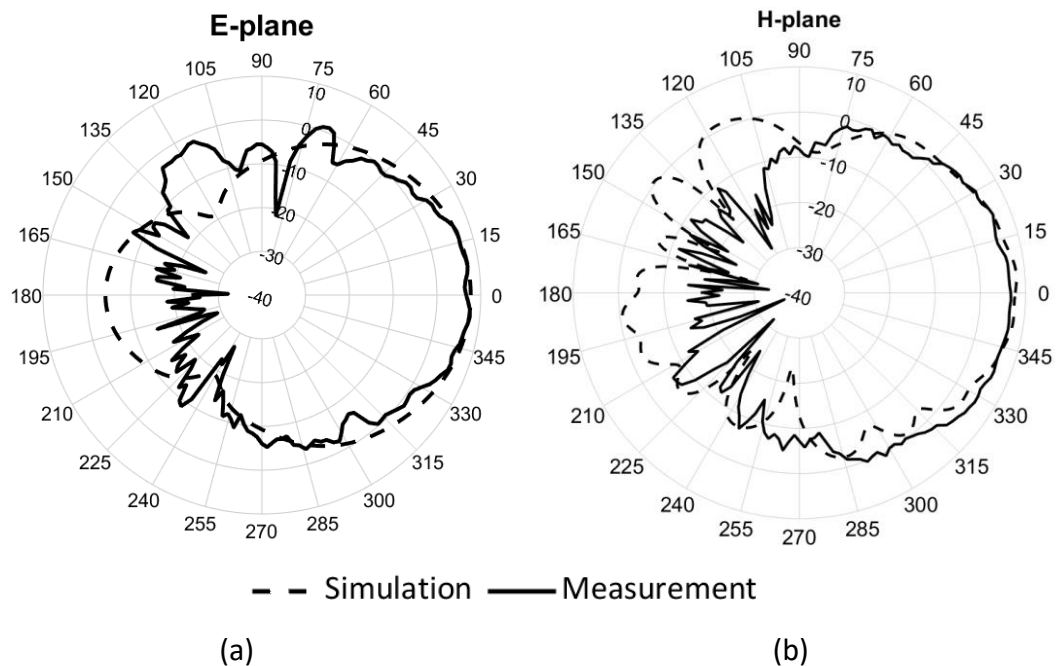


Fig. 3.27 Simulated and measured patch antenna radiation pattern in (a) H-plane and (b) E-plane at 28 GHz.

### 3.4 Conclusion

In this chapter, two types of antennas are proposed, fabricated and measured. The CBSA AFSIW shows its advantages in terms of the wide bandwidth and high efficiency compared to the CBSA SIW. The patch antenna is proposed and fabricated to improve the diversity of the system. Meanwhile, the performance of the patch antenna is less affected by the ground than the CBSA AFSIW. It is important for the antenna system because the ground of the antenna may change due to changes in other components. As shown in Fig. 3.28, the ground of the two antennas increases the same length and width: the length increases 0.1mm (noted Length+) and the width increases 0.1 mm (noted width+) of each side, but the respective radiation center frequencies change differently. The detailed variation of the radiation center frequency is shown in

Tab. 3.3. It can be noted that the variation of the radiation center frequency of CBSA AFSIW is larger than the radiation center frequency of patch antenna. Therefore, the proposed patch antenna is more suitable for an antenna system.

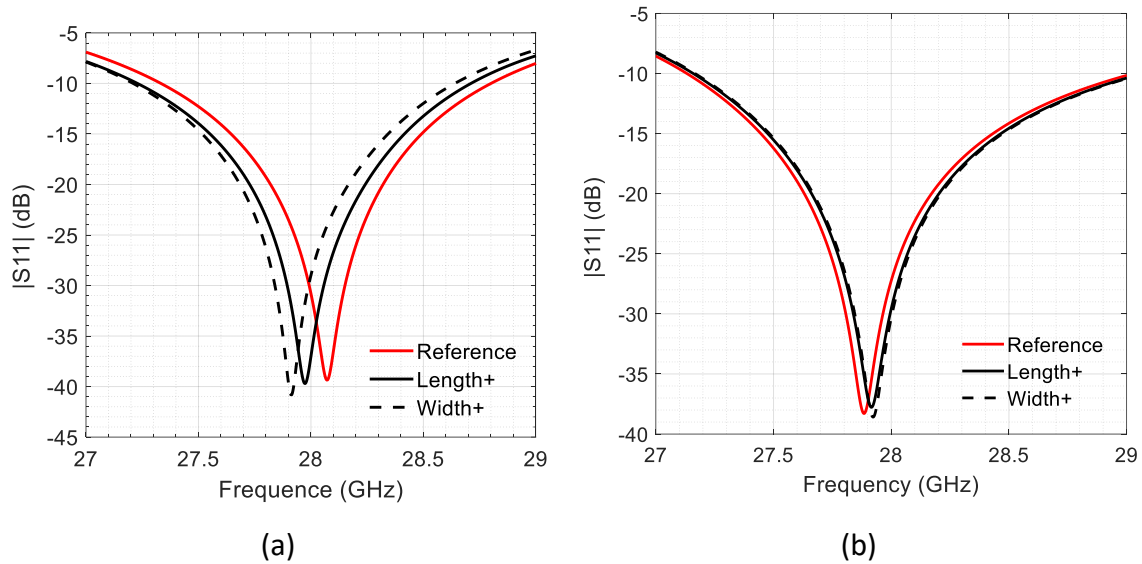


Fig. 3.28 The impact of the size of the ground for: (a) CBSA AFSIW; (b) patch antenna.

Tab. 3.3 Radiation center frequency and variation

	Reference	Length+	Width+	$\Delta F_l$	$\Delta F_w$
CBSA AFSIW	28.07	27.97	27.91	0.1	0.16
Patch antenna	27.88	27.91	27.92	0.03	0.04

\* $\Delta F_l$  is the variation of frequency between the reference and the antenna which has a longer ground.

\* $\Delta F_w$  is the variation of frequency between the reference and the antenna which has a wider ground.

With these two antennas, the antenna system can find out its optimal organization. Because if the component after the antenna is based on AFSIW technology, it can be directly connected to the AFSIW feeder located at the bottom of the patch antenna (Fig. 3.29.a) without the need the transition, or connected to the transition waveguide side by using CBSA AFSIW (Fig. 3.29.b). If the component after the antenna is based

on the microstrip technology, it can be directly connected to the CBSA AFSIW (Fig. 3.29.c) or connected to the transition microstrip side by using a patch antenna (Fig. 3.29.d).

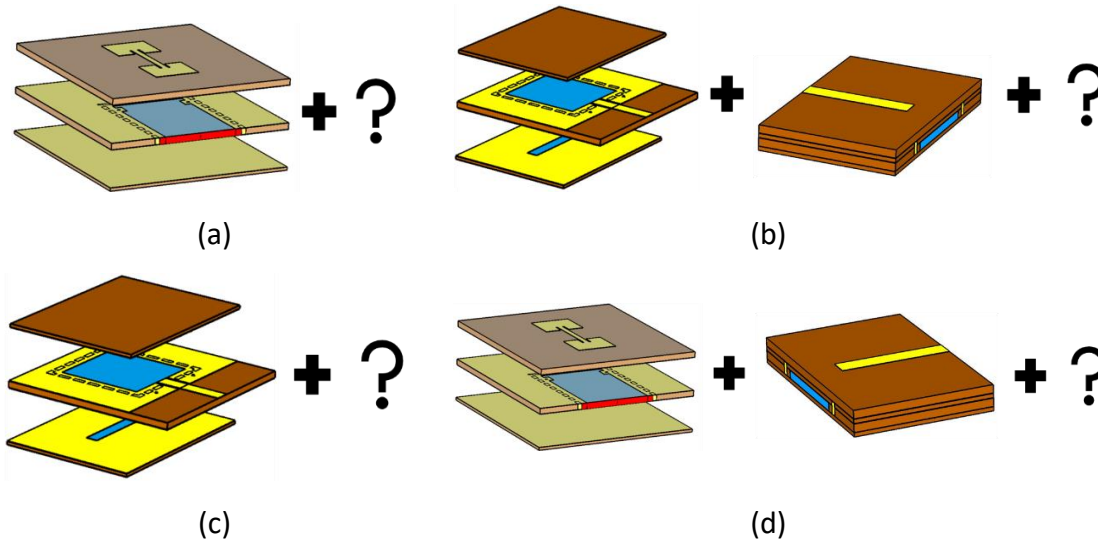


Fig. 3.29 Different organizations of antenna system.

## CHAPTER 4: MULTILAYER FILTER

In the previous chapters, the transition and antenna of the simplified transceiver have been proposed. In this chapter, a multilayer filter as the third component of the vertical simplified transceiver is proposed. The filter is designed and optimized using the CST Studio Suite 2020 software.

### 4.1 Overview

Among the important components that allow advances in the field of communications systems, filters are an essential part [93]. To answer to the market demand, they must offer very good performance in terms of losses (insertion and return losses), while being compact and inexpensive. RF filters come in various types, like lumped element filters [94], [95], planar filters such as microstrip filters [96], [97], dielectric filters [98], [99], cavity filters [100], [101], waveguide filters [19], [102], etc. as shown in the Fig. 4.1.

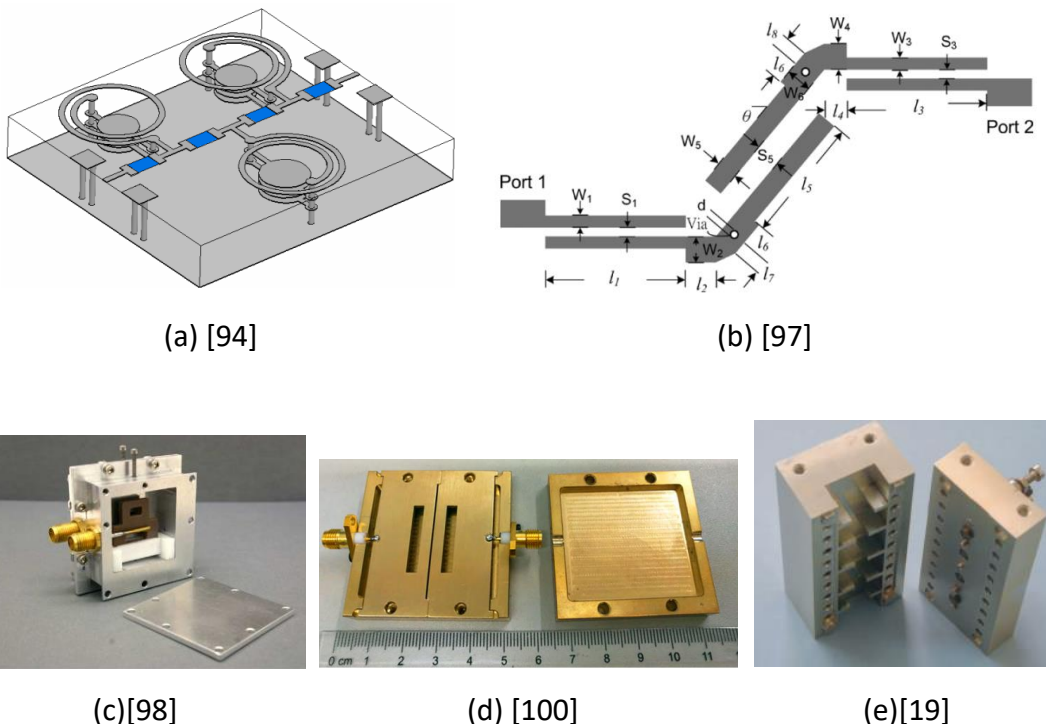


Fig. 4.1 Pictures of filters with different technologies: (a) lumped element filter [15]; (b) microstrip filter [18]; (c) dielectric filter [98]; (d) cavity filter [100] and (e) waveguide filter [19].

Waveguide-based filters are good candidates for communication systems, especially for communications satellites, wireless base stations, earth stations and other point-to-point repeaters [103]. The waveguide has the characteristics of low insertion loss, and its loss mainly comes from the dissipation of current in the waveguide wall. Waveguide resonators also have a high quality factor [104]–[106]. However, a waveguide filter is expensive, so a planar filter, such as a microstrip filter, is usually preferred because of its low cost. Many types of planar filters can be manufactured by cheap PCB, and they can be integrated on the same PCB board to further reduce the extra cost [107], [108]. The SIW or the AFSIW as a waveguide-like structure integrated in planar form can be manufactured by PCB technology and provides a good resonator for filters [71], [109].

The first filter based on the AFSIW technology was proposed in 2015 [8]. The filter inserts a conductive via inside the waveguide to make an inductive post as shown in Fig. 4.2.a. Symmetrical inductive posts were designed based on the inverter theory. In this literature, it shows that the insertion loss of the filter in AFSIW is significantly decreased compared to that of the dielectric-filled SIW counterpart at the expense of an increase in the length of the filter based on the technology of AFSIW.

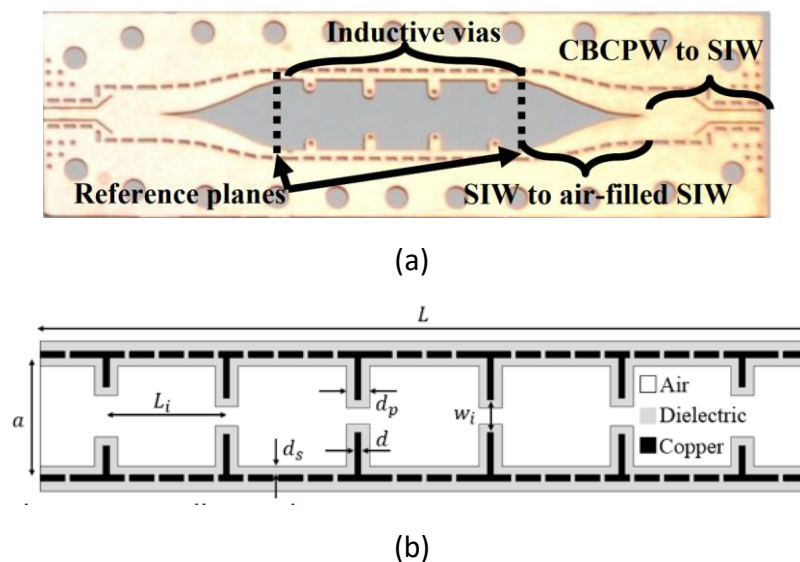


Fig. 4.2 Picture of the air-filled SIW (a) third-order [8] and (b) fifth-order [110] band-pass filter.

Also, with a higher order of the filter, its length increases significantly. For example, a fifth-order air-filled SIW filter shown in Fig. 4.2.b [110] has a length of 46.5 mm, compared to the third-order air-filled SIW filter which is 16.6 mm in length.

To overcome the problem of oversize, different solutions have been proposed [111], namely Partially Air-Filled Substrate Integrated Waveguide Filters [112]–[114], Dielectric Slab Air-Filled Substrate Integrated Waveguide (SAFSIW) [115], AFSIW Filter with Multilayer Cross-Coupling [116], Vertically Stacked SIW Filter [117] all shown in Fig. 4.3.

Because one of the objectives of the thesis is to re-organize the components of the simplified transceiver in three dimensions, the AFSIW Filter with Multilayer Cross-Coupling and the Vertically Stacked SIW Filter are of more interest.

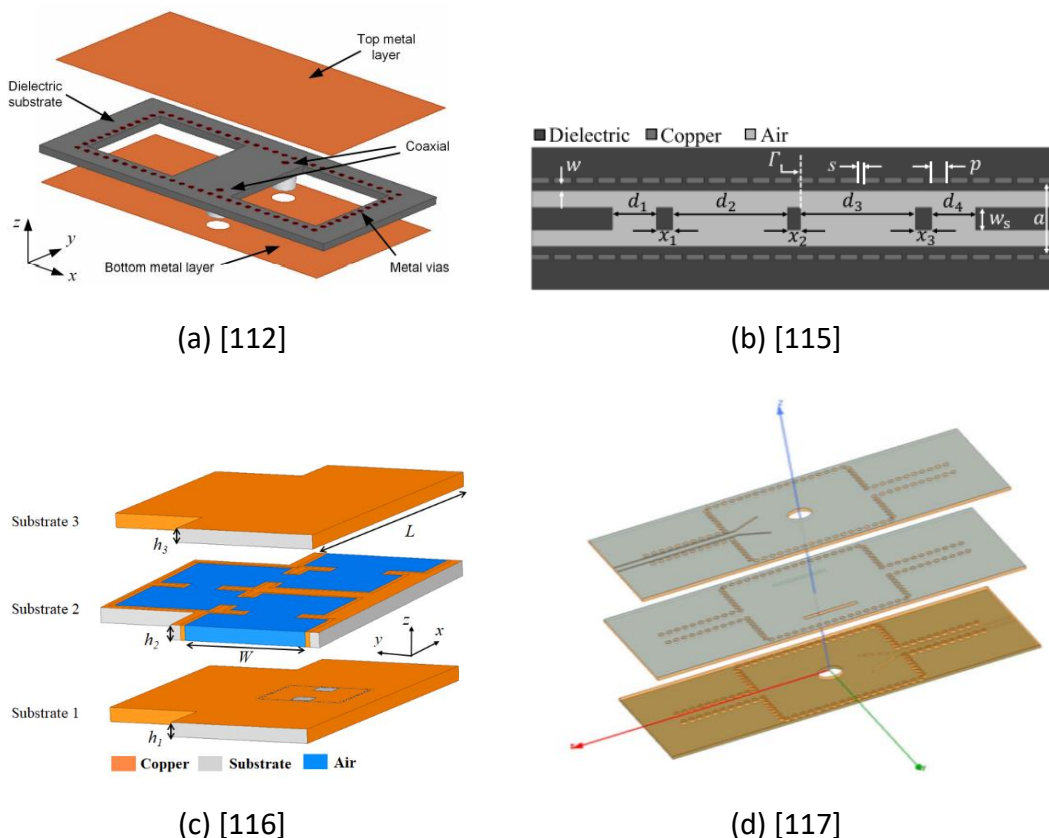


Fig. 4.3 Pictures of filters proposed to overcome the problem of oversize: (a) Partially Air-Filled Substrate Integrated Waveguide Filters [112]; (b) Dielectric Slab Air-Filled Substrate Integrated Waveguide (SAFSIW) [115]; (c) AFSIW Filter with Multilayer Cross-Coupling [116] and (d) Vertically Stacked SIW Filter [117].

In [118], a four-cavity filter simulated in two layers was proposed as shown in Fig. 4.4. One coupling slot is in the center of the cavity between cavities 1 and 4, which is used to generate the transmission zero, and the other is at the end of the cavity between cavities 2 and 3, which is used to transfer the electric field to another layer. By using these slots, the length of this fourth-order filter is greatly reduced.

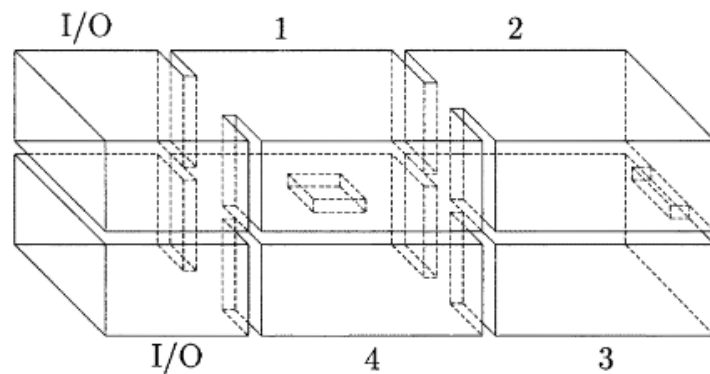


Fig. 4.4 Configuration of the alternative four-cavity filter [118].

The AFSIW filter [116] as shown in the Fig. 4.5 is quite similar to the previous structure when considering the use of multiple layers to realize a coupling between cavities.

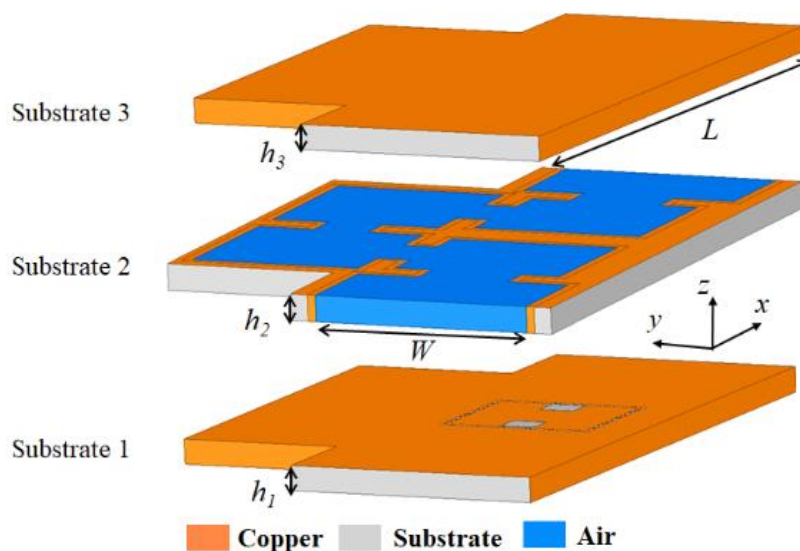


Fig. 4.5 3D view of cross-coupled AFSIW filter [116].

In [116], the advantage of multilayer is used to create the transmission zero in the bottom layer of SIW. Four air resonators are in the hollowed inner middle substrate

(substrate 2) and the phase shift of the cross-coupling is realized by a substrate integrated waveguide (SIW) transmission line in the different substrate (substrate 1). Two slots are used to couple the electric field between the substrate 1 and 2. These four air cavities are also reorganized rather than connected linearly. With these two improvements, this filter not only has the better selectivity around the pass band but also has a smaller footprint compared to its non-cross-coupled counterpart. This filter proposes a possibility of reorganizing the air cavities in the same layer of substrate.

The objective of this chapter is to demonstrate the possibility of reorganization of cavities of the filter. For demonstration purposes, a third-order AFSIW filter with the structure multilayer is proposed, demonstrated and fabricated.

## 4.2 Filter synthesis

The vertical coupling structure for the transition proposed previously can realize the coupling between the quasi-TEM mode and the  $TE_{10}$  mode as well as the coupling between two  $TE_{10}$  modes. The coupling can be adjusted by changing the size and position of the copper patch situated on the inserted substrate. To verify this coupling structure, a multilayer third-order bandpass filter is proposed.

The proposed filter is designed on the basis of a third-order polynomial approximation of the Chebyshev type [119]. The coupling matrix was determined to have a return loss of 22 dB. The coupling topology is shown in Fig. 4.6. The input/output (source/load, "S"/ "L") port and cavity resonator 1/3 situate on one layer of substrate (S2/S6). The cavity resonator 2 situate on another layer (S4). Thanks to the symmetric structure, the coupling between source and cavity resonator 1 is the same as the coupling between load and cavity resonator 3, and the coupling between the cavity resonator 1 and 2 is the same as the coupling between the cavity resonator 3 and 2. The input and output iris is based on the symmetric electrical characteristic equivalence model for a thick iris [119] and two inter-cavity couplings are realized by the vertical coupling structure.

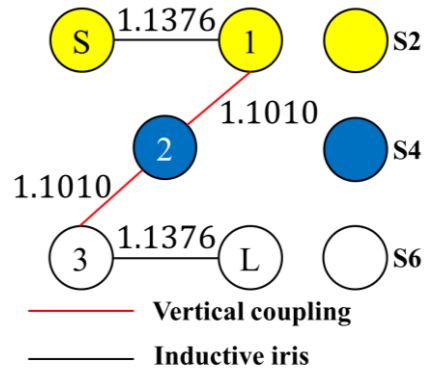


Fig. 4.6 Coupling topology.

For the whole design of the air-filled substrate integrated waveguide filter, only the mode  $TE_{101}$  is considered.

#### 4.2.1 Vertical coupling structure

In order to obtain the coupling between two air cavities of the AFSIW, the structure shown in Fig. 4.7 is proposed.

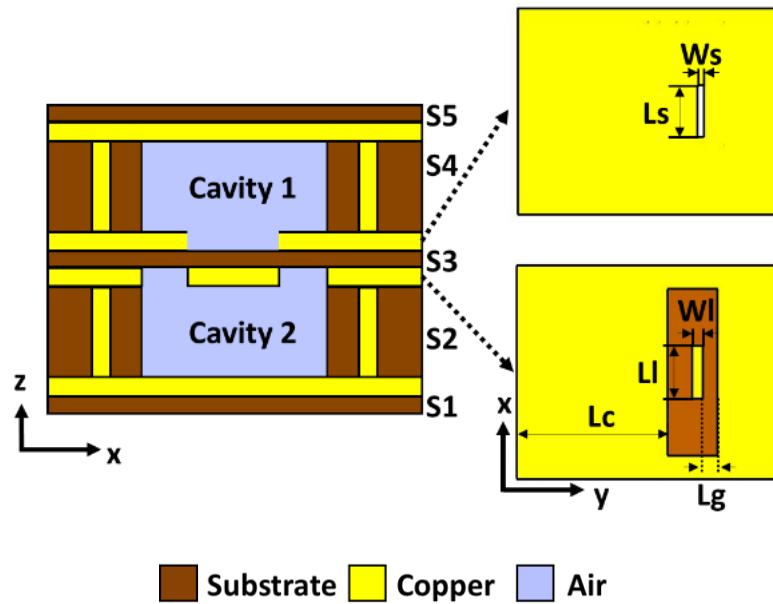


Fig. 4.7 Proposed vertical transition for filter.

The coupling structure corresponds to the asymmetric electrical characteristic equivalence model of thick iris. The K-inverter model is used to determine the dimensions. The design steps for the inter-cavity coupling are as follows:

*a) Step 1: Calculate the coupling matrix*

The coupling matrix given in (4.2.1) for the filter is calculated by [120] with the setup in Tab. 4.1. In order to prove the feasibility of the vertical structure, the filter is designed as the most basic third-order filter.

$$M = \begin{bmatrix} 0 & 1.1376 & 0 & 0 & 0 \\ 1.1376 & 0 & 1.1010 & 0 & 0 \\ 0 & 1.1010 & 0 & 1.1010 & 0 \\ 0 & 0 & 1.1010 & 0 & 1.1376 \\ 0 & 0 & 0 & 1.1376 & 0 \end{bmatrix} \quad (4.2.1)$$

Tab. 4.1 Coupling matrix setup

Return loss	Number of zero transmission	Filter order
-22 dB	0	3

*b) Step 2: Calculate the theoretical K-inverter value*

For TE mode, Inverter values between vertical cavities can be expressed in the following form:

$$\frac{K_{i,i+1}}{Z_0} \approx M_{i,i+1} \frac{\pi W_\lambda}{2} \quad (4.2.2)$$

where  $W_\lambda = \frac{\lambda_{g1} - \lambda_{g2}}{\lambda_{g0}}$  is the guide-wavelength fractional bandwidth,  $\lambda_{g1}$  and  $\lambda_{g2}$  are the guide wavelengths at the band-edge frequencies and  $\lambda_{g0}$  is the guide wavelengths at the central frequency.

In this filter, between the resonators 1 and 2 or 2 and 3, the K is equal to 0.1283.

*c) Step 3: Vary the dimensions until the simulated K-inverter value is equal to or close to the theoretical K-inverter value*

For the asymmetric thick iris, a T-network is chosen as the equivalent circuit as shown in Fig. 4.8 [121].

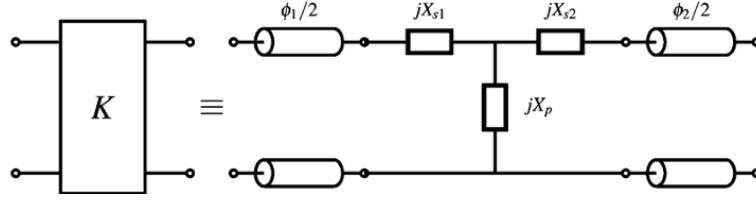


Fig. 4.8 Equivalent T-network for a thick iris.

The normalized values of the T-network elements can be represented by:

$$jX_{s1} = \frac{(1 + S_{11})(1 - S_{22}) + S_{21}^2 - 2S_{21}}{(1 - S_{11})(1 - S_{22}) - S_{21}^2} \quad (4.2.3)$$

$$jX_{s2} = \frac{(1 - S_{11})(1 + S_{22}) + S_{21}^2 - 2S_{21}}{(1 - S_{11})(1 - S_{22}) - S_{21}^2} \quad (4.2.4)$$

$$jX_p = \frac{2S_{21}}{(1 - S_{11})(1 - S_{22}) - S_{21}^2} \quad (4.2.5)$$

$$\phi_1 = -\arctan\left(\frac{\Sigma}{\Pi_-}\right) - \arctan\left(\frac{\Delta}{\Pi_+}\right) \quad (4.2.6)$$

$$\phi_2 = -\arctan\left(\frac{\Sigma}{\Pi_-}\right) + \arctan\left(\frac{\Delta}{\Pi_+}\right) \quad (4.2.7)$$

where

$$\Sigma = X_{s1} + X_{s2} + 2X_p \quad (4.2.8)$$

$$\Delta = X_{s1} - X_{s2} \quad (4.2.9)$$

$$\Pi_+ = 1 + X_{s1}X_{s2} + X_p(X_{s1} + X_{s2}) \quad (4.2.10)$$

$$\Pi_- = 1 - X_{s1}X_{s2} - X_p(X_{s1} + X_{s2}) \quad (4.2.11)$$

Simulated K-inverter value  $K_s$  is obtained using (4.2.3) to (4.2.7) and

$$K_s = \sqrt{\frac{|1 + \Gamma e^{-j\phi_1}|}{|1 - \Gamma e^{-j\phi_1}|}} \quad (4.2.12)$$

where  $\Gamma = \frac{j\Delta - \Pi_+}{j\Sigma + \Pi_-}$ .

The dimensions of the vertical coupling structure are determined by varying each dimension, calculating each  $K_s$ , and thus approximating the theoretical value of  $K$ . All the calculation is realized with the software MATLAB 2021.

Fig. 4.9 shows the influence of each dimension on  $K_s$  which indicates the influence of the coupling for each parameter.

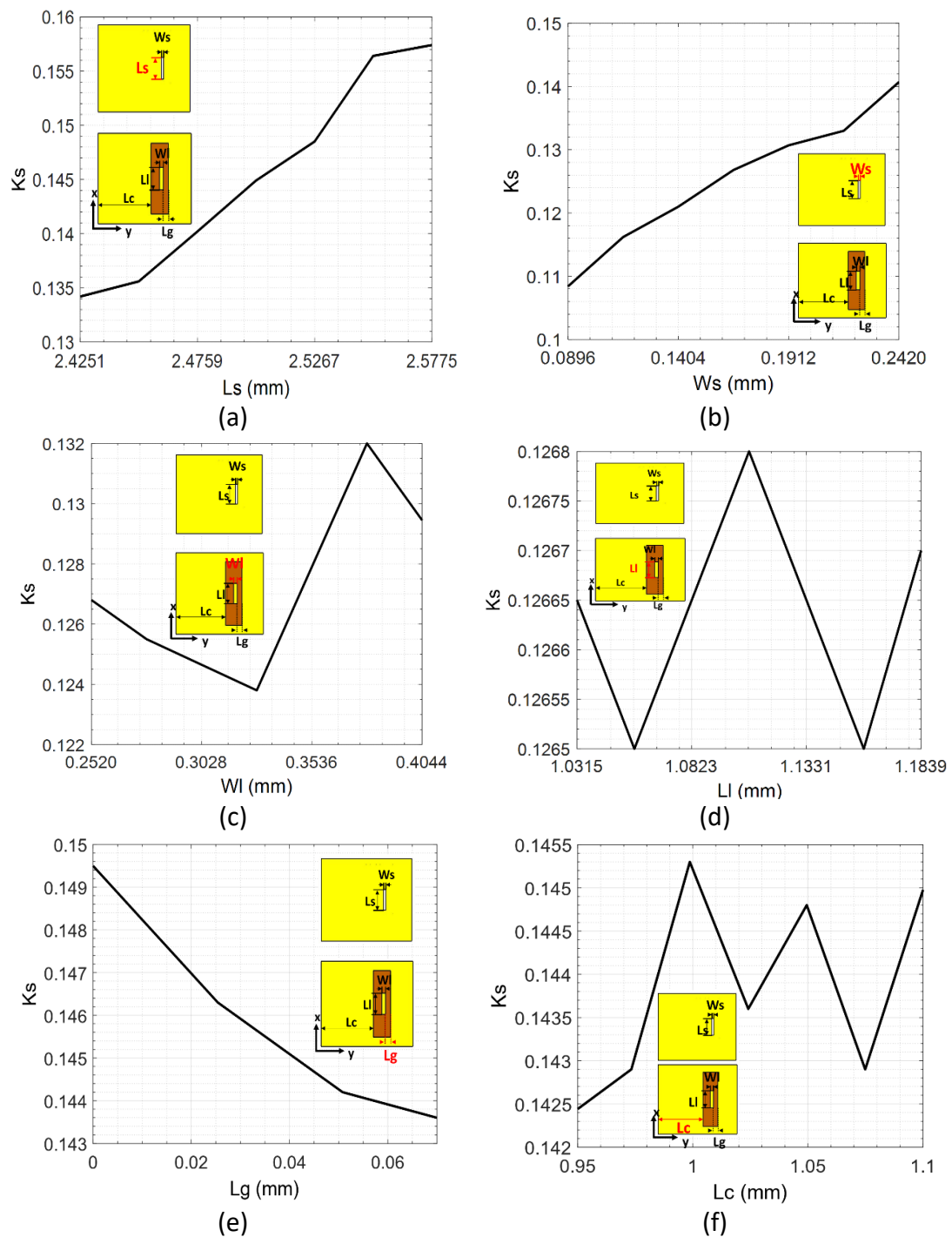


Fig. 4.9 Variation of  $K_s$  for the parameter (a)  $L_s$ ; (b)  $W_s$ ; (c)  $W_l$ ; (d)  $L_l$ ; (e)  $L_g$  and (f)  $L_c$ .

Because the fabrication is based on the unit of mils, the parameters were chosen to vary by 6 mils around the final optimized value except the parameter Lg. The value of the parameter Lg is in the range of 0 to 0.07 mm. As a result of technical manufacturing conditions, the copper patch cannot be too close to the via.

The summary is shown in Tab. 4.2. It can be noted that the size of the slot impact more the coupling between the cavities.

Tab. 4.2 Variation of  $K_s$

Parameter	Ls	Ws	WI	LI	Lg	Lc
Variation	0.0232	0.0323	0.0082	0.0004	0.0059	0.0026

d) *Step 4: Calculate the length of the cavity*

The length of the resonator r can be calculated by using (4.2.6), (4.2.7) and

$$l_r = \frac{\lambda_{g0}}{2\pi} \left[ \pi + \frac{1}{2} (\phi_{r-1} + \phi_r) \right], r = 1, \dots, N \quad (4.2.13)$$

e) *Step 5: Optimize all of the parameters*

By optimization algorithm, the structure size is finally determined as shown in the Tab. 4.3.

Tab. 4.3 Geometry of coupling inter-cavity

Parameters	W <sub>s</sub>	L <sub>s</sub>	WI	LI	Lc	Lg
Dimensions (mm)	0.17	2.50	0.19	1.11	7.47	0.15

#### 4.2.2 Input/Output coupling structure

The input or output iris structure of AFSIW is shown in Fig. 4.10. The thickness of the iris is fixed by the limit of the fabrication.

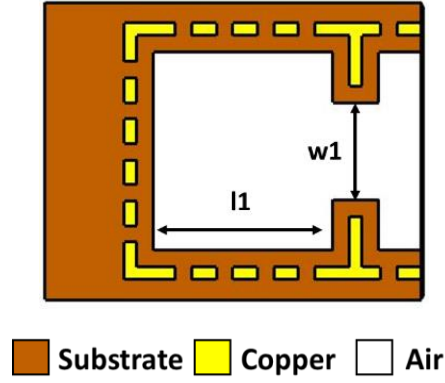


Fig. 4.10 Input/output iris structure.

The design steps for symmetrical iris design are as follows:

a) *Step 1: Calculation of theoretical K-inverter value*

The coupling matrix is calculated in the step 1 of chapter 4.2.1 and the value of coupling matrix between source and cavity 1 ( $M_{S1}$ ) or cavity 3 and load ( $M_{3L}$ ) is 1.1376.

The inverter value of K for input and output can be represented as follows:

$$\frac{K_{S1}}{Z_0} \approx M_{S1} \sqrt{\frac{\pi W_\lambda}{2}} \quad (4.2.14)$$

$$\frac{K_{N,L}}{Z_0} \approx M_{N,L} \sqrt{\frac{\pi W_\lambda}{2}} \quad (4.2.15)$$

where  $W_\lambda = \frac{\lambda_{g1} - \lambda_{g2}}{\lambda_{g0}}$  is the guide-wavelength fractional bandwidth,  $\lambda_{g1}$  and  $\lambda_{g2}$  are the guide wavelengths at the band-edge frequencies and  $\lambda_{g0}$  is the guide wavelengths at the central frequency.

In this filter, between the source and cavity 1 or cavity 3 and load, the K is equal to 0.4124.

b) *Step 2: Vary the dimensions until the simulated K-inverter value is equal to or close to the theoretical K-inverter value*

The input and output iris are based on the symmetric electrical characteristic equivalence model for a thick iris [119] as shown in Fig. 4.11.

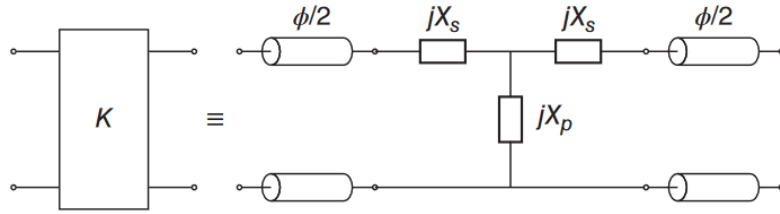


Fig. 4.11 Inverter model (center) for an inductive window in waveguide technology.

The normalized values of the T-network elements can be represented by:

$$jX_s = \frac{1 - S_{12} + S_{11}}{1 - S_{11} + S_{12}} \quad (4.2.16)$$

$$jX_p = \frac{2S_{12}}{(1 - S_{11})^2 - S_{12}^2} \quad (4.2.17)$$

Simulated K-inverter value  $K_s$  is obtained using (4.2.16) to (4.2.17) and

$$K_s = \left| \tan \left[ \frac{\phi}{2} + \arctan(X_s) \right] \right| \quad (4.2.18)$$

$$\phi = -\arctan(2X_p + X_s) - \arctan(X_s) \quad (4.2.19)$$

With each change of parameters  $w_1$ , if  $K_s$  is lower than  $K$ , increase the coupling that's to say open the inductor window (increase the value of  $w_1$ ) and vice versa (shown as Fig. 4.12) until the  $K_s$  approaches the theoretical value of  $K$ .

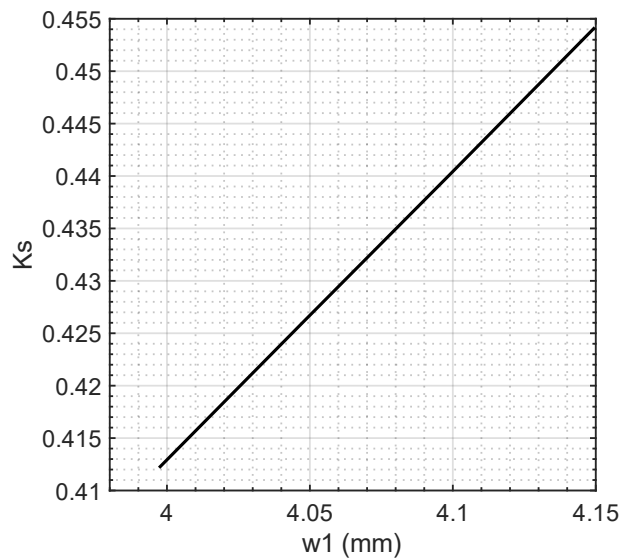


Fig. 4.12 Variation of  $K_s$  for  $w_1$ .

c) Step 3: Calculate the length of the cavity

The length of the resonator  $r$  can be calculated by (4.2.13) and (4.2.19).

d) Step 4: Optimize all of the parameters

By optimization algorithm, the dimensions of the input or output iris structure is shown in the Tab. 4.4.

Tab. 4.4 Geometry of input/output iris.

Parameters	w1	l1
Dimensions(mm)	1.4960	6.3333

#### 4.2.3 Simulation and manufacture

According to the above-mentioned design process, the vertical 3-order passband filter structure is shown in the Fig. 4.13. This filter includes seven substrate layers with the following dimensions in simulation: 7.04 mm (width)  $\times$  2.64 mm (height)  $\times$  11.46 mm (length).

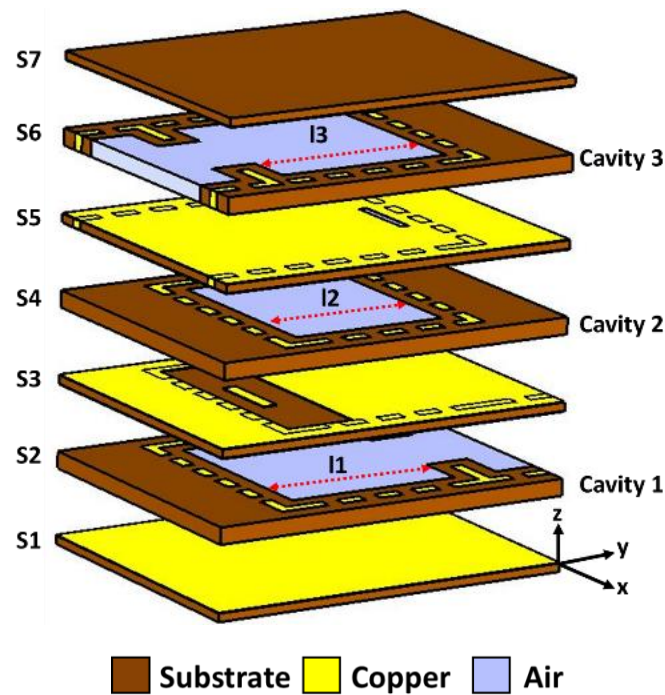


Fig. 4.13 Detailed view of proposed vertical filter.

According to the simulation, with these configurations, the cavities resonate well in the TE<sub>101</sub> mode. The result of the E-field simulation is shown in Fig. 4.14.

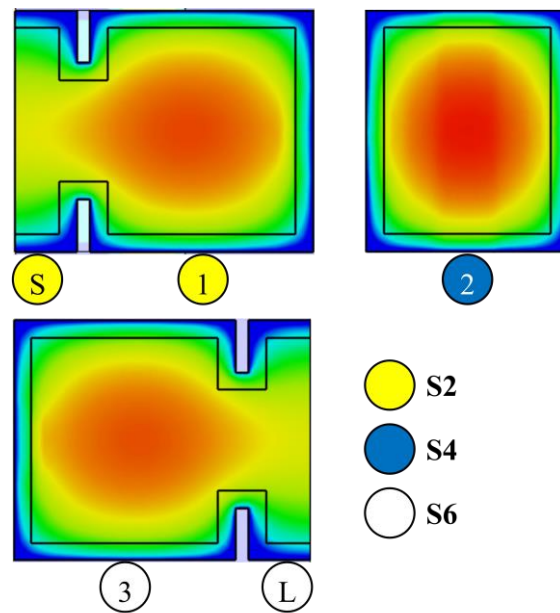


Fig. 4.14 Electric field in the cavity.

The filter frequency response in the simulation is shown in Fig. 4.15.

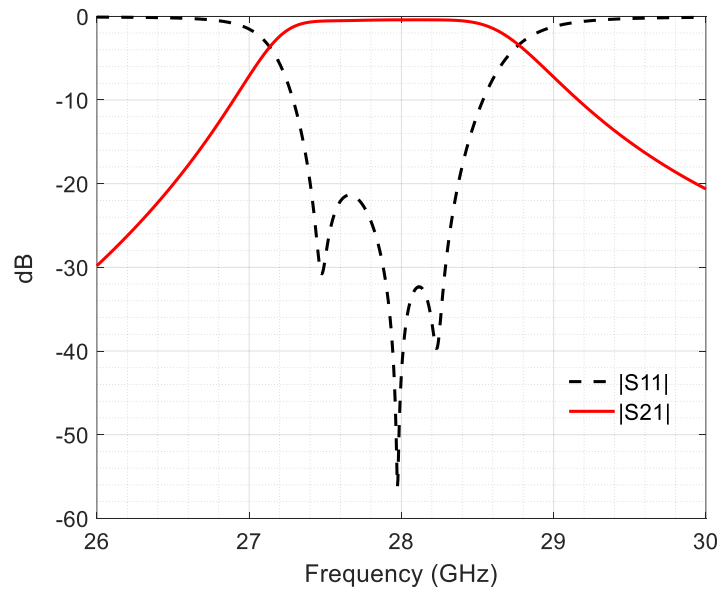


Fig. 4.15 Simulated S-parameters of proposed filter.

It can be noted that the relative bandwidth of -3 dB (BW) at 28 GHz is equal to 6.1% (from 27.2 GHz to 28.9 GHz). The return loss is equal to 23.6 dB while the insertion losses are limited to -0.44 dB in the passband.

But this filter cannot be directly measured because the VNA cannot be directly connected to the waveguide of AFSIW. Therefore, two transitions mentioned in chapter 2 are connected to both ends of the filter for the measurement. The structure of the whole device is shown in Fig. 4.16. With the help of these two transitions, the filter can be connected to the coaxial cable of the VNA. The photo of the fabrication is shown in Fig. 4.17.

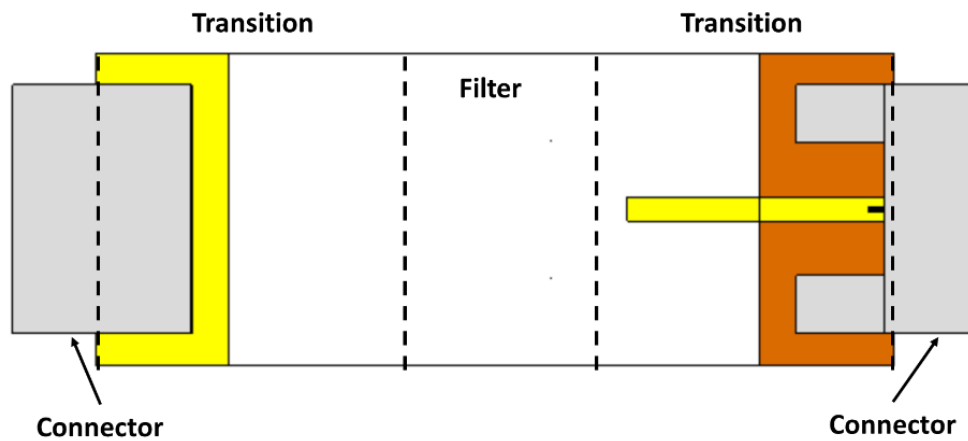
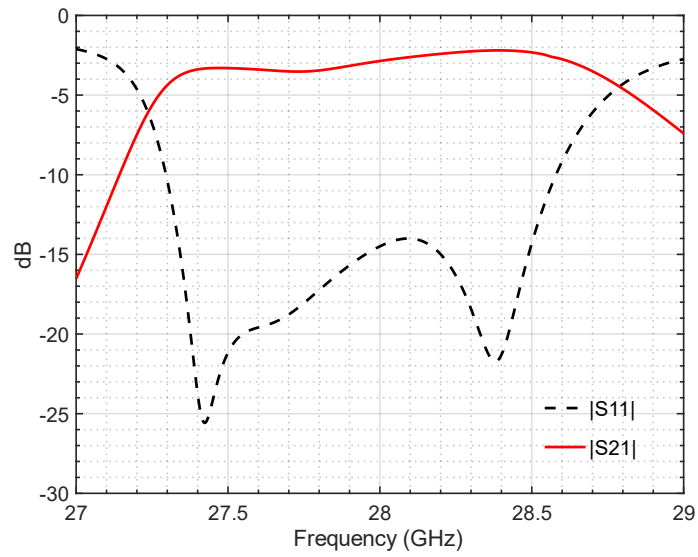


Fig. 4.16 Simulated structure for measurement of proposed filter.

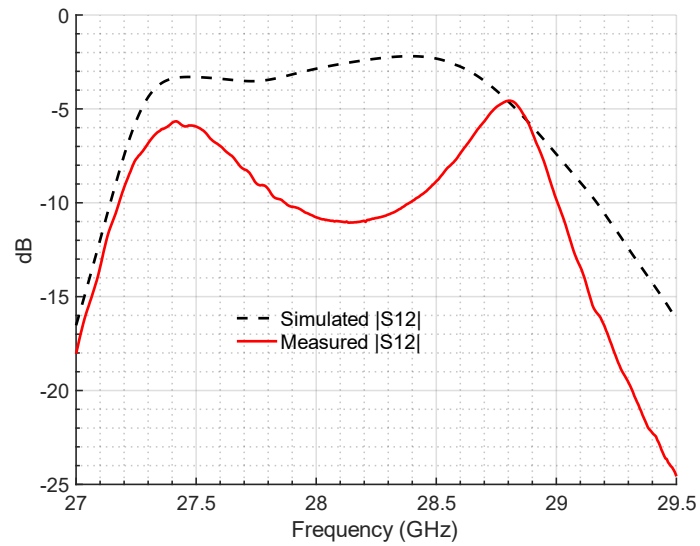
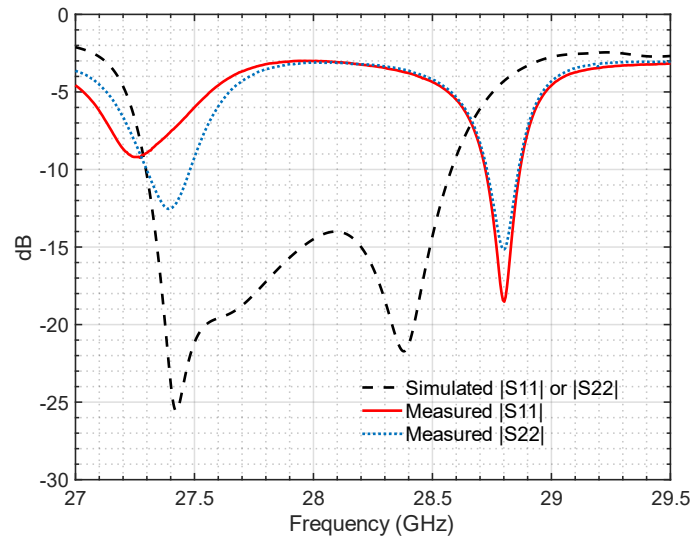


Fig. 4.17 Fabrication of proposed filter.

Fig. 4.18 shows the performance of the proposed filter using two vertical transitions in terms of S-parameters for fabrication and measurement. The used transition has insertion losses between 0.54 dB and 0.77 dB. With a transition and a connector (End Launch Southwest 2.92 mm) connected to the input and output, the whole structure has insertion losses of 3.53 dB with return losses of 14 dB in the simulation. And for the measurement, it can be noted that there was an error in the assemblage.



(a)



(b)

Fig. 4.18 (a) Simulated S-parameters and (b) comparisons of simulated and measured S-parameters of proposed filter.

Due to low human assembly quality, it can be seen from the comparison of measured and simulated results that the coupling of two resonant cavities is too strong. The center pole is offset towards the lower frequencies, as a result, the filter mismatches around 28 GHz.

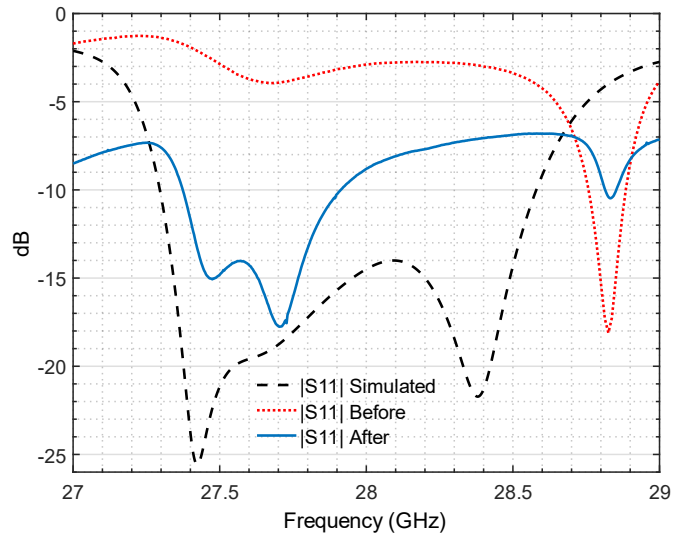
The good phenomenon is that, from the measurement results of  $|S_{12}|$ , it can be seen that the -3dB bandwidth of the filter is close to the simulation results if the mismatch is ignored.

Then in order to compensate for the error, a segment of double-sided conductive self-adhesive is used to change the length of the output and input microstrip lines to tune the input or output coupling. The fabricated filter with correction is shown in Fig. 4.19. The input microstrip line was extended by 1.2 mm.

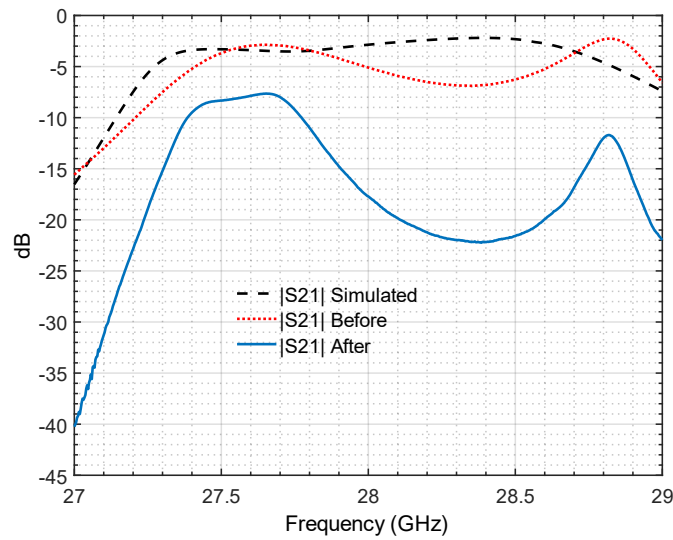


Fig. 4.19 Proposed filter with the correction.

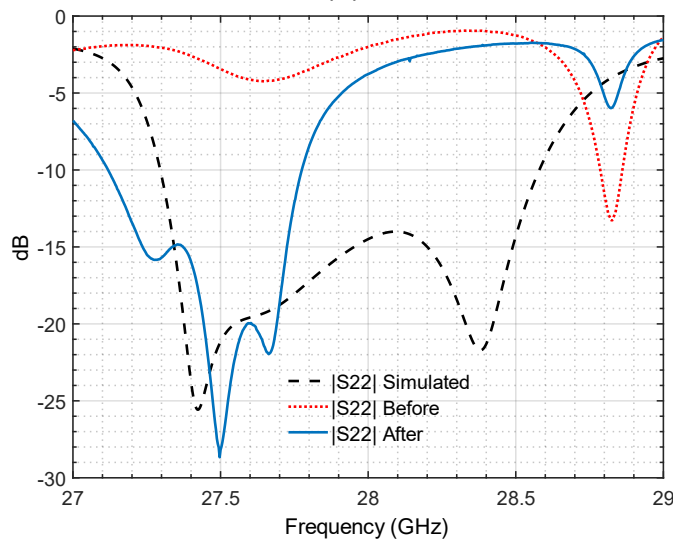
The measurement results and the comparison between simulated, untuned and tuned filters are shown in Fig. 4.20. The tuned results are based on the limits of manual accuracy. It can be noted with the parameters  $S_{11}$  and  $S_{22}$  in Fig. 4.20.a and Fig. 4.20.c that with the correction, the two poles are brought back into the passband. The insertion loss is much lower than the others because the corrected version has been measured without the microstrip line calibration kit.



(a)



(b)



(c)

Fig. 4.20 Comparisons of simulated and measured results with S-parameters of (a) $S_{11}$ ; (b) $S_{21}$ ; (c) $S_{22}$  of proposed filter.

### 4.3 Conclusion

In this chapter, a multilayer filter based on the AFSIW technology is designed, simulated and measured. For the vertical coupling between stacked cavities, it is proved in this chapter that the structure can be synthesized by a T-network for asymmetric thick iris, therefore, the design process is similar to a conventional waveguide filter with the aid of K-inverter model. The design process of inter-cavity coupling and input/output coupling can be summarized by the flow diagram as shown in Fig. 4.21.

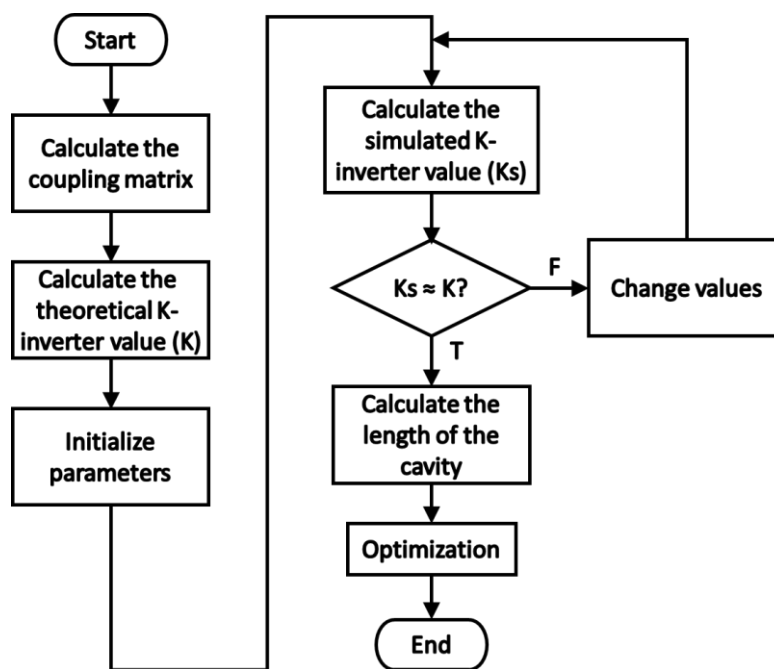


Fig. 4.21 Proposed multilayer filter design approach.

For measurement, two vertical transitions developed in chapter 2 are applied to have access to the VNA. But the whole device has 9 layers and so manual assembly quality gradually decreases. Ultimately, the measurement results of the manufacturing device do not completely match the simulation results. It can be noted in the measured results that around 28 GHz, a mismatch appeared due to the low manual assembly quality between cavities. This result exposes the problem in multi-layer structures: in the assembly of multi-layer vertical structures (such as the 9 layers in this research), the accumulation of low human assembly quality will eventually

cause the device not to work properly. Therefore, more practice with assembly techniques is needed. Comparisons between simulation results without and with transitions and connectors in Fig. 4.15 and Fig. 4.18, show there was a little mismatch in higher frequencies, which can be seen from the result in Fig. 4.18 that the center pole is offset slightly towards the lower frequencies already. Therefore, in order to compensate for low assembly qualities, the first correction was realized by extending the microstrip line with double-sided conductive self-adhesive in Fig. 4.19. Future improvements can be made to make the results as symmetrical as possible while the return loss is acceptable during the simulation.

## CHAPTER 5: SIMPLIFIED TRANSCEIVER

In the previous chapters, the basic components of the simplified transceiver have been designed and measured. In this chapter, all the components: antenna, filter and LNA are assembled together in different layers by transitions to form a simplified transceiver. The schematic is shown in Fig. 5.1.

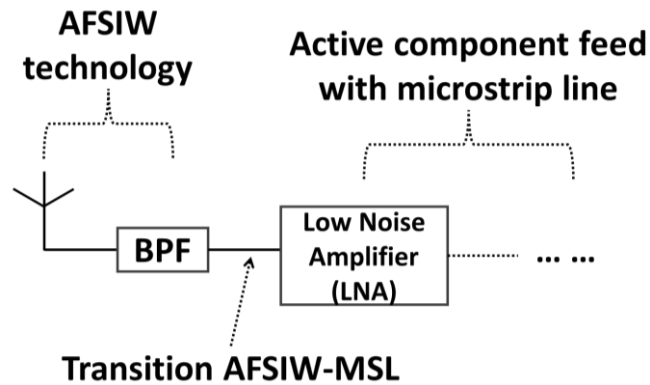


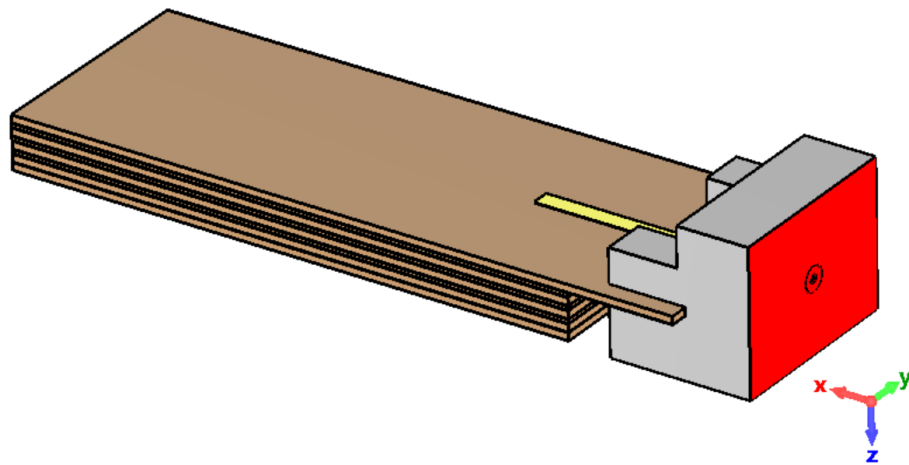
Fig. 5.1 System schematic.

### 5.1 Assembly design

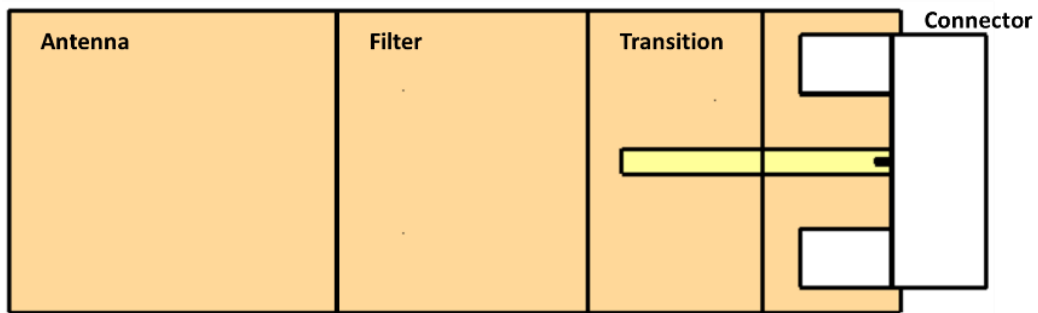
In chapter 3, two antennas have been proposed but for the case of this thesis, the filter with the AFSIW technology is placed behind the antenna. Therefore, the patch antenna is chosen for the final demonstration of the system as it can minimize the system size and it is also more independent of the ground's size. The wave impedance on the side of the AFSIW is the same for the patch antenna and the filter so for the assemblage, the key point lies in the connection of the transition and the filter. The adaptation can be realized by optimizing the relative position of the microstrip line, the slot and the size of the copper patch in the transition.

The simulation model of the system developed in this thesis is shown in Fig. 5.2. This circuit has seven substrate layers. The signal connected with the connector enters the filter by the proposed transition. As presented in chapter 4, this signal is transmitted through three vertical cavities and then enters the feed for the antenna. Finally, the

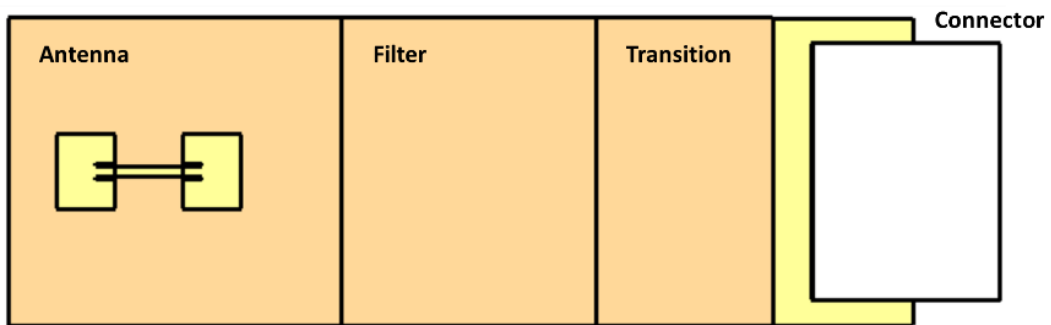
antenna radiates toward the bottom of the system to minimize the impact with the microstrip.



(a)



(b)



(c)

Fig. 5.2 (a) 3D view; (b) top view and (c) bottom view of the system's simulated model.

The trend of the signal can be observed from the E-field simulation shown in Fig. 5.3 and it is shown by the cutting plane according to the XX' axis. According to the E-field,

it can be proved that the signal does have the trend assumed above. The simulated far field result is shown in Fig. 5.4. The antenna has a gain of 8.11 dBi and a total efficiency of 81%.

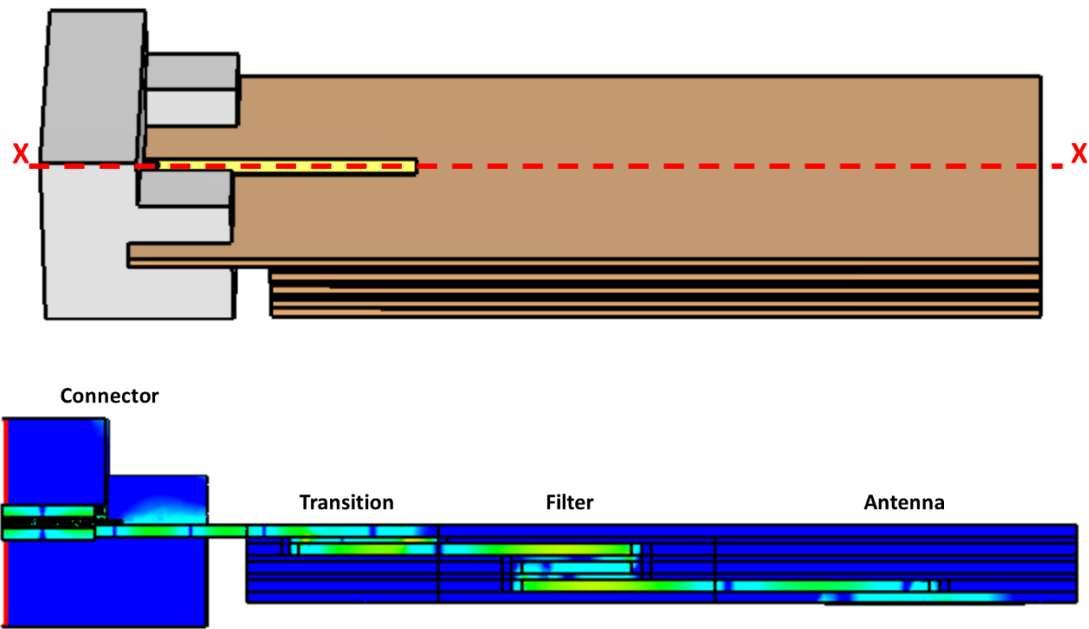


Fig. 5.3 E-field simulation result of the antenna circuit (cross section according to XX').

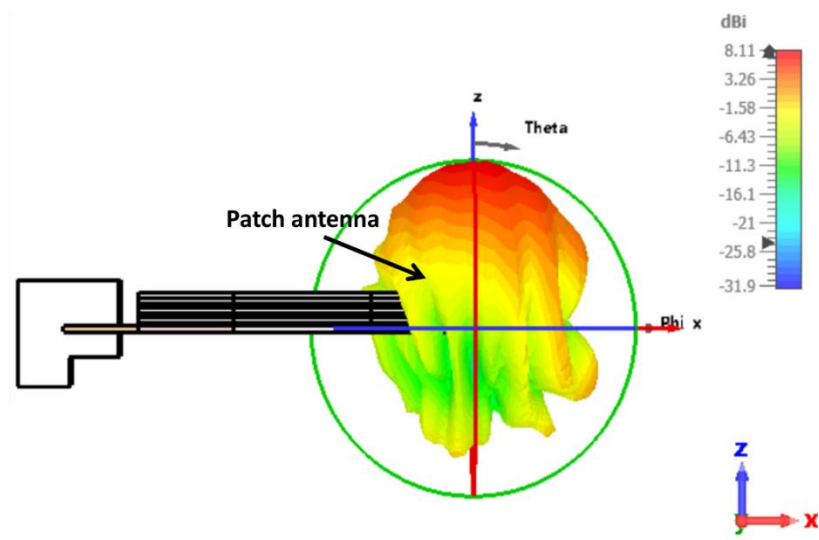


Fig. 5.4 Far field simulation result of the antenna circuit.

## 5.2 Fabrication and measurement

The photo of the fabricated antenna circuit is shown in Fig. 5.5. The radiation patterns were measured in the anechoic chamber shown in Fig. 5.6.a. The proposed system was located at the position of the reception ( $R_x$ ) and it was placed on a support as shown in Fig. 5.6.b. For the S-parameters measurement, blocks of pyramidal absorbers were placed to minimize the radiation interference as shown in Fig. 5.6.c.

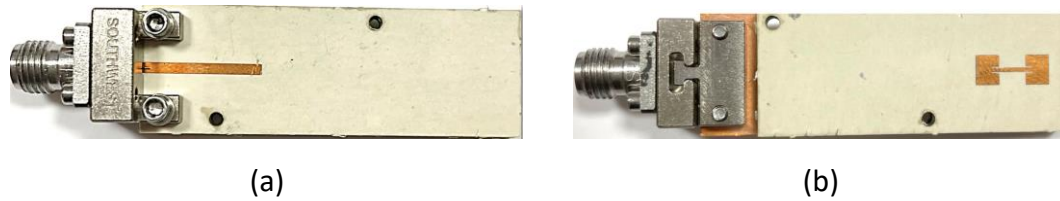


Fig. 5.5 Photos of the (a) front and (b) back of the fabricated antenna circuit.

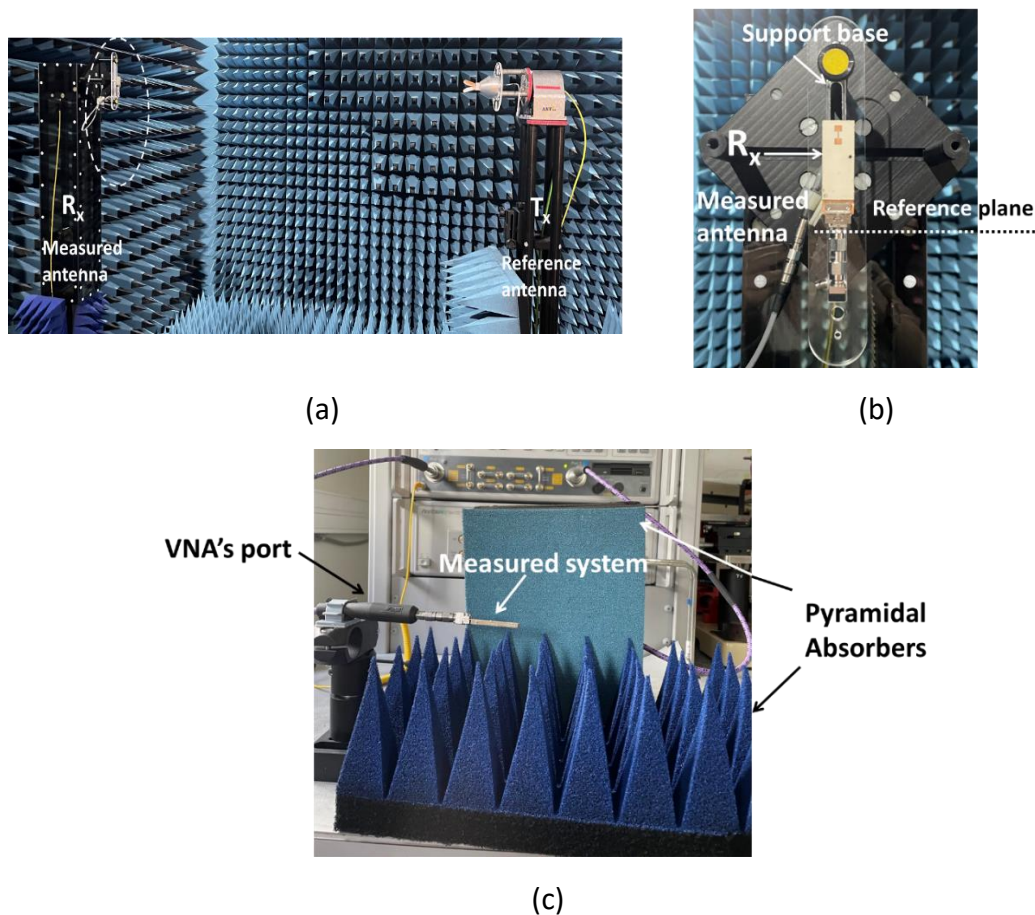


Fig. 5.6 Antenna circuit measurement environment: (a) view in the anechoic chamber; (b) zoom view on the antenna circuit and (c) S-parameters measurement.

The measured S-parameter results compared to the simulated results are shown in Fig. 5.7. It can be noted that the resonant frequency has shifted to low frequency. This error comes from the seven layers of substrate assembly. Therefore, the gain of the antenna is measured at the resonant frequency of 27.3 GHz rather than at 28 GHz for the simulated circuit.

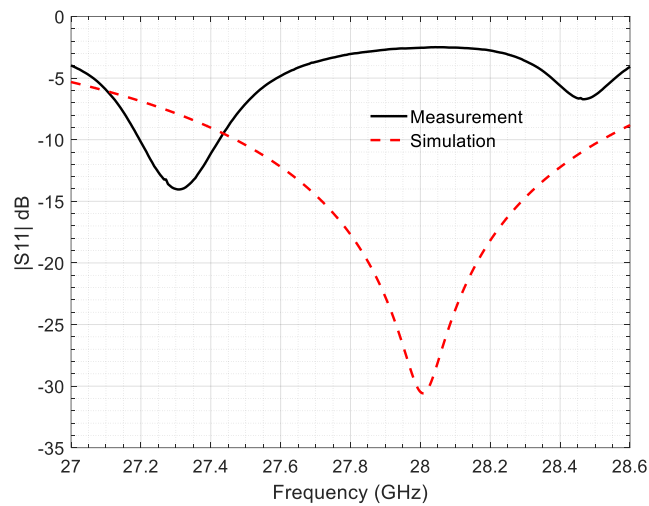


Fig. 5.7 Measured and simulated S-parameter results.

The results of the simulated and the measured radiation patterns are shown in Fig. 5.8. On E-plane, the measured gain is 5 dBi and on H-plane, the measured gain is 6.8 dBi at 27.3 GHz.

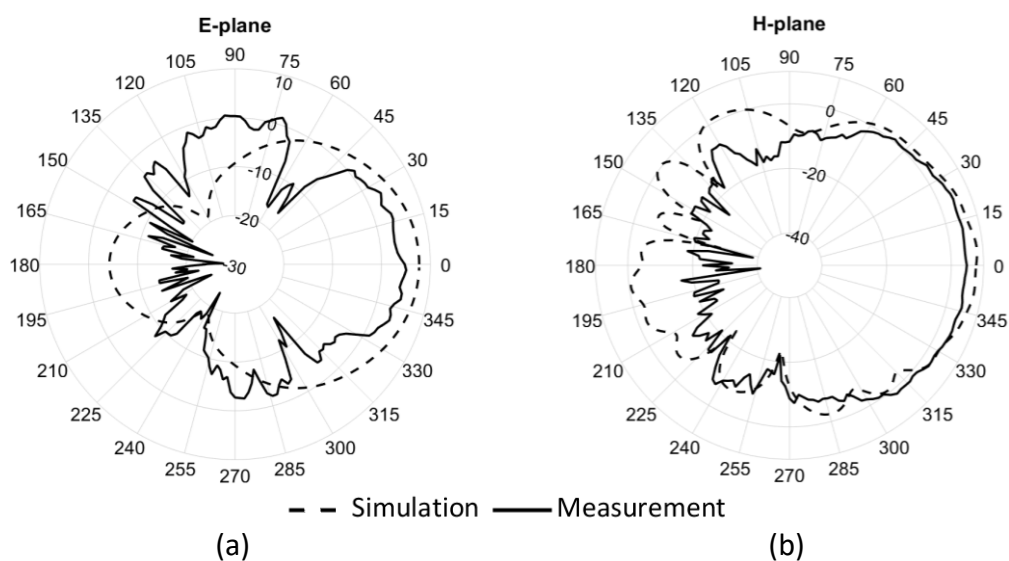


Fig. 5.8 Simulated and measured antenna circuit radiation pattern at their respective resonant frequency (28 GHz and 27.3 GHz) in (a) H-plane and (b) E-plane.

For the amplifier of the simplified transceiver, in this research, the LNA HMC263LP4E fabricated by ANALOG DEVICES is chosen because it has a high gain of 19 - 27 dB within 24 - 36 GHz and its input return loss of 18 dB is the best around 27 GHz. However, within the limited period of the thesis, LNA was not integrated on the same substrate with the rest of the circuit. The performance of the LNA with the rest of the circuit is measured like in Fig. 5.9. The LNA circuit is connected with the other components by a coaxial connector. The bias supply is 5V. The signal sent by the VNA enters the circuit of the LNA through the coaxial cable, and the signal is amplified by the LNA and entered the AFSIW part designed previously by the coaxial cable. The signal then entered the microstrip line through the connector. The signal entering the AFSIW part passed through the vertical filter and was finally radiated by the antenna at the bottom.

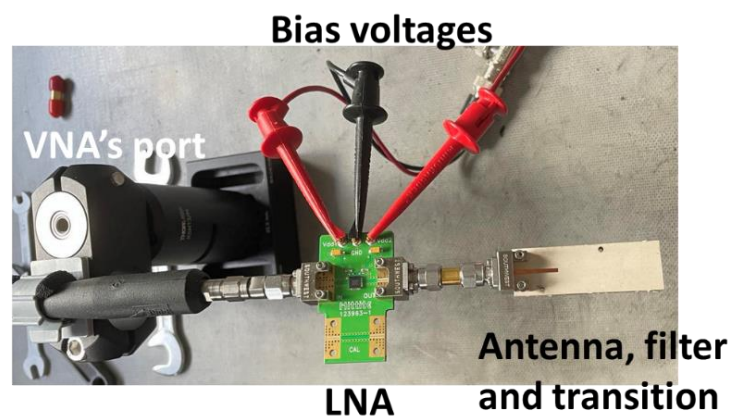


Fig. 5.9 Measurement with the LNA.

The measured S-parameters results are shown in Fig. 5.10. In the results, it can be seen that for the LNA circuit, it has a return loss of -13dB and a gain of 18 dB at the antenna radiation center frequency of 27.3 GHz. This whole circuit has a return loss of -11 dB and a gain of 17 dB. Compared with the circuit containing only LNA and the whole system, at 27.3 GHz, the whole system has a better return loss but it has a slight reduction in gain. Compared with the circuit without LNA and the whole system, the return loss increases by 3 dB due to the return loss of the LNA that can also be marked in Fig. 5.7 and Fig. 5.10.

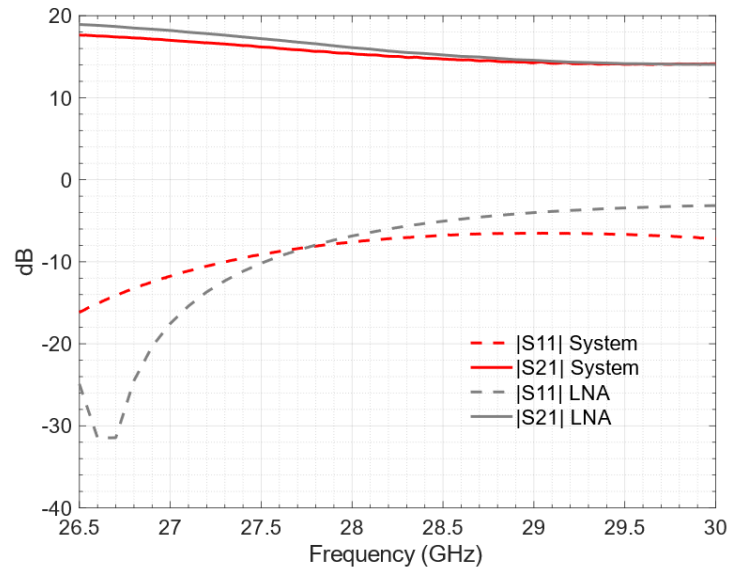


Fig. 5.10 Measured S-parameters results with the LNA.

### 5.3 Conclusion

In this chapter, components of the simplified transceiver circuit have been assembled together. The antenna, filter and LNA are positioned in different layers of substrate. The whole circuit has seven layers and the patch antenna and LNA are in different directions to reduce radiation interference. The whole circuit has seven layers; therefore, the assembly quality is low, which results in the resonant frequency of the circuit being 700 MHz lower than the simulated value. This antenna circuit without LNA resonates at 27.3 GHz with a gain of 5 dBi on E-plane and 6.8 dBi on H-plane. With the LNA connected by a coaxial connector, so far, a simplified transceiver is completed in vertical plane. This simplified transceiver achieves a gain of 17 dB and a return loss of -11 dB at 27.3 GHz.



## CONCLUSION AND PERSPECTIVES

The objective of this thesis is to provide a vertical planar solution for the design of complex circuits. On the one hand, this work realizes the stacking of components based on AFSIW technology and components based on microstrip lines. On the other hand, it realizes the stacking of different cavities in device composed of multiple AFSIW cavities. For the demonstration, a part of a transceiver composed an antenna, a filter and a LNA is designed, fabricated and measured.

The work in this thesis can be summarized as follows:

In chapter 1, the state of the art of satellite communication and the AFSIW technology were presented. For the satellite communication, a general historical review was detailed in chronological order. Different satellite orbits, operation frequency bands and their applications were presented. The general architecture of a satellite includes antennas, transponders, the thermal control, the power supply, the guidance and stabilization, the command and data handling, and the housing. The transceiver in transponder consists of bandpass filter, amplifier, mixer, local oscillator, A/D or D/A and DSP. The research uses the transceiver as the background to demonstrate the advantages of AFSIW technology in vertical system design. The second part of this chapter is an introduction to AFSIW technology. After studying various transmission lines, AFSIW technology was described as an efficient combination between PCB planar transmission lines and metallic waveguides. Performances in terms of transmission loss, power handling capability, Q-factor, size and fabrication complexity were compared between metallic waveguide, planar transmission line, SIW and AFSIW. AFSIW technology has lower transmission loss, higher power handling capability and Q-factor and no dramatic increase in size compared to SIW. The AFSIW technology is widely used in the design of passive components thanks to its above-mentioned advantages. Therefore, this research is dedicated to the system design using AFSIW technology, which realizes the stacking of various components by signal coupling in vertical plane.

In this thesis, the transceiver circuit was used as a carrier to demonstrate the possibility of stacking various devices. For this purpose, in Chapter 2, first, a transition between the AFSIW structure and the microstrip line was proposed. The vertical transition named transition AFSIW-MSL proposed in this research made full use of the upper layer of the AFSIW structure, which is originally only used to close the cavity, to achieve signal coupling. Unlike traditional transitions, it reduced the length of the transition. The microstrip line and the AFSIW cavity were on different substrate layers, so active devices or devices excited by the microstrip line can be stacked on or below the AFSIW structure components. This AFSIW-MSL transition achieved a transmission loss of  $1.16 \pm 0.43$  dB over the frequency range of 27.40 GHz to 29.88 GHz. Compared with the state of the art, this work has acceptable transmission losses in the high frequency band and compared to other transitions, the transition in the vertical plane is a breakthrough and can bring more flexibility to system design.

This transition of two different kinds of ports allows two possibilities for antenna selection. Therefore, in chapter 3, two antennas were designed and proposed for later assembly: a cavity-backed slot antenna fed by microstrip line and a patch antenna fed by AFSIW. The proposed cavity-backed slot antenna achieved a -10dB bandwidth of 420 MHz and a gain of 9.3 dBi at 27.92 GHz. Compared with SIW-based cavity-backed slot antenna, the advantages of AFSIW-based cavity-backed slot antenna is that it has a wider bandwidth. Another proposed antenna is a patch antenna fed by AFSIW. This patch antenna was located in the upper substrate of the AFSIW structure and was fed by the AFSIW cavity below. This antenna was designed on a vertical plane, taking full advantage of the multi-layer structure of AFSIW. The -10 dB bandwidth of this antenna was approximately 6.8% at 27.93 GHz (between 27.02 GHz and 28.95 GHz). It achieved a gain of 7.8 dBi at 28 GHz.

With the same structure of the transition AFSIW-MSL, the coupling can be also realized between AFSIW cavities. A third-order multilayer filter was proposed in chapter 4. This filter had three cavities and each cavity was on a different substrate layer. For the measurement, two transitions proposed before were applied to connect to the VNA. The filter with two transitions had in total 9 layers. This greatly increased the difficulty

of assembly. So unfortunately, due to lack of assembly experience, the accumulation of low human assembly quality in the 9-layer assembly eventually resulted in too strong coupling between two of the resonant cavities, resulting in a mismatched filter around 28GHz. However, it can be seen from the measurement results of  $|S_{12}|$  that if the quality of assembly can be approved, the -3dB bandwidth of the filter matches the simulation results. The first tuning with a segment of double-sided conductive self-adhesive was applied to compensate the error.

In chapter 5, all the components were integrated together to construct a simplified transceiver with the LNA in a vertical plane. The patch antenna fed by AFSIW is directly connected with multilayer filter and a transition AFSIW-MSL was connected at the outlet of the filter. The circuit of LNA was connected with the microstrip line through a coaxial connector due to the limited period of this thesis. Without the LNA, the antenna circuit including an antenna, a filter and a transition achieved a gain of 5 dBi on E-plane and 6.8 dBi on H-plane at 27.3 GHz. In the result, this simplified transceiver has a gain of 17 dB and a return loss of -11 dB behind the LNA at 27.3 GHz which was the resonant frequency of the antenna circuit.

During this thesis research, some contributions in AFSIW technology system design have been made particularly in the reorganization geometrically of the AFSIW system:

A new transition between AFSIW and microstrip line called transition AFSIW-MSL was designed, fabricated and measured. This transition in vertical plane provides the possibilities to connect a AFSIW component with an active device or measurement instruments based on coaxial cable interface in vertical plane to reduce the length of the global system.

Two kinds of antenna named cavity-backed slot antenna and patch antenna fed by AFSIW were proposed to enrich the AFSIW component library and to be used in the vertical system design in this thesis. The cavity-backed slot antenna in AFSIW technology demonstrated that it had a wider bandwidth than the same type of antenna in SIW technology. The patch antenna fed by AFSIW realized a real vertical structure and fit the objective of this thesis.

Using the same structure of transition, a multilayer filter was developed and fabricated. This new filter's three stacked cavities demonstrated the possibilities of the cavity re-organization within an AFSIW component.

A simplified transceiver in AFSIW technology was developed for the first time. In this system, all components are on different layers. This vertical plane organization provides another possibility for system design.

In this period limited thesis, some works have not been completed. Some propositions and some ideas for the improvement are given in follows:

Adjust the filter and connectors to make the return loss more symmetrical so that filter manufacturing is less affected by assembly.

Design the remaining components that make up the transceiver and integrate them into the same integrated circuit.

Combine planar and vertical transitions to limit the length of the device while reducing the error caused by stacking multiple layers of substrate. The final ideal integration circuit will be the same as shown in Fig 6.

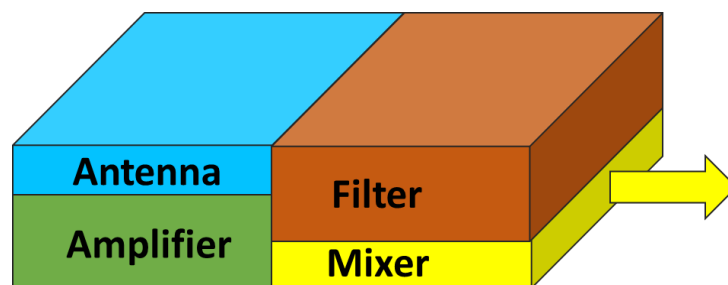


Fig 6. Schematic of the ideal integration circuit.

## References

- [1] J. E. Stutts, "Disposal of PCB transformers: case history," in *Conference Record of 1988 Annual Pulp and Paper Industry Technical Conference*, Jun. 1988, pp. 20–22. doi: 10.1109/PAPCON.1988.10896.
- [2] D. Deslandes and K. Wu, "Integrated microstrip and rectangular waveguide in planar form," *IEEE Microw. Wirel. Compon. Lett.*, vol. 11, no. 2, pp. 68–70, Feb. 2001, doi: 10.1109/7260.914305.
- [3] H. Wang, D.-G. Fang, B. Zhang, and W.-Q. Che, "Dielectric Loaded Substrate Integrated Waveguide (SIW) H-Plane Horn Antennas," *IEEE Trans. Antennas Propag.*, vol. 58, no. 3, pp. 640–647, Mar. 2010, doi: 10.1109/TAP.2009.2039298.
- [4] X.-P. Chen and K. Wu, "Substrate Integrated Waveguide Filters: Design Techniques and Structure Innovations," *IEEE Microw. Mag.*, vol. 15, no. 6, pp. 121–133, Sep. 2014, doi: 10.1109/MMM.2014.2332886.
- [5] J.-X. Chen, W. Hong, Z.-C. Hao, H. Li, and K. Wu, "Development of a low cost microwave mixer using a broad-band substrate integrated waveguide (SIW) coupler," *IEEE Microw. Wirel. Compon. Lett.*, vol. 16, no. 2, pp. 84–86, Feb. 2006, doi: 10.1109/LMWC.2005.863199.
- [6] E. Silavwe, N. Somjit, and I. D. Robertson, "A Microfluidic-Integrated SIW Lab-on-Substrate Sensor for Microliter Liquid Characterization," *IEEE Sens. J.*, vol. 16, no. 21, pp. 7628–7635, Nov. 2016, doi: 10.1109/JSEN.2016.2599099.
- [7] F. Parment, A. Ghiotto, T.-P. Vuong, J.-M. Duchamp, and K. Wu, "Broadband transition from dielectric-filled to air-filled Substrate Integrated Waveguide for low loss and high power handling millimeter-wave Substrate Integrated Circuits," in *2014 IEEE MTT-S International Microwave Symposium (IMS2014)*, Jun. 2014, pp. 1–3. doi: 10.1109/MWSYM.2014.6848524.
- [8] F. Parment, A. Ghiotto, T.-P. Vuong, J.-M. Duchamp, and K. Wu, "Low-loss air-filled Substrate Integrated Waveguide (SIW) band-pass filter with inductive posts," in *2015 European Microwave Conference (EuMC)*, Sep. 2015, pp. 761–764. doi: 10.1109/EuMC.2015.7345875.
- [9] A. Sieganschin, T. Jaschke, and A. Jacob, "A Compact Low-Noise Frontend for Rx/Tx-Integrated SatCom Arrays," Jan. 2021, pp. 820–823. doi: 10.23919/EuMC48046.2021.9338178.
- [10] B. R. Elbert, *The Satellite Communication Applications Handbook, Second Edition*. Artech House, 2004.
- [11] L. Shi, S. Du, Y. Miao, and S. Lan, "Modeling and Performance Analysis of Satellite Network Moving Target Defense System with Petri Nets," *Remote Sens.*, vol. 13, no. 7, Art. no. 7, Jan. 2021, doi: 10.3390/rs13071262.
- [12] A. C. Clarke, "Extraterrestrial radio relays," *Wirel. World*, 1945.

- [13] J. N. Pelton, *Global Communications Satellite Policy: INTELSAT, Politics, and Functionalism*. Lomond Books, 1974.
- [14] J. H. Dellinger, "Analysis of Broadcasting Station Allocation," *Proc. Inst. Radio Eng.*, vol. 16, no. 11, pp. 1477–1485, Nov. 1928, doi: 10.1109/JRPROC.1928.221330.
- [15] R. Beyer and M. GbR, "CAD OF WAVEGUIDE COMPONENTS FOR ANTENNA FEED SYSTEMS: STATE-OF-THE-ART Invited paper," 2001. Accessed: Jul. 10, 2023. [Online]. Available: <https://www.semanticscholar.org/paper/CAD-OF-WAVEGUIDE-COMPONENTS-FOR-ANTENNA-FEED-paper-Beyer-GbR/17c3148878a63f8de7f78b5283f9162e8e24595e>
- [16] R. Fletcher and J. Han, "Low-cost differential front-end for Doppler radar vital sign monitoring," in *2009 IEEE MTT-S International Microwave Symposium Digest*, Jun. 2009, pp. 1325–1328. doi: 10.1109/MWSYM.2009.5165949.
- [17] Lord Rayleigh, "XVIII. On the passage of electric waves through tubes, or the vibrations of dielectric cylinders," *Lond. Edinb. Dublin Philos. Mag. J. Sci.*, vol. 43, no. 261, pp. 125–132, Feb. 1897, doi: 10.1080/14786449708620969.
- [18] K. S. Packard, "The Origin of Waveguides: A Case of Multiple Rediscovery," *IEEE Trans. Microw. Theory Tech.*, vol. 32, no. 9, pp. 961–969, Sep. 1984, doi: 10.1109/TMTT.1984.1132809.
- [19] V. E. Boria and B. Gimeno, "Waveguide filters for satellites," *IEEE Microw. Mag.*, vol. 8, no. 5, pp. 60–70, Oct. 2007, doi: 10.1109/MMM.2007.903649.
- [20] G. Zhao, C. Wen, and Y. Liu, "Design of A Terahertz Waveguide Bidirectional Coupler," in *2020 International Conference on Microwave and Millimeter Wave Technology (ICMMT)*, Sep. 2020, pp. 1–3. doi: 10.1109/ICMMT49418.2020.9387019.
- [21] D. M. Pozar, *Microwave Engineering, 4th Edition*. Wiley, 2011.
- [22] P. Scholar, "Simulation Study on Insertion and Return Loss of Planar Transmission Lines for Different Dielectric Substrates," 2015.
- [23] Y. Y. Wang, G. L. Wang, and Y. H. Shu, "Analysis and synthesis equations for edge-coupled suspended substrate microstrip line," in *IEEE MTT-S International Microwave Symposium Digest*, Jun. 1989, pp. 1123–1126 vol.3. doi: 10.1109/MWSYM.1989.38920.
- [24] J. A. Kostriza, "Microstrip Components," *Proc. IRE*, vol. 40, no. 12, pp. 1658–1663, Dec. 1952, doi: 10.1109/JRPROC.1952.274146.
- [25] C. P. Wen, "Coplanar Waveguide: A Surface Strip Transmission Line Suitable for Nonreciprocal Gyromagnetic Device Applications," *IEEE Trans. Microw. Theory Tech.*, vol. 17, no. 12, pp. 1087–1090, Dec. 1969, doi: 10.1109/TMTT.1969.1127105.

- [26] R. Garg and K. C. Gupta, "Expressions for Wavelength and Impedance of a Slotline (Letters)," *IEEE Trans. Microw. Theory Tech.*, vol. 24, no. 8, pp. 532–532, Aug. 1976, doi: 10.1109/TMTT.1976.1128905.
- [27] H. Howe, "Microwave Integrated Circuits - An Historical Perspective," *IEEE Trans. Microw. Theory Tech.*, vol. 32, no. 9, pp. 991–996, Sep. 1984, doi: 10.1109/TMTT.1984.1132812.
- [28] C. P. Wen, "Coplanar Waveguide: A Surface Strip Transmission Line Suitable for Nonreciprocal Gyromagnetic Device Applications," *IEEE Trans. Microw. Theory Tech.*, vol. 17, no. 12, pp. 1087–1090, Dec. 1969, doi: 10.1109/TMTT.1969.1127105.
- [29] E. A. Mariani, C. P. Heinzman, J. P. Agrios, and S. B. Cohn, "Slot Line Characteristics," *IEEE Trans. Microw. Theory Tech.*, vol. 17, no. 12, pp. 1091–1096, Dec. 1969, doi: 10.1109/TMTT.1969.1127106.
- [30] K. Wu, D. Deslandes, and Y. Cassivi, "The substrate integrated circuits - a new concept for high-frequency electronics and optoelectronics," in *6th International Conference on Telecommunications in Modern Satellite, Cable and Broadcasting Service, 2003. TELSIKS 2003.*, Oct. 2003, p. P-III. doi: 10.1109/TELSKS.2003.1246173.
- [31] K. Wu, D. Deslandes, and Y. Cassivi, "The substrate integrated circuits - a new concept for high-frequency electronics and optoelectronics," in *6th International Conference on Telecommunications in Modern Satellite, Cable and Broadcasting Service, 2003. TELSIKS 2003.*, Oct. 2003, p. P-III. doi: 10.1109/TELSKS.2003.1246173.
- [32] D. Deslandes, M. Bozzi, P. Arcioni, and K. Wu, "Substrate integrated slab waveguide (SISW) for wideband microwave applications," in *IEEE MTT-S International Microwave Symposium Digest, 2003*, Jun. 2003, pp. 1103–1106 vol.2. doi: 10.1109/MWSYM.2003.1212561.
- [33] F. Xu and K. Wu, "Substrate Integrated Nonradiative Dielectric Waveguide Structures Directly Fabricated on Printed Circuit Boards and Metallized Dielectric Layers," *IEEE Trans. Microw. Theory Tech.*, vol. 59, no. 12, pp. 3076–3086, Dec. 2011, doi: 10.1109/TMTT.2011.2168969.
- [34] A. Patrovsky and K. Wu, "Substrate integrated image guide (SIIG)-a planar dielectric waveguide technology for millimeter-wave applications," *IEEE Trans. Microw. Theory Tech.*, vol. 54, no. 6, pp. 2872–2879, Jun. 2006, doi: 10.1109/TMTT.2006.875461.
- [35] Y. Ding and K. Wu, "A 4 × 4 Ridge Substrate Integrated Waveguide (RSIW) Slot Array Antenna," *IEEE Antennas Wirel. Propag. Lett.*, vol. 8, pp. 561–564, 2009, doi: 10.1109/LAWP.2009.2021006.
- [36] Y. Zhang *et al.*, "Slow Wave Substrate-Integrated Waveguide With Miniaturized Dimensions and Broadened Bandwidth," *IEEE Trans. Microw. Theory Tech.*, vol. 69, no. 8, pp. 3675–3683, Aug. 2021, doi: 10.1109/TMTT.2021.3074170.
- [37] F. Parment, "High performance multilayer Substrate Integrated Waveguide (SIW) technics for low-cost millimeter-wave circuits," phdthesis, Université

- Grenoble Alpes, 2016. Accessed: Jun. 11, 2023. [Online]. Available: <https://theses.hal.science/tel-01505416>
- [38] N. Ranjesh and M. Shahabadi, "Reduction of dielectric losses in substrate integrated waveguide," *Electron. Lett.*, vol. 42, pp. 1230–1231, Nov. 2006, doi: 10.1049/el:20061870.
- [39] A. Ghiotto, F. Parment, T.-P. Vuong, and K. Wu, "Millimeter-Wave Air-Filled SIW Antipodal Linearly Tapered Slot Antenna," *IEEE Antennas Wirel. Propag. Lett.*, vol. 16, pp. 768–771, 2017, doi: 10.1109/LAWP.2016.2602280.
- [40] M. Adhikary, A. Sarkar, A. Sharma, A. Biswas, and M. J. Akhtar, "TE<sub>20</sub> Mode Air Filled SIW based Balun Bandpass Filter," in *2018 International Symposium on Antennas and Propagation (ISAP)*, Oct. 2018, pp. 1–2.
- [41] F. Parment, A. Ghiotto, T.-P. Vuong, J.-M. Duchamp, and K. Wu, "Air-to-Dielectric-Filled Two-Hole Substrate-Integrated Waveguide Directional Coupler," *IEEE Microw. Wirel. Compon. Lett.*, vol. 27, no. 7, pp. 621–623, Jul. 2017, doi: 10.1109/LMWC.2017.2711525.
- [42] N.-H. Nguyen, A. Ghiotto, T. Martin, A. Vilcot, K. Wu, and T.-P. Vuong, "Fabrication-Tolerant Broadband Air-Filled SIW Isolated Power Dividers/Combiners," *IEEE Trans. Microw. Theory Tech.*, vol. 69, no. 1, pp. 603–615, Jan. 2021, doi: 10.1109/TMTT.2020.3031924.
- [43] N.-H. Nguyen, A. Ghiotto, A. Vilcot, K. Wu, and T. P. Vuong, "Self-matching Self-compensating Air-filled Substrate Integrated Waveguide (AFSIW) Phase Shifter," in *2022 IEEE MTT-S International Conference on Numerical Electromagnetic and Multiphysics Modeling and Optimization (NEMO)*, Jul. 2022, pp. 1–4. doi: 10.1109/NEMO51452.2022.10038524.
- [44] V. I. Gvozdev and E. I. Nefedov, "Three-dimensional microwave integrated circuits," *Mosc. Izd. Nauka*, Jan. 1985, Accessed: Jan. 24, 2023. [Online]. Available: <https://ui.adsabs.harvard.edu/abs/1985MolzN....V....G>
- [45] V. I. Gvozdev, Yu. V. Gulyaev, and E. I. Nefedov, "Possible use of the principles of three-dimensional integrated microwave circuits in the design of ultrafast digital computers," *Sov. Phys. Dokl.*, vol. 31, p. 760, Sep. 1986.
- [46] V. I. Gvozdev, G. A. Kuzaev, E. I. Nefedov, and A. A. Yashin, "Physical principles of the modeling of three-dimensional microwave and extremely high frequency integrated circuits," *Sov. Phys. Uspekhi*, vol. 35, no. 3, p. 212, Mar. 1992, doi: 10.1070/PU1992v035n03ABEH002223.
- [47] V. I. Gvozdev and E. I. Nefedov, "Some possibilities of three-dimensional integrated UHF structures," *Sov. Phys. Dokl.*, vol. 27, p. 959, Nov. 1982.
- [48] J. S. Izadian and S. M. Izadian, *Microwave Transition Design*. Artech House, 1988.
- [49] A. Pandey, "Waveguide to Microstrip Line Transitions: Different Types of Designs for mmWave Applications," Feb. 2020.

- [50] V. Furtula and M. Salewski, "W-band waveguide bandpass filter with E-plane cut," *Rev. Sci. Instrum.*, vol. 85, no. 7, p. 074703, Jul. 2014, doi: 10.1063/1.4889875.
- [51] H.-W. Yao, A. Abdelmonem, J.-F. Liang, and K. A. Zaki, "Analysis and design of microstrip-to-waveguide transitions," *IEEE Trans. Microw. Theory Tech.*, vol. 42, no. 12, pp. 2371–2380, Dec. 1994, doi: 10.1109/22.339769.
- [52] J. Li, W. Shao, J. Chen, and L. Xue, "A Novel Waveguide-to-Microstrip Transition for Millimeter-Wave Applications," *Int. J. Infrared Millim. Waves*, vol. 25, no. 3, pp. 513–521, Mar. 2004, doi: 10.1023/B:IJIM.0000019318.75753.e2.
- [53] Y. Lou, Q. Xue, and C. H. Chan, "A Broadband Waveguide-to-Microstrip Transition/Power Splitter Using Finline Arrays," *IEEE Microw. Wirel. Compon. Lett.*, vol. 17, no. 4, pp. 310–312, Apr. 2007, doi: 10.1109/LMWC.2007.892993.
- [54] Y. Lou, C. H. Chan, and Q. Xue, "An In-Line Waveguide-to-Microstrip Transition Using Radial-Shaped Probe," *IEEE Microw. Wirel. Compon. Lett.*, vol. 18, no. 5, pp. 311–313, May 2008, doi: 10.1109/LMWC.2008.922114.
- [55] J. Xu, S. Wang, and M. Wang, "Compact in-line waveguide-to-microstrip coaxial probe transition for millimeter-wave," in *2009 Asia Pacific Microwave Conference*, Dec. 2009, pp. 705–707. doi: 10.1109/APMC.2009.5384235.
- [56] N. Tuan, K. Sakakibara, and N. Kikuma, "Bandwidth Extension of Planar Microstrip-to-Waveguide Transition by Controlling Transmission Modes Through Via-Hole Positioning in Millimeter-Wave Band," *IEEE Access*, vol. PP, pp. 1–1, Nov. 2019, doi: 10.1109/ACCESS.2019.2952073.
- [57] A. U. Zaman, V. Vassilev, P.-S. Kildal, and H. Zirath, "Millimeter Wave E-Plane Transition From Waveguide to Microstrip Line With Large Substrate Size Related to MMIC Integration," *IEEE Microw. Wirel. Compon. Lett.*, vol. 26, no. 7, pp. 481–483, Jul. 2016, doi: 10.1109/LMWC.2016.2574995.
- [58] Y.-C. Leong and S. Weinreb, "Full band waveguide-to-microstrip probe transitions," in *1999 IEEE MTT-S International Microwave Symposium Digest (Cat. No.99CH36282)*, Jun. 1999, pp. 1435–1438 vol.4. doi: 10.1109/MWSYM.1999.780219.
- [59] L. Hyvonen and A. Hujanen, "A compact MMIC-compatible microstrip to waveguide transition," in *1996 IEEE MTT-S International Microwave Symposium Digest*, Jun. 1996, pp. 875–878 vol.2. doi: 10.1109/MWSYM.1996.511077.
- [60] H. Iizuka, T. Watanabe, and K. Nishikawa, "Millimeter-wave microstrip line to waveguide transition fabricated on a single layer dielectric substrate," *IEICE Trans. Commun.*, vol. vol.85, pp. 1169–1177, Jun. 2002.
- [61] H. Aliakbarian *et al.*, "Fully micromachined W-band rectangular waveguide to grounded coplanar waveguide transition," *IET Microw. Antennas Propag.*, vol. 6, no. 5, p. 533, 2012, doi: 10.1049/iet-map.2011.0301.
- [62] H. Nam, T.-S. Yun, K.-B. Kim, K.-C. Yoon, and J.-C. Lee, "Ku-band transition between microstrip and substrate integrated waveguide (SIW)," in *2005 Asia-*

*Pacific Microwave Conference Proceedings*, Dec. 2005, p. 4 pp.-. doi: 10.1109/APMC.2005.1606310.

- [63] Y. Ding and K. Wu, "Substrate Integrated Waveguide-to-Microstrip Transition in Multilayer Substrate," in *2007 IEEE/MTT-S International Microwave Symposium*, Jun. 2007, pp. 1555–1558. doi: 10.1109/MWSYM.2007.380571.
- [64] A. Belenguer, H. Esteban, and V. E. Boria, "Novel Empty Substrate Integrated Waveguide for High-Performance Microwave Integrated Circuits," *IEEE Trans. Microw. Theory Tech.*, vol. 62, no. 4, pp. 832–839, Apr. 2014, doi: 10.1109/TMTT.2014.2309637.
- [65] H. Esteban, A. Belenguer, J. R. Sánchez, C. Bachiller, and V. E. Boria, "Improved Low Reflection Transition From Microstrip Line to Empty Substrate-Integrated Waveguide," *IEEE Microw. Wirel. Compon. Lett.*, vol. 27, no. 8, pp. 685–687, Aug. 2017, doi: 10.1109/LMWC.2017.2724011.
- [66] Tsung-Hsun Yang, Chi-Feng Chen, Ting-Yi Huang, Chun-Long Wang, and Ruey-Beei Wu, "A 60GHz LTCC Transition between Microstrip Line and Substrate Integrated Waveguide," in *2005 Asia-Pacific Microwave Conference Proceedings*, Suzhou, China: IEEE, 2005, pp. 1–3. doi: 10.1109/APMC.2005.1606294.
- [67] C. Yau, T.-Y. Huang, T.-M. Shen, H.-Y. Chien, and R.-B. Wu, "Design of 30GHz Transition between Microstrip Line and Substrate Integrated Waveguide," in *2007 Asia-Pacific Microwave Conference*, 2007, pp. 1–4. doi: 10.1109/APMC.2007.4554565.
- [68] A. Belenguer, J. A. Ballesteros, M. D. Fernandez, H. E. González, and V. E. Boria, "Versatile, Error-Tolerant, and Easy to Manufacture Through-Wire Microstrip-to-ESIW Transition," *IEEE Trans. Microw. Theory Tech.*, vol. 68, no. 6, pp. 2243–2250, Jun. 2020, doi: 10.1109/TMTT.2020.2984474.
- [69] T.-Y. Huang, T.-M. Shen, and R.-B. Wu, "Design and Modeling of Microstrip Line to Substrate Integrated Waveguide Transitions," in *Passive Microwave Components and Antennas*, V. Zhurbenko, Ed., InTech, 2010. doi: 10.5772/9418.
- [70] C.-W. Ting, K.-C. Chen, S. Chen, and T.-L. Wu, "A mm-Wave Low-Loss Transition from Microstrip Line to Air-Filled Substrate Integrated Waveguide on Printed Circuit Board Technology," in *2019 Electrical Design of Advanced Packaging and Systems (EDAPS)*, KAOHSIUNG, Taiwan: IEEE, Dec. 2019, pp. 1–3. doi: 10.1109/EDAPS47854.2019.9011622.
- [71] D. Deslandes and K. Wu, "Integrated microstrip and rectangular waveguide in planar form," *IEEE Microw. Wirel. Compon. Lett.*, vol. 11, no. 2, pp. 68–70, Feb. 2001, doi: 10.1109/7260.914305.
- [72] I. BAHL and T. DK, "A DESIGNER'S GUIDE TO MICROSTRIP LINE.," *Des. GUIDE MICROSTRIP LINE*, 1977.
- [73] F. Parment, A. Ghiotto, T.-P. Vuong, J.-M. Duchamp, and K. Wu, "Broadband transition from dielectric-filled to air-filled Substrate Integrated Waveguide for low loss and high power handling millimeter-wave Substrate Integrated Circuits,"

- in *2014 IEEE MTT-S International Microwave Symposium (IMS2014)*, Jun. 2014, pp. 1–3. doi: 10.1109/MWSYM.2014.6848524.
- [74] M. S. Arunima, S. Bhuvana Nair, and K. A. Unnikrishna Menon, “An Overview of Millimeter-wave Antennas,” in *2020 5th International Conference on Communication and Electronics Systems (ICCES)*, Jun. 2020, pp. 395–400. doi: 10.1109/ICCES48766.2020.9137985.
- [75] P. Kumawat and S. Joshi, “Review of Slotted SIW antenna at 28 GHz and 38 GHz for mm-wave applications,” in *2020 12th International Conference on Computational Intelligence and Communication Networks (CICN)*, Sep. 2020, pp. 8–13. doi: 10.1109/CICN49253.2020.9242587.
- [76] Guo Qing Luo, Zhi Fang Hu, Lin Xi Dong, and Ling Ling Sun, “Planar Slot Antenna Backed by Substrate Integrated Waveguide Cavity,” *IEEE Antennas Wirel. Propag. Lett.*, vol. 7, pp. 236–239, 2008, doi: 10.1109/LAWP.2008.923023.
- [77] H. Zhan, X.-C. Li, L. Ji, and J.-F. Mao, “A Tri-Band SIW Single-Slot Antenna Fed by Asymmetric GCPW,” in *2020 International Conference on Microwave and Millimeter Wave Technology (ICMMT)*, Sep. 2020, pp. 1–3. doi: 10.1109/ICMMT49418.2020.9386648.
- [78] N. Ghassemi and K. Wu, “Planar High-Gain Dielectric-Loaded Antipodal Linearly Tapered Slot Antenna for E- and W-Band Gigabyte Point-to-Point Wireless Services,” *IEEE Trans. Antennas Propag.*, vol. 61, no. 4, pp. 1747–1755, Apr. 2013, doi: 10.1109/TAP.2012.2232269.
- [79] K. Gong and X. H. Hu, “Low-Profile Substrate Integrated Dielectric Resonator Antenna Implemented With PCB Process,” *IEEE Antennas Wirel. Propag. Lett.*, vol. 13, pp. 1023–1026, 2014, doi: 10.1109/LAWP.2014.2325033.
- [80] M. Esquius-Morote, B. Fuchs, J.-F. Zürcher, and J. R. Mosig, “Novel Thin and Compact H-Plane SIW Horn Antenna,” *IEEE Trans. Antennas Propag.*, vol. 61, no. 6, pp. 2911–2920, Jun. 2013, doi: 10.1109/TAP.2013.2254449.
- [81] X. Zou, C.-M. Tong, J.-S. Bao, and W.-J. Pang, “SIW-Fed Yagi Antenna and Its Application on Monopulse Antenna,” *IEEE Antennas Wirel. Propag. Lett.*, vol. 13, pp. 1035–1038, 2014, doi: 10.1109/LAWP.2014.2327161.
- [82] K. Y. Kapsuz, A. V. Berghe, S. Lemey, and H. Rogier, “Compact, Broadband, and Highly Efficient Leaky-Wave Antenna in Air-Filled Substrate Integrated Waveguide Technology,” in *2021 18th European Radar Conference (EuRAD)*, Apr. 2022, pp. 126–128. doi: 10.23919/EuRAD50154.2022.9784510.
- [83] A. Ghiotto, F. Parment, T.-P. Vuong, and K. Wu, “Millimeter-Wave Air-Filled SIW Antipodal Linearly Tapered Slot Antenna,” *IEEE Antennas Wirel. Propag. Lett.*, vol. 16, pp. 768–771, 2017, doi: 10.1109/LAWP.2016.2602280.
- [84] Y. Cai, Z.-P. Qian, Y.-S. Zhang, J. Jin, and W.-Q. Cao, “Bandwidth Enhancement of SIW Horn Antenna Loaded With Air-Via Perforated Dielectric Slab,” *IEEE Antennas Wirel. Propag. Lett.*, vol. 13, pp. 571–574, 2014, doi: 10.1109/LAWP.2014.2312917.

- [85] J. Wang, F. Wu, Z. H. Jiang, Y. Li, and D. Jiang, "A Millimeter-Wave Substrate Integrated Waveguide H-Plane Horn Antenna With Enhanced Gain and Efficiency," *IEEE Antennas Wirel. Propag. Lett.*, vol. 21, no. 4, pp. 769–773, Apr. 2022, doi: 10.1109/LAWP.2022.3145883.
- [86] Y. Yoshimura, "A Microstripline Slot Antenna (Short Papers)," *IEEE Trans. Microw. Theory Tech.*, vol. 20, no. 11, pp. 760–762, Nov. 1972, doi: 10.1109/TMTT.1972.1127868.
- [87] S. Mukherjee, A. Biswas, and K. V. Srivastava, "Broadband Substrate Integrated Waveguide Cavity-Backed Bow-Tie Slot Antenna," *IEEE Antennas Wirel. Propag. Lett.*, vol. 13, pp. 1152–1155, 2014, doi: 10.1109/LAWP.2014.2330743.
- [88] G. Q. Luo, Z. F. Hu, L. X. Dong, and L. L. Sun, "Planar Slot Antenna Backed by Substrate Integrated Waveguide Cavity," *IEEE Antennas Wirel. Propag. Lett.*, vol. 7, pp. 236–239, 2008, doi: 10.1109/LAWP.2008.923023.
- [89] M.-H. Ho, K. A. Michalski, and K. Chang, "Waveguide excited microstrip patch antenna-theory and experiment," *IEEE Trans. Antennas Propag.*, vol. 42, no. 8, pp. 1114–1125, Aug. 1994, doi: 10.1109/8.310003.
- [90] M. Kanda, D. C. Chang, and D. H. Greenlee, "The Characteristics of Iris-Fed Millimeter-Wave Rectangular Microstrip Patch Antennas," *IEEE Trans. Electromagn. Compat.*, vol. EMC-27, no. 4, pp. 212–220, Nov. 1985, doi: 10.1109/TEMC.1985.304292.
- [91] N.-H. Nguyen, A. Ghiotto, M. T. Le, and T.-P. Vuong, "High Gain Microstrip Patch Antenna Array using Air-Filled Substrate Integrated Waveguide (AFSIW) Feeding Structure," in *2022 International Conference on Advanced Technologies for Communications (ATC)*, Oct. 2022, pp. 54–57. doi: 10.1109/ATC55345.2022.9943028.
- [92] C. A. Balanis, *Antenna Theory: Analysis and Design*. John Wiley & Sons, 2016.
- [93] D. Budimir, "Millimeter-Wave Filters for Wireless Communications and Radar Applications - An Overview," in *2007 International Kharkov Symposium Physics and Engrg. of Millimeter and Sub-Millimeter Waves (MSMW)*, Jun. 2007, pp. 648–650. doi: 10.1109/MSMW.2007.4294765.
- [94] G. Brzezina, L. Roy, and L. MacEachern, "A miniature LTCC bandpass filter using novel resonators for GPS applications," in *2007 European Microwave Conference*, Oct. 2007, pp. 536–539. doi: 10.1109/EUMC.2007.4405246.
- [95] L. Hepburn and J. Hong, "Compact Integrated Lumped Element LCP Filter," *IEEE Microw. Wirel. Compon. Lett.*, vol. 26, no. 1, pp. 19–21, Jan. 2016, doi: 10.1109/LMWC.2015.2505631.
- [96] J. W. Bandler, R. M. Biernacki, S. H. Chen, D. G. Swanson, and S. Ye, "Microstrip filter design using direct EM field simulation," *IEEE Trans. Microw. Theory Tech.*, vol. 42, no. 7, pp. 1353–1359, Jul. 1994, doi: 10.1109/22.299729.

- [97] C.-H. Wu, Y.-S. Lin, C.-H. Wang, and C. H. Chen, "Novel microstrip coupled-line bandpass filters with shortened coupled sections for stopband extension," *IEEE Trans. Microw. Theory Tech.*, vol. 54, no. 2, pp. 540–546, Feb. 2006, doi: 10.1109/TMTT.2005.862710.
- [98] R. Zhang and R. R. Mansour, "Dual-Band Dielectric-Resonator Filters," *IEEE Trans. Microw. Theory Tech.*, vol. 57, no. 7, pp. 1760–1766, Jul. 2009, doi: 10.1109/TMTT.2009.2022876.
- [99] M. Memarian and R. R. Mansour, "Quad-mode and dual-mode dielectric resonator filters," *IEEE Trans. Microw. Theory Tech.*, vol. 57, no. 12, pp. 3418–3426, Dec. 2009, doi: 10.1109/TMTT.2009.2034310.
- [100] B.-L. Zheng, S.-W. Wong, S.-F. Feng, L. Zhu, and Y. Yang, "Multi-Mode Bandpass Cavity Filters and Duplexer With Slot Mixed-Coupling Structure," *IEEE Access*, vol. 6, pp. 16353–16362, 2018, doi: 10.1109/ACCESS.2017.2766293.
- [101] B. Yassini, M. Yu, and B. Keats, "A  $\text{\$Ka\$}$  -Band Fully Tunable Cavity Filter," *IEEE Trans. Microw. Theory Tech.*, vol. 60, no. 12, pp. 4002–4012, Dec. 2012, doi: 10.1109/TMTT.2012.2224367.
- [102] A. E. Atia and A. E. Williams, "Narrow-Bandpass Waveguide Filters," *IEEE Trans. Microw. Theory Tech.*, vol. 20, no. 4, pp. 258–265, Apr. 1972, doi: 10.1109/TMTT.1972.1127732.
- [103] M. Yu, "The recent advances of high performance filters and multiplexers," in *2015 Asia-Pacific Microwave Conference (APMC)*, Dec. 2015, pp. 1–1. doi: 10.1109/APMC.2015.7413071.
- [104] I. Hunter, *Theory and design of microwave filters*. in IEE electromagnetic waves series, no. 48. London: Institution of Electrical Engineers, 2001.
- [105] F. R. Connor and F. R. Connor, *Wave transmission*. in Introductory topics in electronics and telecommunication / F. R. Connor, no. 3. London: Arnold, 1972.
- [106] L. A. Belov, S. Smolskiy, and V. N. Kochemasov, *Handbook of RF, microwave and millimeter-wave components*. in Artech House microwave library. Boston, Mass.: Artech House, 2012.
- [107] A. Das and S. K. Das, *Microwave Engineering*. Tata McGraw-Hill Publishing Company, 2000.
- [108] R. B. Waterhouse and R. B. Waterhouse, *Microstrip patch antennas: a designer's guide*. Boston: Kluwer Academic, 2003.
- [109] S. Moscato, C. Tomassoni, M. Bozzi, and L. Perregrini, "Quarter-Mode Cavity Filters in Substrate Integrated Waveguide Technology," *IEEE Trans. Microw. Theory Tech.*, vol. 64, no. 8, pp. 2538–2547, Aug. 2016, doi: 10.1109/TMTT.2016.2577690.
- [110] N. H. Nguyen, F. Parment, A. Ghiotto, K. Wu, and T. P. Vuong, "A fifth-order air-filled SIW filter for future 5G applications," in *2017 IEEE MTT-S International*

*Microwave Workshop Series on Advanced Materials and Processes for RF and THz Applications (IMWS-AMP)*, Sep. 2017, pp. 1–3. doi: 10.1109/IMWS-AMP.2017.8247355.

- [111] N. Delmonte, L. Silvestri, C. Tomassoni, L. Perregrini, and M. Bozzi, “Overview of Air-Filled SIW Filter Topologies,” in *2021 IEEE MTT-S International Microwave Workshop Series on Advanced Materials and Processes for RF and THz Applications (IMWS-AMP)*, Nov. 2021, pp. 308–310. doi: 10.1109/IMWS-AMP53428.2021.9643962.
- [112] L. Silvestri, A. Ghiotto, C. Tomassoni, M. Bozzi, and L. Perregrini, “Partially Air-Filled Substrate Integrated Waveguide Filters With Full Control of Transmission Zeros,” *IEEE Trans. Microw. Theory Tech.*, vol. 67, no. 9, pp. 3673–3682, Sep. 2019, doi: 10.1109/TMTT.2019.2926356.
- [113] C. Tomassoni, L. Silvestri, M. Bozzi, L. Perregrini, and A. Ghiotto, “A novel filter based on a dual-mode air-filled substrate integrated waveguide cavity resonator,” in *2017 IEEE MTT-S International Conference on Numerical Electromagnetic and Multiphysics Modeling and Optimization for RF, Microwave, and Terahertz Applications (NEMO)*, May 2017, pp. 290–292. doi: 10.1109/NEMO.2017.7964263.
- [114] C. Tomassoni, L. Silvestri, A. Ghiotto, M. Bozzi, and L. Perregrini, “Substrate-Integrated Waveguide Filters Based on Dual-Mode Air-Filled Resonant Cavities,” *IEEE Trans. Microw. Theory Tech.*, vol. 66, no. 2, pp. 726–736, Feb. 2018, doi: 10.1109/TMTT.2017.2786212.
- [115] N.-H. Nguyen, A. Ghiotto, T.-P. Vuong, A. Vilcot, T. Martin, and K. Wu, “Dielectric Slab Air-Filled Substrate Integrated Waveguide (SAFSIW) Bandpass Filters,” *IEEE Microw. Wirel. Compon. Lett.*, vol. 30, no. 4, pp. 363–366, Apr. 2020, doi: 10.1109/LMWC.2020.2974993.
- [116] T. Martin, A. Ghiotto, T.-P. Vuong, K. Wu, and F. Lotz, “Compact Quasi-Elliptic and Highly Selective AFSIW Filter with Multilayer Cross-Coupling,” in *2019 IEEE MTT-S International Microwave Symposium (IMS)*, Jun. 2019, pp. 718–721. doi: 10.1109/MWSYM.2019.8700728.
- [117] C. Tomassoni, L. Silvestri, M. Bozzi, and L. Perregrini, “Substrate Integrated Waveguide Filters with Stacked Cavities,” in *2020 IEEE MTT-S International Wireless Symposium (IWS)*, Sep. 2020, pp. 1–3. doi: 10.1109/IWS49314.2020.9359927.
- [118] T. Shen, H.-T. Hsu, K. A. Zaki, A. E. Atia, and T. G. Dolan, “Full-wave design of canonical waveguide filters by optimization,” *IEEE Trans. Microw. Theory Tech.*, vol. 51, no. 2, pp. 504–511, 2003, doi: 10.1109/TMTT.2002.807829.
- [119] “Microwave Filters for Communication Systems: Fundamentals, Design, and Applications | Wiley eBooks | IEEE Xplore.” Accessed: Nov. 22, 2022. [Online]. Available: <https://ieeexplore-ieee-org.gaelnomade-1.grenet.fr/book/8341843>
- [120] R. Cameron, “Advanced Filter Synthesis,” *IEEE Microw. Mag.*, vol. 12, no. 6, pp. 42–61, Oct. 2011, doi: 10.1109/MMM.2011.942007.

- [121] S. Cogollos *et al.*, “A Systematic Design Procedure of Classical Dual-Mode Circular Waveguide Filters Using an Equivalent Distributed Model,” *IEEE Trans. Microw. Theory Tech.*, vol. 60, no. 4, pp. 1006–1017, Apr. 2012, doi: 10.1109/TMTT.2012.2183381.



## LIST OF PUBLICATIONS

### International conferences

1. J. Zhang, Y. Duroc, A. Ghiotto, K. Wu and T. -P. Vuong, "Air-Filled Substrate Integrated Waveguide (AFSIW) Cavity-Backed Slot Antenna for 5G Applications," IEEE International Symposium on Antennas and Propagation and North American Radio Science Meeting, Montreal, QC, Canada, 2020, pp. 395-396, doi: 10.1109/IEEECONF35879.2020.9329764.
2. J. Zhang, Y. Duroc, K. Wu, A. Ghiotto and T. -P. Vuong, "A Vertical Transition between Microstrip Line and Air-Filled SIW at Ka-band," 52<sup>nd</sup> European Microwave Conference (EuMC), Milan, Italy, 2022, pp. 484-487, doi: 10.23919/EuMC54642.2022.9924415.

### National conferences

1. J. Zhang, Y. Duroc, A. Ghiotto, K. Wu and T. -P. Vuong, "Transition verticale à faibles pertes entre ligne microruban et guide d'ondes intégré au substrat creux en bande Ka," 22<sup>ème</sup> édition des Journées Nationales Microondes, Limoges, France, 2022.
2. J. Zhang, Y. Duroc, A. Ghiotto, K. Wu and T. -P. Vuong, "Filtre passe-bande d'ordre trois à guide d'ondes intégré au substrat creux (AFSIW) multicouche en bande Ka," 22<sup>ème</sup> édition des Journées Nationales Microondes, Limoges, France, 2022.